Chemical weathering on Eldsfjellet, Meland municipality, western Norway

Oliver Queck

Master Thesis in Geology – Quaternary Geology and Paleoclimatology

Department of Earth Science

University of Bergen

Autumn 2012

Acknowledgment

I would like to thank my supervisor Henriette Linge for her constructive ideas during field work, laboratory work and the writing process. I also want to thank Prof. Haakon Fossen and Prof. Ingunn H. Thorseth for their supervision. A big thanks goes to Prof. Svein-Olaf Dahl, Henrik Løset Jansen and Bjørn Eikeland for helping me to collect sediment samples from Storatjørna (local lake). Special thanks go to Dr. Romain Meyer for his guidance in the laboratory and the help with analysing my results. I want to thank Ole Tumyr, Hildegunn Almelid, Yuval Ronen and Siv Hjort Dundas for the help with preparing and processing my samples. For the clay analysis of my sediment samples I want to thank Markus Peltz and Dr. Georg Grathoff at the University of Greifswald (Germany). Big thanks also go to Benjamin Aubrey Robson for reading through my thesis and correcting my English. I am very thankful for always having the support of my parents, my friends and my girlfriend during my thesis. Without them it would have been much harder to write this thesis.

Bergen, November 2012

Oliver Queck

Abstract

The Subject of this master thesis was to define the chemical weathering processes, create a weathering chain from sink to source and to evaluate the degree of weathering on Eldsfjellet, Meland municipality in western Norway. Rock, water and sediment samples were collected in the field area using a corer for hard rock and sediment samples, water samples were bottled in laboratory flasks and afterwards cleaned with a filter to remove colloids and other particles. Multiple analyses such as XRF, XRD, ICP-MS, ICP-OES and microscopy were carried out. The major element, trace element and rare earth element composition of the various samples were acquired. The comparison between trace elements from water and rock samples showed a good agreement which leads to the presumption that water is the major weathering and transport agent in the field area. Because of the low temperature range between summer and winter in the field area, mechanical weathering is assumed to be a less important weathering factor for most of the year. Derived sediment samples from organic rich top layers in the local catchment lake were analysed using XRD. Clay minerals were found which could be directly linked to the local bedrock, therefore it was possible to create a weathering chain. First the bed rock is slowly dissolved due to the permanent supply with fresh water. Secondly, because of the reaction between water and bedrock, clay minerals get produced which then will be, together with other particles, transported to the local catchment lake and finally deposited in the lake sediments. To determine the degree of weathering, different chemical indexes of weathering have been used, all of which show a slight level of weathering. The Elsdfjellet data were compared with data on similar rock types from India, which shows that climatic difference (higher temperature, more precipitation) and a longer transport distance favour chemical weathering in India. To define weathering rates, a formula was used which includes a *gain-loss* factor calculated from the weight % concentration of different major elements in bedrock and sediment samples. The calculation also displays a low loss of fresh rock material.

Contents

1. Introduction

Chemical weathering is a process happening all over the world and in every geological environment. Every rock type is affected by chemical weathering and dependent on the rock stability rocks will resist against it longer or shorter time periods. The composition of a rock and the climate conditions in which the rock is located plays a major role for the weathering rate. The chemical weathering is stronger in tropical and humid climate zones compared to nival and aride climate zones. Chemical weathering is a crucial part of the geological cycle and is partly responsible for the erosion of mountains. The chemical weathering has been subject of extensive studies in tropical climate zones but has recieved less attention in higher latitudes. The major weathering processes in cold and arid climate are related to mechanical weathering but chemical weathering plays also in these areas an important role, while both processes have significant influence in humid zones.

The focus of this thesis is to determine the dominating chemical weathering process and the average rates of weathering after the deglaciation. Another question is how to detect and quantify chemical weathering processes and which chemical information can be used to achieve that. What kind of weathering products will be produced and are these products in agreement with the local bedrock composition. Another important point is to obtain information about the rate of weathering, since the field area is a mountain situated on the strandflat. It is necessary to acquire information about the weathering chain to use this information for the description of weathering processes and speed on other mountains at the western coast of Norway. Another question is to characterise the rate and degree of chemical weathering compared to other areas in the world with different climate conditions to show the effect of climate on chemical weathering. Eldsfjellet gives the opportunity to characterise and quantify the post-glacial weathering in western Norway. To do so, geochemical methods have been utilised.

The Eldsfjellet area has previously been subject of intensive structural geological analysis (e.g., Austrheim 1987; Boundy et al. 1992; Erambert and Austrheim 1993; Austrheim et al. 1997).

This research project started with a review of the published literature, and fieldwork was initiated in August 2011. The fieldwork was carried out on Eldsfjellet, a mountain on the island of Holsnøy in Meland municipal approximately 40 km north of Bergen (Fig. 1 and 2). After an investigation of the field area, locations were carefully selected for collecting cores sample from bedrock surface, sediment cores from a catchment lake, and water samples from different small puddles within the area. The core samples from the bedrock were taken from horizontal and vertical surfaces in the south-east, south-west and north-west parts of the study area. These samples were analysed using the geochemical methods described in Chapters 3 and 4. The data derived from the chemical analysis will be used for describing the weathering chain from source area to the sink (sediments from a local lake).

Eldsfjellet is part of the Lindås Nappe which was partly subducted in the Silurian during the Caledonian orogeny (Bingen et al. 2004) and has since been strongly eroded. The dominating rocks constituting Eldsfjellet are anorthosites followed by eclogite. The main goals of this thesis are to characterise the most important chemical weathering agents, describing the weathering chain from source to sink, determine the degree of weathering in the area after the deglaciation and compare the degree of weathering with chemical weathering of similar rocks in other climate zones.

The major and trace element composition of the rocks and also the chemistry of sediments and water in the area were investigated. The methods used are polarized light microscopy, scanning electron microscopy (SEM), X-ray fluorescence (XRF), X-ray diffraction (XRD), inductive coupled plasma mass spectrometry (ICP-MS), inductively coupled plasma atomic emission spectroscopy (ICP-AES) and ion chromatography (IC). Another way to study the processes was the use of secondary minerals such as various types of clay minerals to construct a weathering chain that shows the parental material and the secondary (weathering related) minerals.

During the fieldwork two sediment cores were taken from a local lake using a gravity corer device. One of the cores was cut in slices of 3 cm thickness for the analysis of the

chemical composition of the sediments and to find out which secondary minerals are in the samples.

Details related to the different methods used will be addressed in the methodology chapter (chapter 3). In the results chapter (chapter 4) the data will be objectively described. In the discussion chapter (chapter 5) the results will be interpreted together to become a picture of the different processes leading to the local weathering. The results will be compared with data from other areas to critically discuss and support them

1.1. Study site

The field area is situated on the island of Holsnøy (Nordhordaland) approximately 40 km north of Bergen (Fig. 1).

Figure 1: The green square marks the field area, the blue square the position of Bergen (source: Statens Kartverk).

Eldsfjellet is located in the northern part of Holsnøy and has a maximum altitude of 324 m a.s.l (Fig. 2). The whole field area covers approximately 7 km². To the west of Holsnøy are the islands of Herdla and Askøy and to the east lies the island of Radøy. The island is surrounded

by the Hatlefjorden to the west, the Mangersfjorden to the north-east and the Radøyfjorden to the east (Fig. 1).

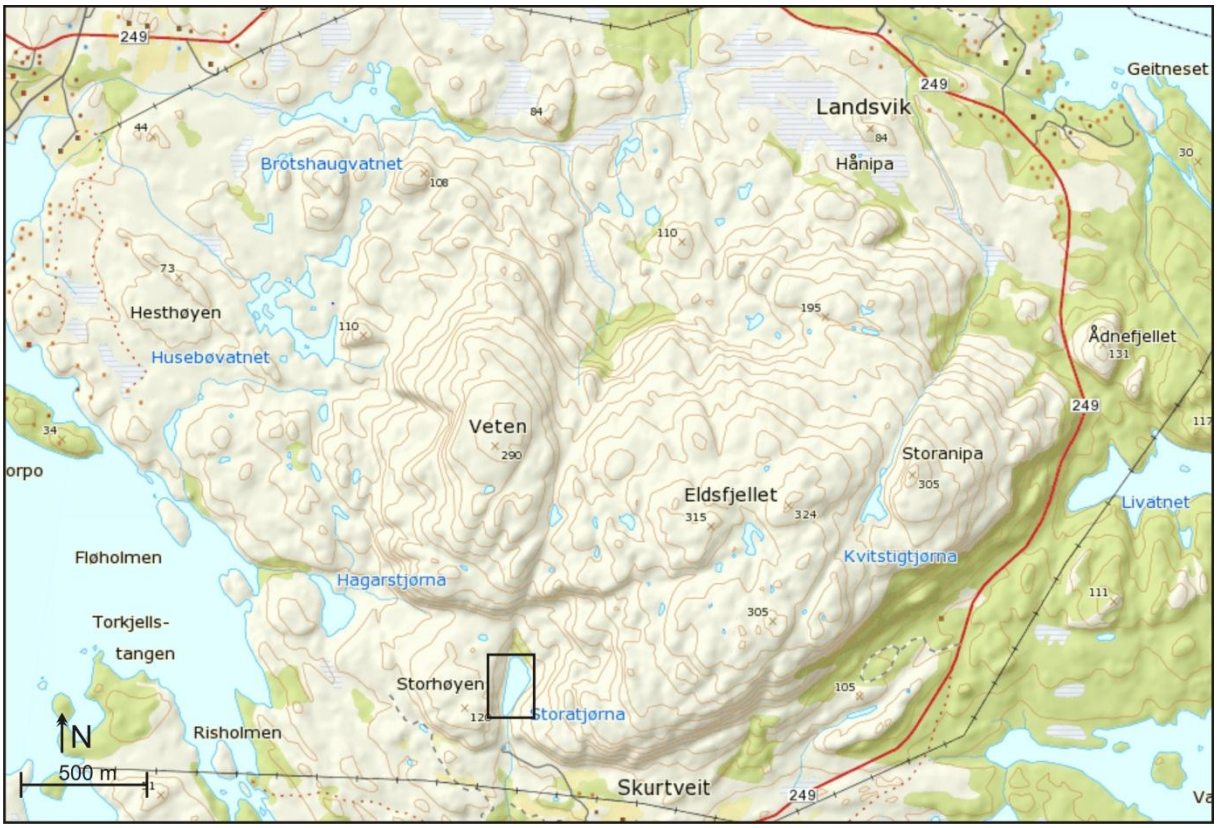

Figure 2: A topographic map of Eldsfjellet, marked with a black square is Storatjørna a local lake which has been cored (source: Statens Kartverk).

The mountain has several peaks (Fig. 2) which are, partly, difficult to access because of a steep topography. The southern and eastern flank is steep. The access from the coastal side is gentler. The northern and north-eastern lower parts of the field area consist of a heavily vegetated marsh landscape.

1.2. Bedrock geology

The field area is located in the Bergen arcs, which is a series of arcuate Caldeonian trust sheets centered on the town of Bergen (Austrheim 1986). The whole mountain is dominated by anorthosite, a plagioclase-rich felsic rock, but it also consists of various mafic rocks like gabbroic anorthosite and rocks of the charnokite group (Raimbourg et al. 2005) (Fig. 3).

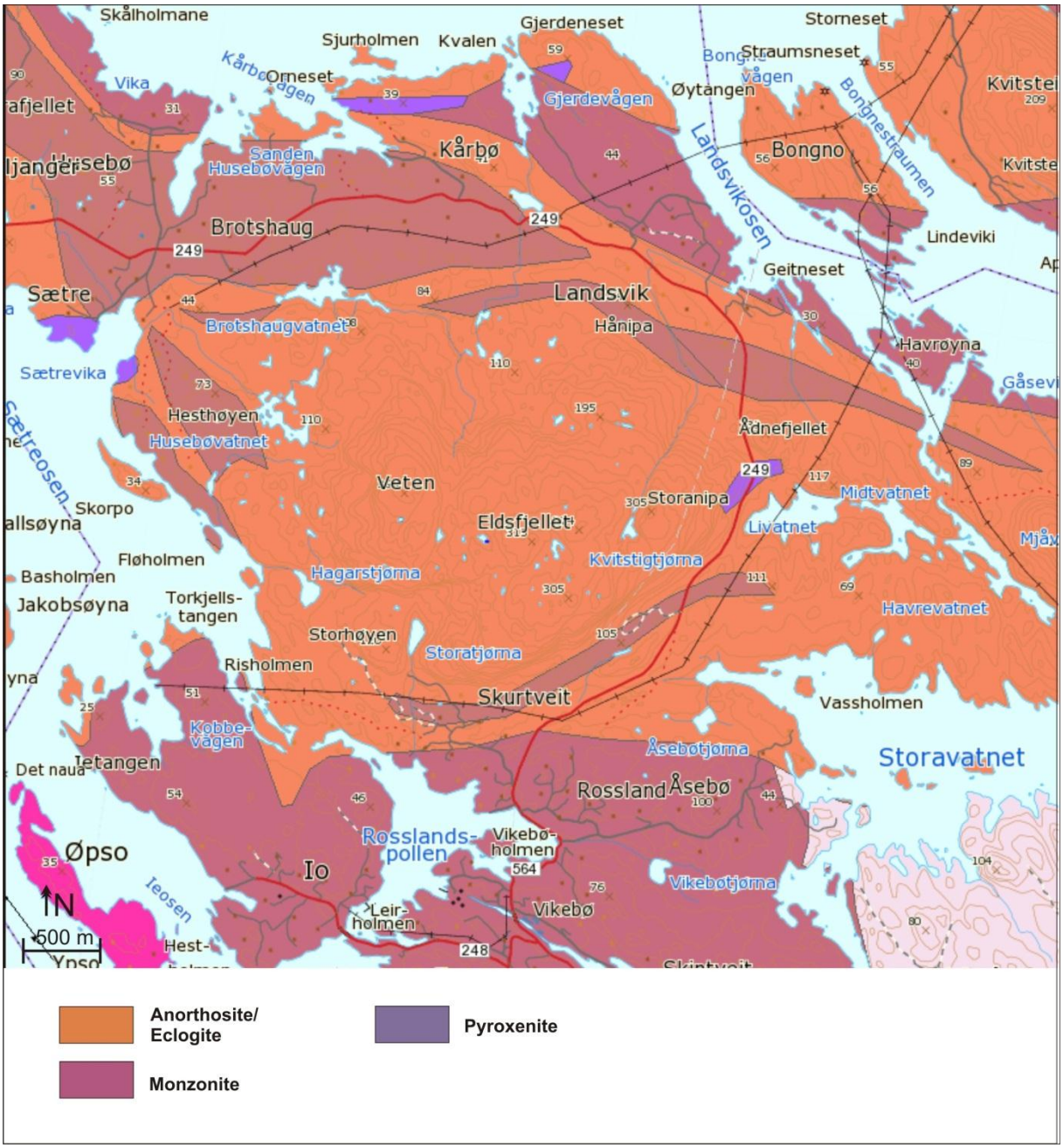

Figure 3: A geological map showing the different main rock types in the field area (Source: bedrock map from http://geo.ngu.no/kart/berggrunn/).

The geological history of the Bergen arcs is dominated by two events. The first, the Grenvilian orogeny of Proterozoic age, is an event dominated by extensive magmatic activity, deformation and granulite facies metamorphism. This was then followed by localized Caledonian reworking. Austrheim (1986) considers the anorthositic material to be a lower-crustal suite based on composition and mineralogy. The island of Holsnøy is part of the Lindås Nappe, which is in the highest tectonic position of the Bergen Arc nappe pile. Eclogite is common in the field area; this has an age of approximately 425 Ma and is referred

to be older than the widespread eclogites in the Western Gneiss Region to the north. Proterozoic granulitic anorthosites and mangerites, which are similar to the basement of the Western Gneiss Region, form the core of the Lindås nappe and the local field area (e.g. Griffin, 1985). A common feature of the local geology is a coronitic mineral texture called corona textures, they can be found all over the mountain and range in size from a few centimeters up to a few meters. The corona textures consist of a core made up by pyroxene and (locally) olivine, and are surrounded by a layer of garnet of variable thickness (Fig. 4). Due to their mafic components, the core of these textures weather more easily than the anorthositic host rock, and are therefore typically spotted as holes in the weathered bedrock. The degree of weathering of these textures varies and probably depends on the exposure of the bedrock to the prevailing wind direction and the amount of meteoric precipitation.

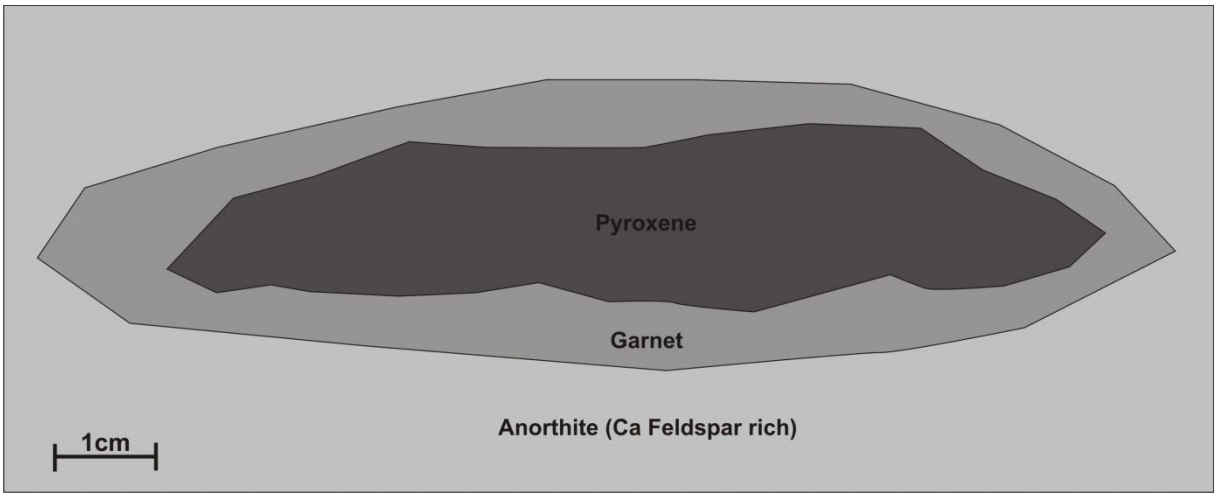

Figure 4: A schematic sketch of a corona texture, the mineral composition can vary.

1.3. Geomorphology and sediment cover

The field area shows very distinct morphological features. Eldsfjellet is a well-rounded mountain with several round peaks of approximately the same elevation (approximately 300 m). The rounded shape of the mountain is essentially due to erosional processes during Quaternary which strongly affected the landscape. The maximum elevation of Eldsfjellet is 324 m a.s.l. A very distinct geomorphological feature on Holsnøy is the strandflat, which was first described by Reusch (1894). The lowland surrounding Eldsfjellet is part of the strandflat and has mostly an elevation of only a few tens of meters above sea level while a number of

hills and small mountains with heights of several hundred meters rise up from this flat level. These features are very common on the western Norwegian coast.

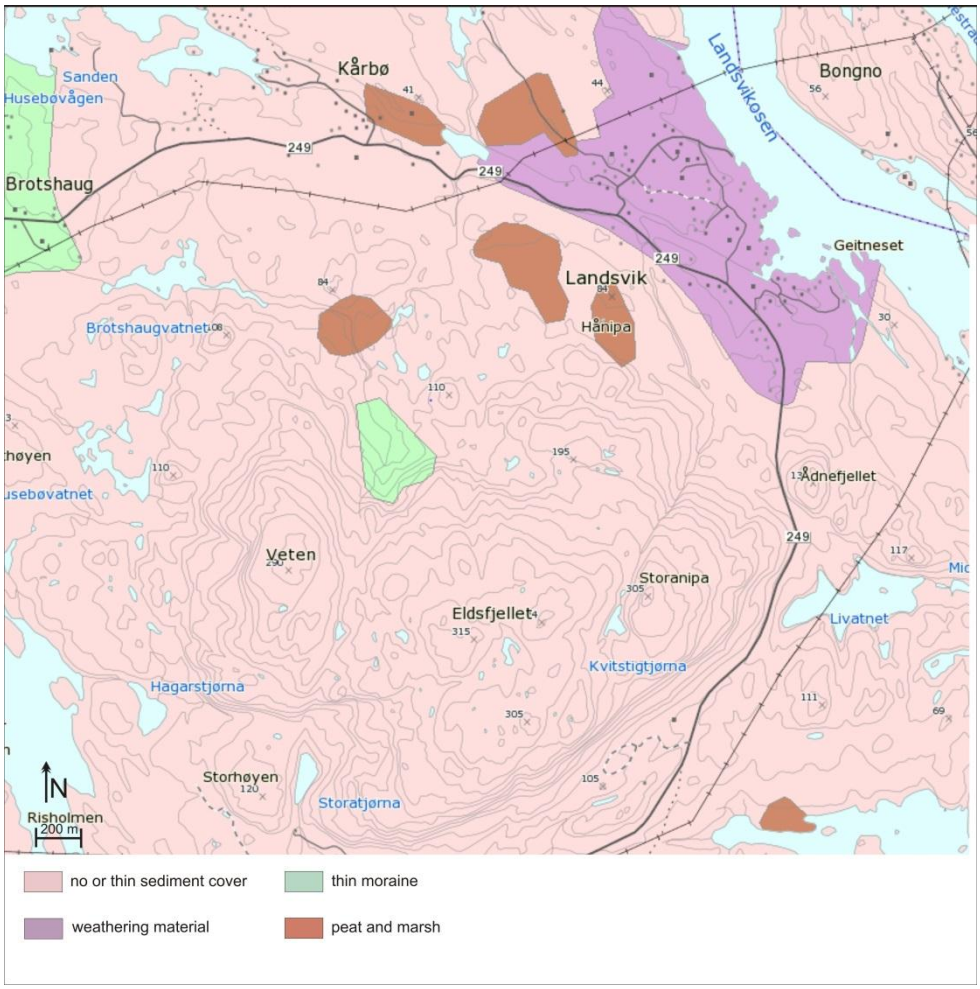

Figure 5: A Quaternary map showing the sediment cover in the field area (source: Løsmassekart from NGU).

As seen in the Quaternary map of the area (Fig. 5), the area has very little sediment cover. One exception is the central part of Eldsfjellet with a thin till cover and some areas which are covered by peat deposits and swamps. The purple area in the north is, according to NGU, deposits of local weathered material.

1.4. Present weather conditions

The weather conditions in the field area are heavily influenced by its coastal position. The area has a relatively narrow annual temperature range with typical temperatures varying between -1°C (January) and 12°C (July-August) (Fig. 6). The temperature data shown in this master thesis is sourced from www.eklima.no. The temperature data are from Bergen-Florida station (Nr. 50540). The reported temperature readings span from 01.01.1990 to 31.12.2011. The average temperature for 1990 was of approximately 5.5°C, which continuously increased in the last years to around 5.6°C. Two years with extreme low average annual temperature are 1996 with 4.3°C and 2010 with 3.4°C. The Bergen-Florida station has been chosen because it had temperature data.

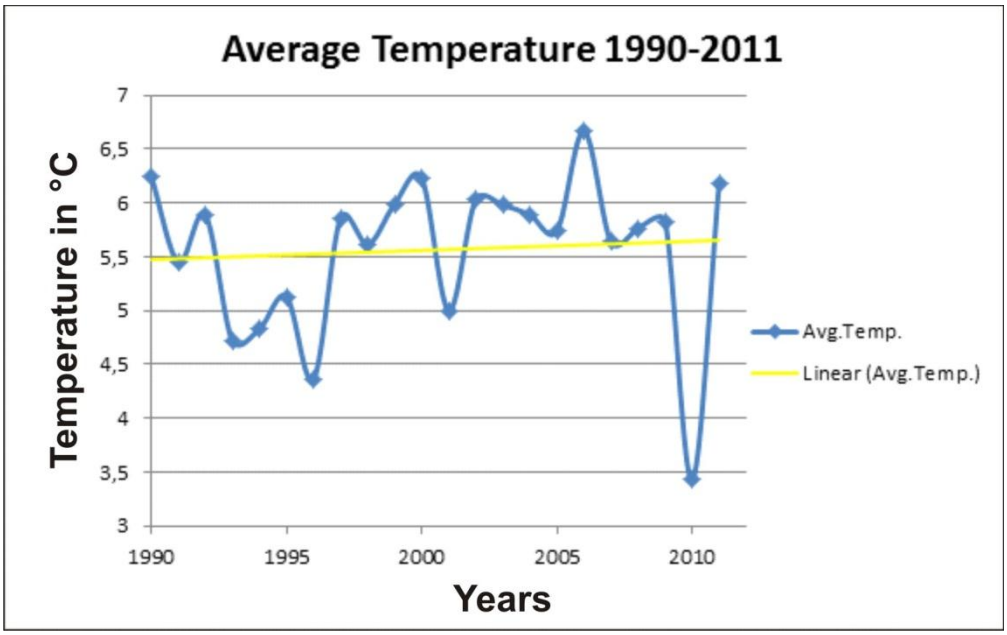

Figure 6: The blue graph shows the yearly average temperature in the period 1990 to 2011. The yellow line in the figure is a linear trend for the average temperature and shows an increase in the yearly average temperature over the presented time period (source: eklima.no).

The amount of precipitation is strongly dependent on the wind direction. The most dominant direction is from west, which sends moist air from the sea on land. Due to the orographic effect behind the coastal area where Holsnøy is located, water saturated clouds cannot go over the mountains and therefore will precipitate at the close coastal area. The average annual precipitation on Holsnøy is more than 2000 mm/a (Fig. 7).

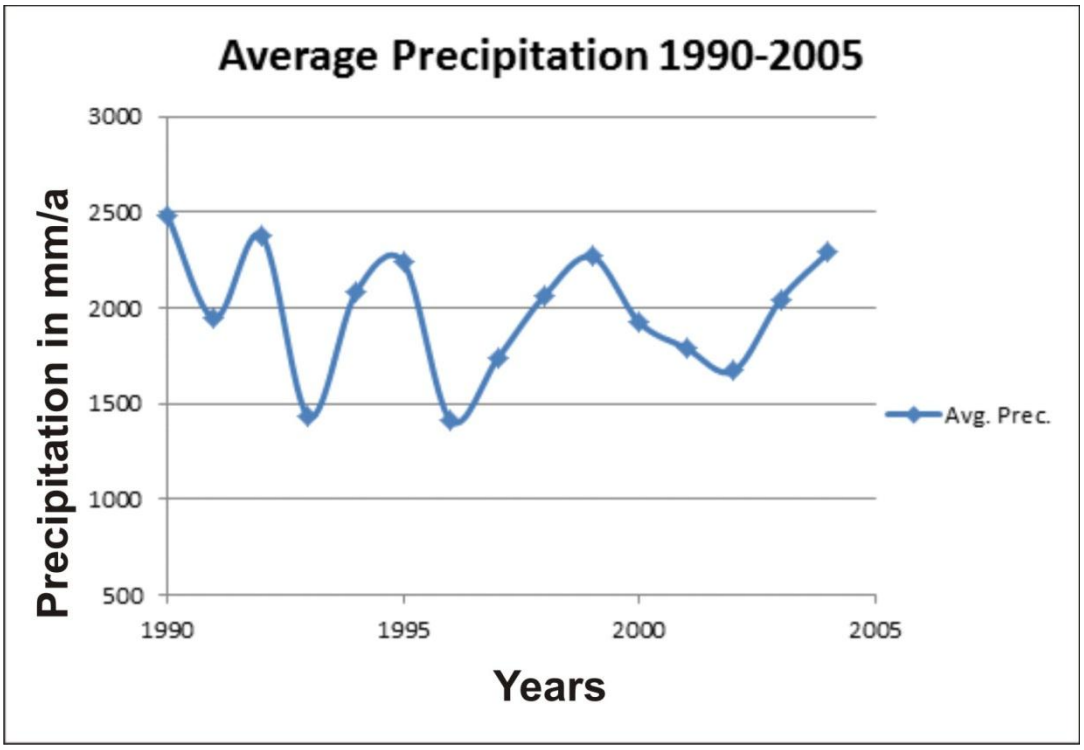

Figure 7: The blue line shows the average precipitation from 1990 to 2011 (source: eklima.no).

The station used for precipitation is called Holsnøy – Landsvik (Nr. 52440). This station has only precipitation data and no temperature data. The data range is from 1990 to 2005. The average precipitation has been circa 2000 mm/a. Lowest precipitation periods were 1993 and 1996 with precipitation below 1500 mm/a. Maximum precipitation has been 1990 with 2500 mm/a.

1.5. Quaternary geology

The glaciation history in the region is important since glacial erosion has removed pre-existing weathering products and the intensity of chemical weathering is different in an interglacial period compared to a glacial period. Mechanical weathering is expected to be dominant during the latter periods, whereas chemical weathering would play a minor role. Reconstruction of the Scandinavian ice sheet during the Weichselian period has resulted in time-distance diagrams showing the change in ice-margin position with time for the Bergen area. Mangerud (1970) conducted mainly ^{14}C-dating and pollen analysis to determine the advance and retreat of the ice sheet during the last glacial period. Figure 8 shows the different ice-margin fluctuations during the late Weichselian.

It is important to note the position of Herdla moraine (11.760 ± 120 cal a BP)(which lies further west than Holsnøy). The distance between Herdla and Holsnøy is approximately 3 km. Herdla is located north of the island of Askøy north-west of Bergen. This means if the ice margin of the Scandinavian ice sheet retreated on Herdla, it also was retreating on Holsnøy, albeit slightly later. If the ice sheet readvanced, then it re advanced first on Holsnøy and slightly later on Herdla. Therefore it is possible to correlate the ice margin changes on Herdla with the changes on Holsnøy.

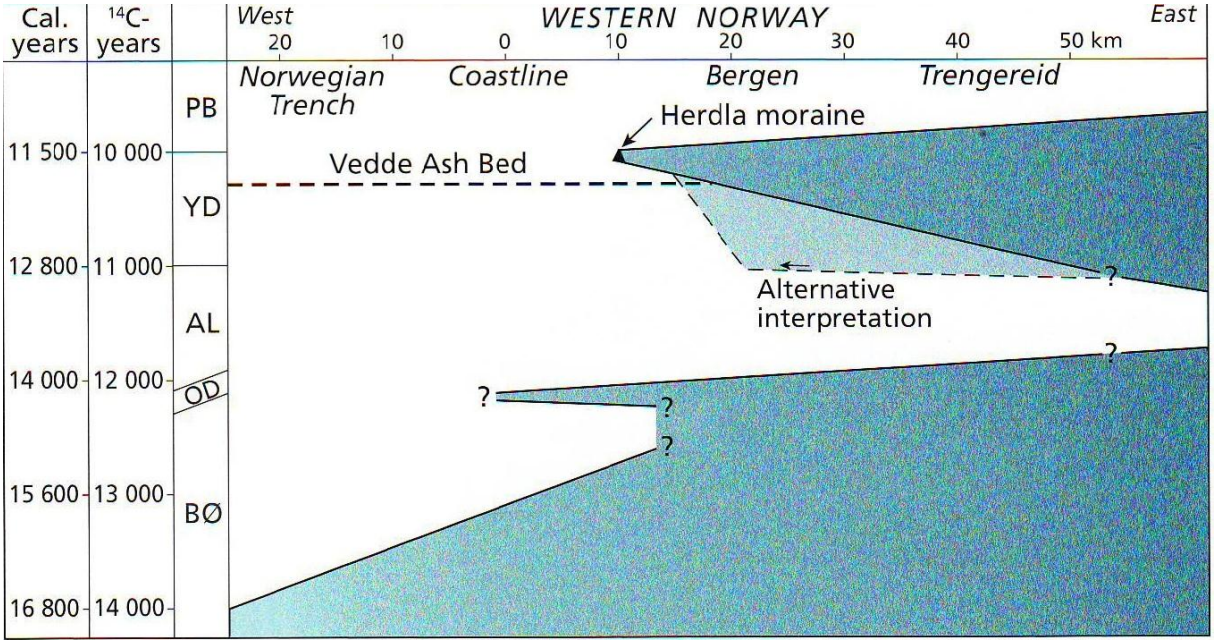

Figure 8: A time-distance diagram showing the ice sheet oscillation during the late Weichselian (Ramberg et al. 2008).

The fluctuations in Figure 8 is based on ^{14}C measurements from the Bergen area and is partly obtained from marine mollusks, gyttja, wood and bryozoan carbonate. The precision of these measurements is in order of ± 110 to ± 350 cal a BP.

At 19 k cal a BP the Norwegian Channel was deglaciated (Sejrup et al. 2009) and the ice sheet margin entered a period of stagnation that lasted around 4000 years (Mangerud et al. 2011). Then the ice retreated further until about 14.5 k cal a BP, when the outermost islands became ice-free (Lohne et al. 2011) and also Herdla and Holsnøy became ice-free (see Fig. 8). The ice margin advanced again during the Allerød Interstadial (Lohne et al. 2007) and reached Herdla during the late Younger Dryas (Fig. 9) (Andersen et al. 1995; Bondevik

and Mangerud 2002; Lohne, 2006). In Figure 9 the reconstructed ice margin position for the Younger Dryas is marked with a red line. Based on the map, Eldsfjellet was proximal to the ice margin. Since Eldsfjellet is 324 m (a.s.l.) high and the surrounding area is the strandflat, it is possible that the summit of Eldsfjellet was ice free, with ice flowing around the mountain. At around 11.5 k cal a BP the ice margin finally retreated and from that time on Holsnøy was ice free.

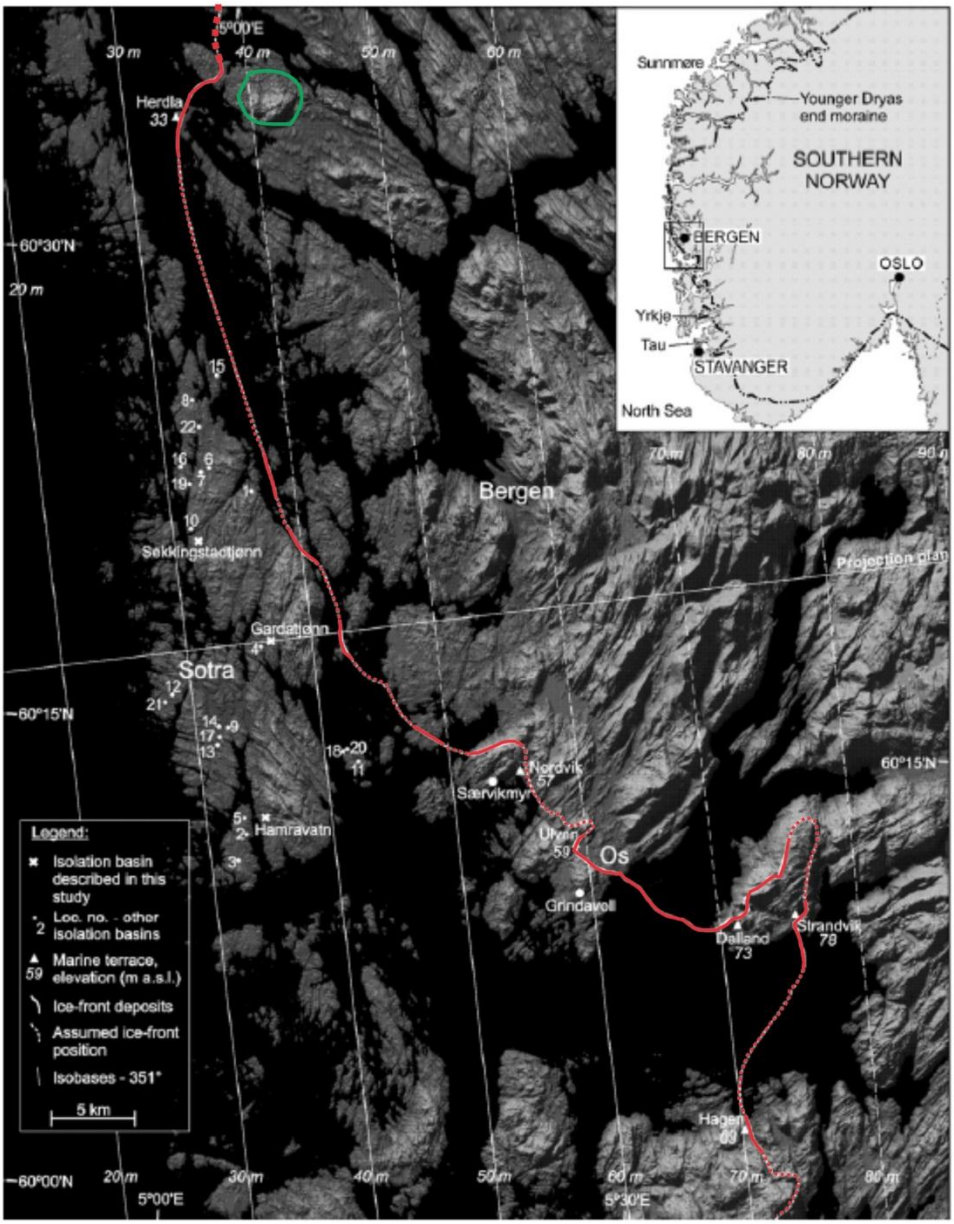

Figure 9: The red line marks the outermost boundary of the Younger Dryas ice advance before the final retreat of the ice sheet. The dotted line show assumed boundaries while the full lines show boundaries based on moraines and sediments of isolation basins. The green circle marks the field area (Lohne et al. 2007).

The glaciation history prior to the late Weichselian is only preserved at a few localities, for example Fjøsanger and Skjonghelleren. In most parts of the western coast of Norway the pre-Weichselian glaciation history is missing due to the glacial erosion. Therefore it can be assumed that the investigated surfaces were well eroded and freshly exposed after the last deglaciation. That means chemical weathering features and products observed can be assumed to be the product of weathering after the retreatment of the last ice sheet about 11.5 k cal a BP.

2. Theory and definitions

In this part, the focus will be on the theoretical background of processes which are common in the presented field area. The main active processes which form the landscape today are chemical and mechanical weathering; these are strongly influenced by the climate in this area. The information in this chapter are mostly based on textbook literature from Ollier (1984), Bahlburg and Breitkreuz (2004), Faure (1998) and Deer et al. (1966).

2.1.1. Chemical weathering

The basis for all chemical weathering processes is the desire of a system to be in equilibrium. Every chemical reaction will cease to run if the system reaches a state of equilibrium. Equilibrium relations determine the maximum amount of mineral that can be dissolved in any system (Ollier 1984). Due to the slow chemical reaction rate of most rocks, they will not reach a chemical equilibrium at the earth surface. The continuous supply of meteoric water keeps the reactions going.

The most important process which keeps weathering active at the earth surface is the permanent removal of weathered products. If the weathering products are continuously removed, the reaction will continue indefinitely since no equilibrium will be reached within the system. In closed systems, the chemical weathering will stop earlier after it reaches equilibrium.

The basis for chemical weathering is the reaction of minerals with air and water. Solutions play an important role since many weathering products will be transported away in a solution. Oxidation happens if minerals are exposed to air. Reduction happens mostly in waterlogged anaerobic environments. One of the most important processes is hydrolysis which is a chemical reaction between minerals and water. Hydrolysis is important for the breakdown of silicate minerals. Silicates are the most important group of minerals due to their high abundance on Earth. There are several other processes like carbonation, hydration and chelation. A mixture of various chemical and mechanical processes can happen due to the presence of organisms; these can strongly affect the weathering rate and are often referred to as biological weathering.

The most important ion in solution is hydrogen (H^+). Hydrogen controls many reactions and is expressed as the pH of a solution. The solubility of minerals is dependent on the pH of a solution. A neutral pH is 7. Dissolved iron in slightly acidic water will be precipitated when fresh water reaches the alkaline sea water

The oxidation states also play an important role in geochemical weathering. Fe, for example, can have several oxidation states. The oxidation stages depend on energy changes which are involved in adding or removing electrons.

Ions in solution attract water molecules; the strength of the attraction depends on the proportion to its charge (Z) and radius (*r*). The factor Z/*r* is known as ionic potential. Elements with low ionic potential, such as Na, K, and Ca, remain in solution during weathering; elements with intermediate ionic potential are precipitated by hydrolysis; whereas elements with still higher ionic potential form complex anions with oxygen which are again soluble (Ollier, 1984).

The first stage of weathering is a liquid mixture. It can be running water or a film of water around a solid particle. The amount of dissolution is strongly dependent on the water passing the surface of the particle. A continuous supply of fresh water will lead to increased weathering since the solution stays undersaturated due to the open system behaviour. Different minerals have different solubilities in a solution. Halite, for example, is easily soluble, gypsum is less soluble. In areas with higher temperatures, silicates can be easier dissolved. This means that the solubility of minerals is also climate dependent.

Oxidation is simply the loss of electrons or increase in oxidation state by a molecule, ion or atom. The oxidation of minerals always involves water. It is often enough to have a thin film of water. It mostly takes place in aerated zones. Typical are iron oxides and hydroxides which have a distinct red and yellow colour. Reduction is the opposite effect to oxidation and visible because of the colour change from red and yellow to greyish and greenish. Reduction is often a result of bacteria. The oxidation - reduction potential of soils is determined by the oxygen and CO_2 dissolved in water and the soil organic matter. It is therefore strongly dependent on the partial pressure of the gaseous oxygen and CO_2 in the soil air and on the pH of the soil solution.

The kinetics of dissolution is also dependent on the temperature. Temperature can have a stronger effect on rate constants than other effects. For example a temperature increase of 10 °C doubles the rate. But compared to the transport of species through solution, the effect of temperature is insignificant. This effect can be important as an indirect effect. If the temperatures are too low for organisms to live, they cannot affect the weathering.

2.1.2. Mechanical weathering

Mechanical weathering is based on the breakdown mainly by physical processes. The forces can come from inside the rocks (residual stress in the rocks) and externally due to, for example, tectonic processes, glaciers movement, freezing water, roots or running water. Stresses can lead to strain and eventually to rupture of the material. Gilbert (1904) proposed that expansion of rock masses, when their confining pressures are reduced by uplift and erosion, finds relief in the development of cracks. Thermal cooling also generates contraction that may cause the rock to fracture at or near the surface. This happens preferentially in granites, sandstones and limestone.

Structures in the rocks play an important role for the mechanical weathering. When bedrock is exposed to surface conditions, the rocks will decompact and cool down. These processes lead to the production of cracks in the rock. A typical example for decompaction processes is exfoliation. Exfoliation happens when the overlaying rock material is eroded and the rocks below are decompacting. Due to the release of pressure, chunks of material will be peeled from the rocks. This process is common in massive rocks like granites. The foliation and schistosity also make certain types of rock more vulnerable against mechanical weathering.

Mechanical weathering can be strongly dependent on temperature and temperature changes. A strong change between day and night temperature, such as in deserts, leads to rapid contraction and expansion of rock material. This causes a mechanical weakening of the rock structure and subsequently a breakdown of rock material.

Another important mechanical weathering factor is frost wedging. If water in cracks in a rock freezes, it leads to an expansion of water by 11 %. Due to the expansion, the rock structure will become weakened and collapse if a critical point is reached. If the mountain wall

collapses, new cracks will open and the mechanical weathering can continue. Frost wedging depends on cold climate and is therefore more common than chemical weathering at high latitudes and altitudes.

Mechanical weathering generally affects the rocks much stronger in extreme climates or under conditions with strong daily or seasonal temperature changes.

Another type of mechanical weathering, commonly found in coastal, arid areas, is known as salt wedging. It works similar to frost wedging. Saline water is transported from the sea by wind. The fine aerosol can settle in cracks. If the water evaporates, the salt starts to recrystallise. This leads to pressure built by the evaporation of 13 MPa and 4 MPa due to the growth of salt crystals. Sandstones are especially susceptible to this type of weathering. Typical weathering structures built by this type of weathering are tafoni.

Clay minerals can play an important role in mechanical weathering. Due to its capability for incorporating water in the mineral structures, clay has a high potential for swelling. The swelling will lead to a strong expansion of the clay and lead to failure in the rock structure. It also works the other way around. If clay loses its water content, it will shrink. This can lead to sagging and therefore also to rock failure.

2.2. Factors that affect weathering

There are several factors that strongly affect the weathering of rocks. In this part a short summary of the most important factors will be given.

2.2.1. Climate

Climate plays a crucial role and strongly affects the weathering. The main climatic controls are related to water and temperature. As mentioned previously the supply of water is very important for geochemical processes, while temperature is crucial for mechanical as well as geochemical weathering processes.

The water supply is not necessarily a warrant for strong weathering. Arizona has an annual precipitation of 7.5 cm and is considered to be arid, most of the water evaporates due to the high annual temperatures. On the other hand Alaska has partly the same amount of

precipitation but is full of swamps and due to the lower evaporation water plays a more important role as weathering agent. It is therefore a combination of different factors that make water an efficient weathering agent. Precipitation is important for the leaching of for example Na, K, Mg and Ca in humid regions. If the precipitation is greater than the evaporation, there will be a movement of solutions and therefore a removal of weathered products. If evaporation exceeds precipitation there will be an upward movement of water, drying out of soils, crystallization of salts and a lack of removal of weathered products. This could lead to stronger mechanical weathering in dry areas.

Temperature can be a crucial factor for weathering too. The annual temperature range can be significant for mechanical weathering due to the phase change of water from liquid to solid which leads to a volume increase of 11 %. Also for chemical weathering, the temperature is important. It is expected that a temperature change of 10 °C leads to a doubling or trebling of chemical reactions. The biological activity will also increase. An opposite effect has an increase of temperature on CO_2, it will be less soluble at higher temperature. This is particularly important for the weathering of calcite. Its solubility depends on the solubility of CO_2 and is less at higher temperatures. The silicate rocks have an increasing solubility with increasing temperature.

2.2.2. Frost

Frost weathering is a very important mechanical weathering process. It is most effective if there is a frequent alternation between freeze and thaw, together with an abundance of water. This has the strongest weakening effect on rocks. The effectiveness of frost is therefore dependent on the frequency of temperature fluctuations and of course the amount of water.

2.2.3. Aspect

Aspect describes the orientation of a mountainside. In the northern hemisphere a south facing mountain slope has a higher frequency of freeze and thaw cycles than a north facing slope due to longer sun exposure. Therefore the mechanical weathering rate will be higher. The biological weathering should also be stronger on south facing slopes because of more vegetation (sun light availability), therefore more root wedging. The higher temperatures on

the southward facing slope in combination with fresh water will increase the chemical weathering as well.

2.2.4. Atmospheric pollution

Atmospheric pollution can play an important role in industrial areas with a high amount of released SO_X, NO_X, CO_2 and other gases. These will produce acidic rain which reacts especially with limestone. Since the world is highly industrialized, the problem of atmospheric pollution is today stronger than pre-industrial revolution. The acidity of precipitation in Norway has also increased due to the air pollution from the industrial centers in Europe like Germany, France, Poland etc.

2.3. Mineral weathering

The chemical composition of rocks is not the only factor influencing weatherability since different minerals with the same composition can have different weathering rates. Two examples are calcite and aragonite. Both have an identical chemical composition ($CaCO_3$) but they have different crystal structure and because of this difference, aragonite is ten times more soluble than calcite. Next to its chemical composition and structure there are other factors which are controlling the weatherability, each of which is discussed below.

2.3.1. Crystal size

The size of mineral crystals can be important for weathering. Large crystals weather much slower than smaller ones. This is due to the so called surface activity. Many small minerals grains have altogether a much bigger reaction surface then one big mineral.

2.3.2. Crystal shape

The shape of crystals can be very different and depending on the shape, the weatherability will also vary. A platy crystal is in comparison with a chunky one easier to weather. That is because larger parts of the crystal are closer to a crystal face and that means also closer to a weathering surface. Another factor influencing the weatherability is the mineral cleavage. These are crystallographic structure planes on which crystals preferentially split. This leads to a weakening of the crystal. Minerals can have micro fractures which increasing the

reaction surface for chemical weathering and which make it possible for water to enter and break down the mineral. For effective chemical weathering, the micro fractures have to be wide enough so water can run through. The minimum width of a crack for water to flow is $8*10^{-3}$ mm which is the double amount than the maximum thickness of adhesive water on cracks (Hölting and Coldewey 2008)

2.3.3. Crystal perfection

The weathering ability of every single crystal is affected by the position of every single atom in the crystal lattice. A perfectly shaped crystal is harder to weather because all atoms are in perfect position in the lattice. They are kept place because of strong bonding and therefore do not react easily with the weathering agent. If there are defects in the lattice or impurities and substitutions, the weathering can affect the crystal much easier and weathering will always start to dissolve a crystal at these points. The weakest bonds can be found on the crystal surface and the edges, here the weathering will start.

2.3.4. Access for weathering agents and removal of weathering products

The accessibility for weathering agents on a mineral crystal will affect the weathering rate. In porous rocks where water can reach and attack all grains, the weathering will be more effective than in a massive chunk of rock. As mentioned earlier, one of the most important factors for weathering is an open system behavior. This means transport of solutes by water ensuring that the rock/water ratio will not reach equilibrium and stop reacting. If a constant removal of dissolved material is taking place and a permanent supply with fresh water happens, weathering will be active.

2.4. Weathering of rock forming minerals

The following minerals are some of the most abundant minerals on earth. I chose only the once which are important for my thesis.

2.4.1. Feldspar

The main rock type in the field area is anorthosite. The anorthosite has a high concentration of plagioclase which is a mineral of the feldspar group. Feldspar weathering is therefore important in the area and provides the most parent material for the production of secondary minerals.

The two main feldspar series are orthoclase $(K,Na)AlSi_3O_8$ and plagioclase $(Na,Ca)Al(Al,Si)Si_2O_8$. Feldspar can be found in most igneous and metamorphic rocks. The feldspars are less weathering resistant than quartz, due to their cleavages. The members of the feldspar group, have different weathering rates. Ca-rich plagioclase will weather faster than Na-rich plagioclase. If the weathering is very effective, kaolinite will be the main secondary clay mineral produced. The dominant plagioclase type on Eldsfjellet, based on the major element composition results, is a Ca-rich plagioclase.

2.4.2. Pyroxene

The minerals of the pyroxene group have a silicate tetrahedral structure, which is organized in a chain-like manner. Therefore they have a good cleavage and weather easily. The most common member is augite which is found in intermediate and basic rocks. Augite weathers through ion exchange and lattice alteration and will produce clay minerals. The main types of pyroxene found in the thin section of rock samples from the field area are orthopyroxene and clinopyroxene (see section 4.1.1.).

2.5. Clay minerals

Clay minerals are usually an important part of the weathering chain. They are secondary minerals, which are the products of rock alteration, notably from phyllosilicates and feldspars. Since it is possible to determine the source rock based on the different types of

clay minerals which are produced, they are very helpful to define the rock composition of the bedrock in the area.

2.5.1. Structures of clay minerals

Clays are usually very fine grained and incorporated with common minerals and sometimes amorphous colloids. The basic structure is a simple Si-O tetrahedral layer which never occurs in isolation. Sometimes atoms of other elements substitute for silicon in the structure.

Another important atomic layer, called octahedral, consists of aluminum and oxygen or hydroxyl (which is virtually the same size as oxygen) (Ollier, 1984). The basic structure of kaolinite is a silica tetrahedral layer and an alumina octahedral layer arranged together. Kaolinite plays an important role in many industrial purposes. This is a very simple structure and is called a 1:1 clay mineral.

If clay minerals are arranged in two silica layers sandwiching one alumina layer the structure is called 2:1 clay minerals. These structural types include minerals like the mica group minerals, montmorrilonite, smectite and illite (hydrous mica).

2.5.2. Properties of clay minerals

2.5.2.1. Spacing

The unit cell thickness or basal spacing is the distance between successive similar layers. This is characteristic for different minerals, and is used in the X-ray (XRD) identification of clay minerals (Ollier 1984). There is a very wide variation of basal spacing in different clay minerals.

2.5.2.2. Expanding lattice

A special property of some clay minerals is their ability to expand the lattice by absorbing water or other solvents. This happens because water can produce an extra sheet in the clay. The thickness is dependent on the associated cations. An exception is clay minerals with a 1:1 structure; they do not expand except for hydrated halloysite.

The expansion during wetting and the shrinking during drying are important for rock weathering since it will mechanical weakening the rocks around.

2.5.2.3. Water absorption

The water absorption is dependent on the structure of the clay mineral. If a clay mineral is subdivided into, for example fine layers, it has a high ability of absorbing water into its structure. There are three different ways for water to be attached to clays; it can be absorbed on the surface, it can be interlayer water, or it can be attached as hydroxyl water to the crystal lattice (Ollier, 1984).

2.5.2.4. Ion exchange

The bonds in clay minerals are not equally strong everywhere, especially on the edges of clay minerals, weak bonds can be found which connect ions not related to the actual structure. The importance of this depends on the type of minerals and its crystal lattice. In kaolinite the weak bonds are restricted to the edges and their importance is therefore low. In minerals like mica there will also be a substitution with the general structure, therefore ion exchange plays a more important role.

2.5.2.5. Dialysis of clays

Clay minerals act as semi-permeable membranes, and if a fragment of clay mineral is placed in water it will lose some ions into solution, and again gain hydrogen ions to balance the charge (Ollier 1984). This will happen until equilibrium is achieved and is called the Donnan equilibrium.

2.5.3. Weathering of clay minerals

The alteration of clay minerals is possible if the surrounding conditions are changing. When clay minerals weather, their structure becomes more or less entirely destroyed and a new structure is produced. Tropical swamps develop a characteristic clay mineral distribution, where kaolinite minerals can be found on hill slopes and montmorrilonite in the valleys. The type of weathering products that can be produced from weathering of clays is dependent on the parent rocks. For example basalt and similar basic rocks provide plenty of cations and

tend to produce montmorrilonite (Ollier, 1984). Siliceous rocks which have typically more sodium than calcium or magnesium have the tendency to produce kaolinite (Ollier, 1984).

Based on Ollier (1984), divalent ions are effective agents in flocculating otherwise soluble silica and therefore impede desilicification. If there is Ca^{2+} or Mg^{2+}, kaolinite would not be produced, because the kaolinite lattice does not include them. They will be only incorporated in clay minerals other than kaolinite. The monovalent ions K^{+} and Na^{+} do not flocculate silica like the divalent; therefore silica and alkalis are lost during weathering until the silica-alumina ratio of kaolinite is reached. Therefore alkali-rich rocks are predisposed to weather to kaolinite (Ollier 1984).

2.6. Corona textures

Corona textures can be found in significant amount on the Lindås nappe and locally the Jotun nappe. They are typical features of medium to high pressure amphibolite and granulite facies metamorphism (de Haas et al. 2002) (Fig. 10). Dam et al. (1995) propose a production temperature of 825°C in gabbro and therefore regards them to cooling-related phenomena.

A typical example of corona textures is a plagioclase-olivine corona with an inner shell made of orthopyroxene surrounded by olivine, which is rimmed by clinopyroxene and/or amphibole (Fig. 11). Sometimes the outermost shell can consist of garnet (as it is the case for Eldsfjellet corona textures). In these structures orthopyroxene minerals grow at the expense of olivine (de Haas et al. 2002).

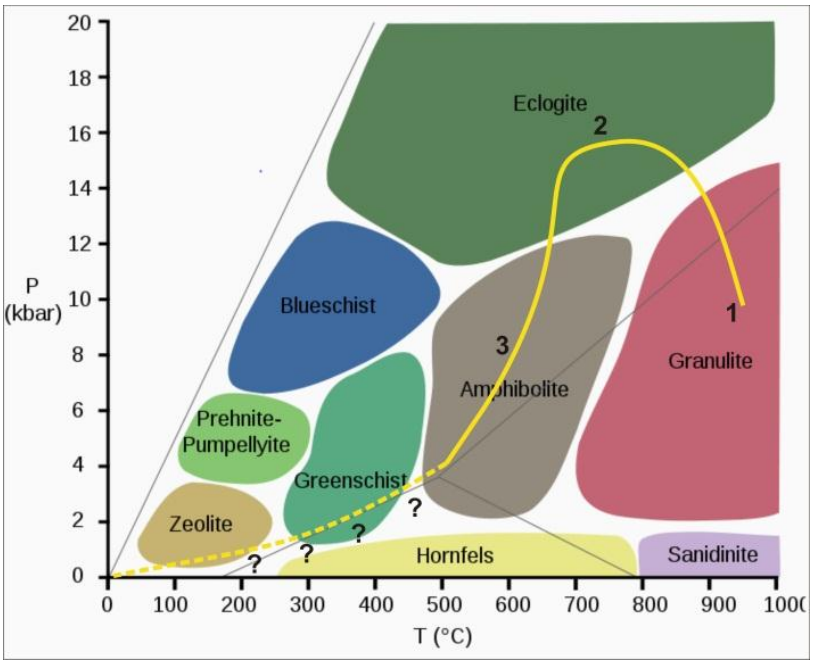

Figure 10: This P-T diagram shows the different metamorphic facies, marked with a yellow line are the expected metamorphic stages of the Eldsfjellet area (source: Wikipeadia).

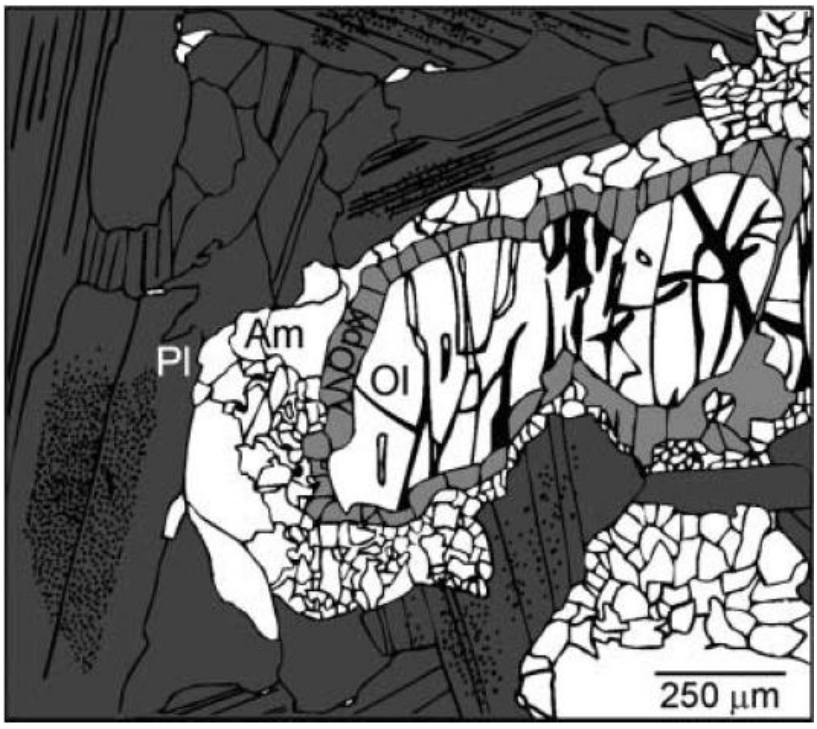

Figure 11: An example of a corona texture, Ol=olivine, OPX=orthopyroxene, Am=amphibole and Pl=plagioclase (de Haas et al. 2002).

De Haas et al. (2002) states that the development of corona textures in gabbroic rocks is due to interaction of the crystalised face with late stage magmatic liquids and finally fluids. There is a strong interaction between minerals of the different shells. Also important are liquids filling the micro cracks in the coronas which then lead to new mineral production due to the supply of different elements. Since the Eldsfjellet geology includes gabbroic anorthosites and anorthositic gabbro it can be assumed that a similar process has occurred here.

Weathering depends on many different factors including climate variations, amount of precipitation, vegetation, tectonic activities and crystal structures. It is not possible to strictly divide into two major modes of weathering. Both chemical and mechanical weathering works together in the weakening of rocks. Often climate conditions in the local area are the tip on the scale to favour one of them. Whereas mechanical weathering is more dominant in nival and aride climate zones, chemical weathering is more dominant in tropical and humid climate zones. In temperate climate, both processes are relevant and the dominance of either mechanical or chemical weathering is dependent on the seasons.

3. Methodology

In this chapter the focus will be on the different methods used to collect samples, process them and gain results. The methods used are very important and are dependent on the type of samples and even on the chemical composition of samples. An unsuitable technique can lead to incorrect results.

3.1. Fieldwork techniques

During fieldwork several methods were used to collect rock samples, water samples and sediment samples.

3.1.1. Drilling

A BT45 rock drill (Fig. 12) was used for taking bedrock core samples from different locations in the field area.

Figure 12: Picture of a Stihl Bt45. (source: http://www.westauction.com/user_images/2999267.jpg)

The drill was used with a core drill adapter to collect core samples. The core drill adapter had a valve to support the coring with water to reduce the wear and tear of the diamond coated saw cylinder. The drill adapter was coupled with a coring device (diameter 4.2 cm). During

the drilling a permanent supply with fresh water was given to prevent the core drill bit from overheating. The maximum length of the bit was 20 cm, but a core of this length was never collected during field work because of cracks and stress zones which led to breakage of the rock core while drilling.

Figure 13: Shows a whole HTH sediment corer (Renberg 1991).

3.1.2. HTH sediment corer

For the sediment coring, a HTH devise (Fig. 13) was used. This is a so called gravity corer. All metal parts such as weight, frame and the closing mechanism are made of stainless steel, all other parts of polyoxymethylene plastic (POM) (Renberg 2008). This makes cleaning of this corer simple and reduces the contamination of samples with metals from the coring device. During the fieldwork a version with 90/86 mm tubes and a length of 50 cm was used. The sub-sampling of the core was managed by using an extruding device of the HON-Kajak corer (Renberg 1991).

The whole extruding device consists of different parts. The first part is the piston which is constructed out of polyethylene, it is partly hollow with a rubber ring to seal it properly so no sediments can escape. The piston is constructed of the lighter polyethylene so it floats in case it gets dropped in the water. The second part is the threaded rod which is built exactly for this type of device. The core tube draws down exactly 5 mm when the extruder head is turned 360° clockwise and 2.5 mm when turned 180°. The third part is the extruder head which consists of two pieces, the upper stationary piece consisting of a large stainless steel hose clamp which holds the core tube in position. The other part is the lower rotatable piece. These two pieces are attached to each other using two guiding pins that move freely in an incision on the stationary piece (Renberg 2008). The fourth piece is the foot plate which is used for taking out sediment samples from the core afterwards. The core can be mounted on the foot plate and stand free. The sectioning tray is a very useful tool for collecting amounts of the sediment samples. It can be put on the tube and then slices of sediment in chosen thickness can be scraped off and bagged. The whole sediment coring process is fast. The whole device

is brought down on a wire to the lake bottom and then dropped there. Due to the weight of the device it will sink down into the sediment. When the device is pulled up again the sediment will be kept in the tube. It is Important that the second person puts the piston on the core while it is in the water so the sediments do not escape.

3.1.3. Water samples

The water samples from the area were collected in order to measure concentrations of dissolved elements. Samples were therefore taken from different puddles in the area. This was done because of higher concentrations of dissolved minerals in puddles compare to running surface water. Laboratory plastic bottles with a volume of 250 ml were used for sampling. After the samples were taken, the bottles were stored at 4 °C to prevent chemical reactions in the water. Soon after the field sampling, the water samples were filtered using syringes with small filter on top to remove the particulate matter. The last preparation stage before further storage was to add 2% HNO_3 to the water samples.

3.2. Laboratory methodology

Several different analytical techniques were used for chemical analyses of the rock, sediment and water samples. Different techniques and preparations will be now explained briefly.

3.2.1. Rock sample preparation

3.2.1.1. Grinding of sample material

After the rock samples were collected in the field area, different preparation procedures were performed in the laboratory. The first step was to grind rock samples down to powder size. This is necessary to produce glass disks to analyse the bulk rock composition. There are several machines at the Department of Geology, which can be used for this purpose. Since it is necessary to know the chemical composition of rocks, mills which use metal plates for grinding down the samples are not suitable for this use. The risk of sample contamination with Fe is high. Therefore two different agate mills were used. A large one from Tesch Siebtechnick was used, which needed a minimum sample amount of approximately 100 g. In

most cases there was not enough material to use the large agate mill. For smaller sample sizes, the agate mill from Retsch (PM100) (Fig. 14) was used. Here it was possible to grind down small amounts (down to a few grams) of sample material. Both machines use the same technique. The machine is filled with an agate ring and a so called puck (large agate mill) or with several small agate balls (small agate mill). The sample, which consists of coarse grained material, will be equally distributed between the agate rings/balls. After the distribution is finished, the machine rotates and the rings/balls will grind down the sample. The length of time necessary for this varies and depends on the hardness of the sample. The large mill usually uses 8 minutes to grind down the samples to powder size, the small mill can take several hours for pulverising the sample. A problem with the small mill is a low efficiency due to the agate balls which can get stuck, preventing them from grinding. A problem with the large mill is the sample distribution; if the sample material is distributed unevenly it can destroy the ring or the puck in the machine.

Figure 14: The Retsch PM 100 agate mill (using agate balls) (source: http://www.unb.ca/fredericton/science/chem/smcgrady/hrl/images/Equipment/Retsch-PM100-Ballmill.jpg)

3.2.1.2. Ignition of rock samples

Before the rock samples can be analysed, they need to be ignited to determine the LOI (loss on ignition). The LOI is important to obtain information about the organic content of the samples and also the loss of volatile elements.

The rock powder was heated up to 1000 °C in a Carbolite ELF 11/14B muffle furnace for two hours. The sample material was weighed before and after ignition. The weight difference represents the loss of organics, volatile compounds and water from the sample. The rock samples show, as expected, a much lower LOI compared to the organic rich lake sediment samples from the catchment lake.

3.2.1.3. Chemical digestion of samples for analysis of trace elements and rare earth elements

Chemical digestion is used to prepare rock samples for further geochemical analysis using ICP-MS. Chemical digestion is a process which takes, depending on the composition of the rock sample, several days to weeks. During this master thesis 8 samples were prepared using this technique to determine the REE and trace element composition. First the sample had to be ground down to powder size, afterwards the samples were weighted to almost exactly 0,100000 g to ensure precise results later during the analysis. After the weighing, the samples were stored in labeled Teflon containers. In the next step acid digestion was used, concentrated HNO_3 were added to the samples and the mixtures were boiled at ca. 135 °C for several hours. It is important to keep the containers closed so that no acid can escape. Following this, the samples were fumed at 135 °C so that the concentrated HNO_3 could escape. It is important to avoid complete drydown. In the next step concentrated hydrofluoric acid was added to the samples before they were boiled for several hours. It is necessary to check if there are still particles in the solution. After that step, the acid was evaporated again. Since there were still particles in the solution, an aqua regia solution was prepared by mixing 2 parts concentrated HNO_3 with 3 parts concentrated HCl. The steps are the same as described above. After the whole sample is dissolved in the solution and the acid is evaporated again, the sample is added 4 ml HNO_3 (2%) and boiled again so everything is dissolved. Afterwards 45 ml HNO_3 (2%) was added to get a specific concentration for the analyses.

3.2.1.4. Preparation of glass disks for XRF

The ground and ignited samples were used for preparing glass disks for XRF analysis. First 0.96 g of the sample powder was mixed with 6.72 g lithium tetraborate. The lithium tetraborate is used as a flux to reduce the melting temperature and melting time of the sample material. Afterwards the mixed powder was put into platinum cups and mounted in the melting facility (Claisse, model fluxy). The cups are mounted on top of gas torches. On top of the cups is a container mounted which collects the molten material for cooling and producing the disk shaped glass tablets. The process is fully automatic and takes about 30 min for three glass disks. The cups rotate on top of the gas torch so that the whole material in the cups will be equally heated. After the material is melted, the machine drops it into the container. The disadvantage is that only one program is possible to use. That means if there are rocks with many volatile elements the resulting values may not be representative for the volatiles.

3.2.2. Sediment sample preparation

The preparation of lacustrine sediment samples is quite similar to the rock sample preparation. First the samples were dried at 50 °C for a day to reduce the amount of water in the sediments. Afterwards the samples were ignited and glass tablets prepared.

3.2.3. Preparation of water samples

The water samples were filtered using a syringe with a small filter and 50 ml was taken from the 250 ml of sample water. These samples were added ultrapure 2 % HNO_3 to reduce the reactions in the water. Alkalinity and pH were measured shortly after sample collection and water samples were bottled especially for anion analysis and nutrient analysis. Afterwards the preparation the water was stored at 4 °C.

3.3. Geochemical analysis

3.3.1. X-ray fluorescence spectroscopy

X-ray fluorescence is a nondestructive technique for analysis of element composition. The samples are irradiated by a strong X-ray beam which leads to emission of X-rays. These X-rays can be measured using an energy dispersive or a wavelength dispersive detector. Energies or wavelengths make it possible to detect which elements are present in the samples. The intensity of these characteristic X-rays give information about the abundance of different elements. A common analysis range of elements is between sodium and uranium.

First the source X-rays are produced inside a tube by freeing electrons due to a high electron voltage energy. Then the X-rays are accelerated towards a metal target (anode). When they hit the metal target X-rays are produced. These x-rays are directed towards the sample were they interact or exchange with electrons in the atoms of the sample. This leads to a release of X-rays from the samples, which are characteristic for the different elements and can be measured in the tube.

3.3.2. ICP-MS

ICP-MS stands for **i**nductively **c**oupled **p**lasma **m**ass **s**pectrometer. The instrument used was a Thermo Finnigan Element 2 (Fig. 15). It is used for trace element analysis in the ppm and ppb range. The ICP-MS can be used to analyse solution samples, but also solid samples with laser ablation technique, which facilitates dating of accessory like U-Th-Pb.

Figure 15: Thermo Finnigan Element 2 with solution autosampler (Foto: source BGF)

The system is built in a manner known as Nier-Johnson geometry. There are two different approaches, both based on the same principle. They consist of two analysers, a "traditional" electromagnet and an electron analyzer (ESA). In the standard version the ESA is positioned before the electromagnet and in the reverse design it is positioned behind the electromagnet (Fig. 16) (Thomas 2001).

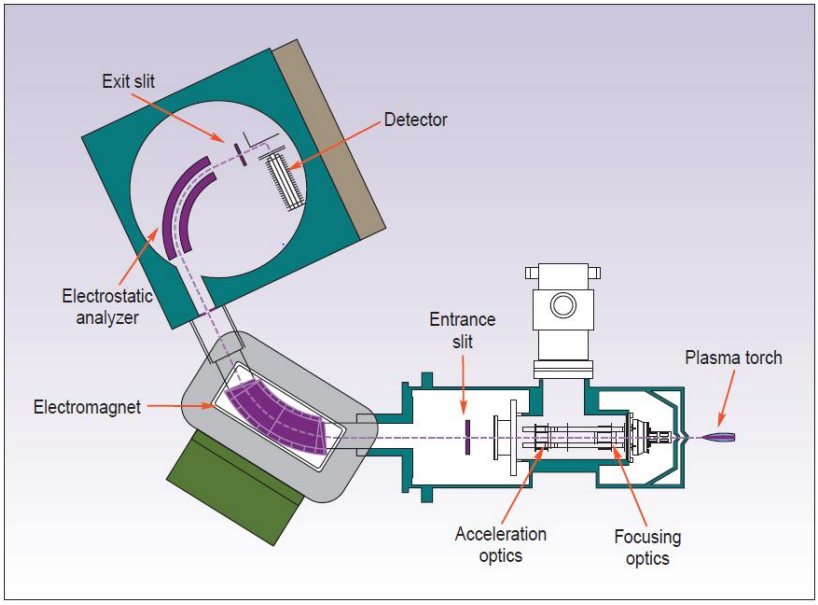

Figure 16: A schematic of a reverse Nier-Johnson double-focusing magnetic-sector mass spectrometer (from Thomas 2001).

The ions will be sampled from the plasma by accelerating them into the ion optic region up to a few kilovolts before they enter the mass analyzer (Thomas 2001). A magnetic field is

dispersive only for ions and mass, all ions with diverging angles will be focused to the entrance slit. After that the ESA (which is only dispersive for ion energy) will focus them to the exit slit into the detector (Fig. 17). In the detector is a possibility that the energy dispersion of the magnet and the ESA are having the same magnitude but opposite directions, in this case they will focus both ion angles (first focusing) and ion energy (second or double focusing) (Thomas 2001). The electric field will be changed to the opposite direction to the field strength of the magnet during the cycle time of the magnet which has the effect that the mass is stopped for detection. If a certain magnet field strength is reached, it turns back to the original values and the next mass becomes frozen (Thomas 2001). The used voltage can be fixed by the operator of the machine which makes it possible to only measure the peaks of interest. This is very helpful if trace element analyses are processed regularly, because it saves detection time. The quantification of the peaks happens through taking multiple data points over a preset window and integrating it over a fixed time. A full mass scan takes between 400-500 ms which is long compared to quadrupole technique which takes 100 ms. It also takes much longer for the magnet to measure (30-50 ms) compared to 1-2 ms for quadrupole (Thomas 2001). This difference in analysis speed compared to the quadrupole based ICP-MS makes the system much less effective for routine analyzes of samples. The data resolution is depends on the width of the slits used in the machine, the wider the slits, the lower the resolution. Therefore a change in the slit entrance and exit width will affect the resolution (Fig. 17). It is important to note is that with increasing resolution, the transmission will decrease. At a resolving power, the transmission will be 100 %, but at a resolving power of 10.000 only ca. 2 % transmission will be achievable (Thomas 2001).

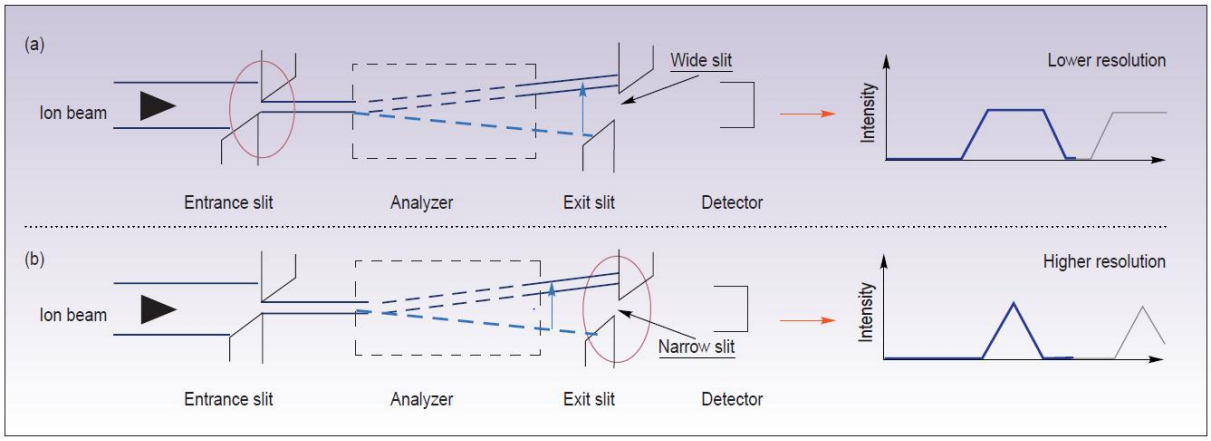

Figure 17: The scheme shows the same installation with different width of the exit slit and the differences in resolution. Installation A has a wide slit and a flat peak which shows low resolution. Installation B has a narrow exit slit and a triangular peak and shows high resolution (Thomas 2001).

Another advantage of this technique is a high sensitivity of typically 100-200 million counts per second (mcps) per ppm while the background levels from dark current noises are very low and typically only in a range of 0.1-0.2 cps. A quadrupole only has a sensitivity of 10-50 mcps and background levels in a range of ca. 10 cps. This makes it possible to determine elements which would be not possible to identify like the polyatomic interference of $^{40}Ar^{16}O$ and ^{56}Fe. The results of the measurements are mostly in a range of 0.01-0.05 % (RSD = relative standard deviation) at low-resolution mode.

3.3.3. ICP-OES

This instrument is used for trace element analysis (ppm) and major element analysis (wt%) on solution samples. The machine used at the University of Bergen is a Thermo Elemental Iris (Fig. 18).

Figure 18: Picture of the ICP-OES (Source: BGF).

The method uses emission of light. Samples will be dissociated in a coupled plasma source into their constituent atoms or ions. They become excited until they emit light in their specific wavelength. The light intensity is measured by a detector and used to calculate the concentration of the element. The temperatures reached are approximately 10.000 °C which atomizes also the most refractory elements to a high degree. The detection limit is therefore in range of 1-10 ppb. The simultaneous ICP technique is, compared to other techniques, very fast. The RSD for this type of technique is good, the short term precision is between 0.1-2 % and over a longer period of hours it will be between 1-5 %. In the simultaneous spectrometer the precision will be better than in the sequential spectrometer. The use of internal standards increases the precision of measurements. The risk for spectral interference problems is minimal. Background effects exist and it is therefore necessary to use background correction techniques. OH from the water solvent can lead to peak or band structures. This risk can be minimized by careful selection of plasma conditions or moving to an unaffected analyte line. Due to physical effects such as viscosity and surface tension in the spray chamber it is important to use internal standards to minimize these problems.

3.3.4. Polarized light microscopy

The basic installation of a polarized light microscope is the same as a normal microscope; the only difference is the polarizer. Light is usually “vibrating”, this means the waves are not concentrated in one direction. A polarizer is focusing the otherwise circular polarized light in a linear polarized light. In the polarizer the light can only pass through on their polarizing axis. In these filters are particles which absorb the light going in their direction so only the light which is going in a straight line will reach the microscope stage. If this filter is in an angle of exactly 90° it will absorb all light.

The system consists of two parts, the polarizer which is directly under the stage and fixed to a left-right or east-west position and the analyzer which is mounted above the stage and fixed in a north-south position. This part can be slit in and out from the path of the source light. If the light is turned on under the microscopy stage it will go through the polarizer under the stage were light moving East-West will only be able to move through. If the analyzer is active, the light can only go through North-East, but since it was before forced to go east-west, no light will be visible, that is called a crossed polarization. Since the light from the source has to go first through the polarizer and the sample, the direction of light will be changed. Crystals have their specific structures and angles which make it possible for light to go through in the specific angle. If the angle is right, the light can pass. Since the angle of the light is now different, light will not be blocked completely anymore and the crystals will be visible in their specific light spectrum.

The microscope used for analyzing thin section is a Nikon Eclipse LV100PDL. The thin sections were prepared at the Independent Petrograph Service in the UK.

3.3.5. SEM-scanning electron microscope

The difference between a normal microscope, which uses light as a source for creating a picture, is that a SEM uses electrons to create a picture. SEM have many advantages compared to normal light microscopes, the specimens which can be investigated are much more variable. Since SEM works with electromagnets and not lenses, the magnification of samples can be controlled in a much finer way (http://www.purdue.edu/rem/rs/sem.htm).

The depth of magnification is much higher than under a common microscope and the quality of the pictures is better too.

An electron beam is produced by an electron gun. The beam follows a vertical path down through the microscope which has a vacuum inside. Lenses and electromagnetic fields focus the beam until it hits the samples which start to emit X-rays and electrons. A detector is collecting the back-scattered electrons, X-rays and secondary electrons and transforms them into a signal which will be send to a screen as an image.

3.4. Evaluation of measurement precision

To evaluate the quality of measurements, different standards of known reference values were used. The standards used have values which are internationally used. They have similar reference values all over the world. The values of standards are constantly revised with the latest laboratory technology and updated on web pages like GeoReM (Max Planck Institute at University of Mainz, Germany) to compare with the most precise standard value data. To evaluate the measurements of samples, the precision of the laboratory equipment must be evaluated. For this, the measured values of standards are compared with the GeoReM data base from Max Planck Institute (MPI) at the University of Mainz (Germany) (http://georem.mpch-mainz.gwdg.de/) (Tab. 1)

Table 1: Comparison of standard values measured at the Department of Earth Science (UiB) with values from the MPI. The yellow marked columns show the average BCR-2 values measured at the Department of Earth Science in comparison with the latest values from MPI. The deviation is given in per cent. The green marked columns show the values for the GSP-1 standard measured at the Department of Earth Science and the MPI, respectively.

values in weight %	Na_2O	MgO	Al_2O_3	SiO_2	P_2O_5	K_2O	CaO	TiO_2	MnO	Fe_2O_3
BCR-2 average	3,2	3,6	13,4	54,8	0,4	1,8	7,1	2,3	0,20	13,9
standard MPI	3,2	3,6	13,5	54,1	0,4	1,8	7,1	2,3	0,20	13,8
% deviation	0,9	-0,4	-0,9	1,4	3,6	-0,1	-0,2	3,7	0,00	1,1
GSP-1 average	2,8	1,0	15,1	68,2	0,3	5,5	2,0	0,7	0,04	4,3
standard MPI	2,8	1,0	15,1	67,2	0,3	5,5	2,1	0,7	0,04	4,3
% deviation	-1,6	3,7	-0,2	1,4	1,8	0,0	-2,8	2,7	0,00	-0,3

4.

The table shows values of XRF standards (for major elements) which were used for analysing the major element composition of glass disks from different samples. The standards used are W-2 and BCR2. The measured values and the standard values from MPI show a maximum error of 3.8 % and is in agreement between standards measured at the Department of Earth

Science and the once from MPI, therefore it can be expected that sample results are trustworthy. This procedure was done for all the laboratory measurements by comparison with their associated standard values. It has been used for standard values of ICP-MS, ICP-OES, XRF and different techniques for analysing water samples. The uncertainties of all comparisons are mostly less than 5%.

3.5. Potential Uncertainties for fieldwork and laboratory methods

During field work and laboratory work different uncertainties be produced because of wrong sample taking, contamination of samples and the use of unsuitable laboratory techniques. In this section, possible pitfalls and errors will be explained.

3.5.1. Pitfalls during field work

During the field work of this thesis, different types of samples were taken. Sample taking in natural environments always has the risk of contamination; therefore the sample taking has to be well planned.

During the drilling of rock cores, water is involved to cool the drill and avoid the risk of damaging the drill. The problem is that the water will also partly remove clay minerals, salt crystals and other sediments from the surface of the drilled samples. Therefore it will not be possible to quantify the amount of these particles and minerals when sampling is done in this manner.

Lake sediment samples were taken to extract sediment for geochemical analysis. The coring process has to be taken out very carefully, if the tube with the sediments inside is not sealed properly, material can get lost or mix, structures can be destroyed and exchange between pore water from different depth can occur. Another potential pitfall is the bagging of sample material, there is a risk of cross-contamination.

3.5.2. Potential uncertainties during laboratory work

Laboratory work can have potential for many different pitfalls, very important is contamination. A laboratory is a clean environment with high precision instruments; small contaminations can lead to large errors in measurements. An important source for pitfalls is

the sample preparation; certain samples have to be treated in a special way to obtain proper results. Very important is a clean environment with sterile weights, clean equipment, clean flasks and containers. Another important factor is to separate samples from each other so sample material does not become cross-contaminated.

Weighing is another potential pitfall, it is crucial to weigh as exactly as possible since the concentrations of elements will be calculated based on the amount of sample material. The more exact the weighing is, the more exact the result will be.

A potential error can be caused by the ignition of samples for example for removal of organics or during melting of glass disks for XRF analysis. The heating of samples can lead to a loss of volatile elements in the sample and might give uncertainties for the volatiles.

Another potential source for errors during sample preparation is during the grinding of sample material, using a jaw crusher to crush rock samples can lead to a contamination with Fe in the sample. The jaw crusher was chosen for crushing since the contamination risk is lower than using a disk mill, since the contact between sample and metal parts in the machine is less long. The same problem can arise during pulverization. To avoid contamination in this step, an agate mill was chosen for grinding the samples.

During chemical digestions, a typical pitfall can be a too short dissolution period. If the sample material is not properly dissolved, particles will be left in the sample and this can produce errors during the measurements of element content and concentrations.

Laboratory measurements have always a high risk for potential errors. A typical source for errors is using a wrong or inaccurate calibration curve and inadequate preparation procedures. To detect potential errors during measurements, standards are run together with the measured sample material. These standards have a known element concentration, by comparison with the derived results from the measurement, the error can be calculated. This bears again a potential source for error since the standards will be always updated and the results will be constantly refined. Using old data for standards can be risky since the new standard data can have significantly different values. To exclude this error, the latest standard values derived by the Max Planck Institute database for reference materials

of geological and environmental interest (http://georem.mpch-mainz.gwdg.de/) were used to combine measured standards with the latest data.

4. Results

In this chapter the results of the different analytical techniques will be presented, evaluated and partly interpreted. The interpretation will be based only on the specific data set. Further interpretation and the link of different data sets will be done in the discussion chapter (chapter 5).

4.1. Rock samples

During the field work altogether 26 rock samples were taken (Fig. 19). The samples were collected in the south-western, southeastern and north-western area of Eldsfjellet.

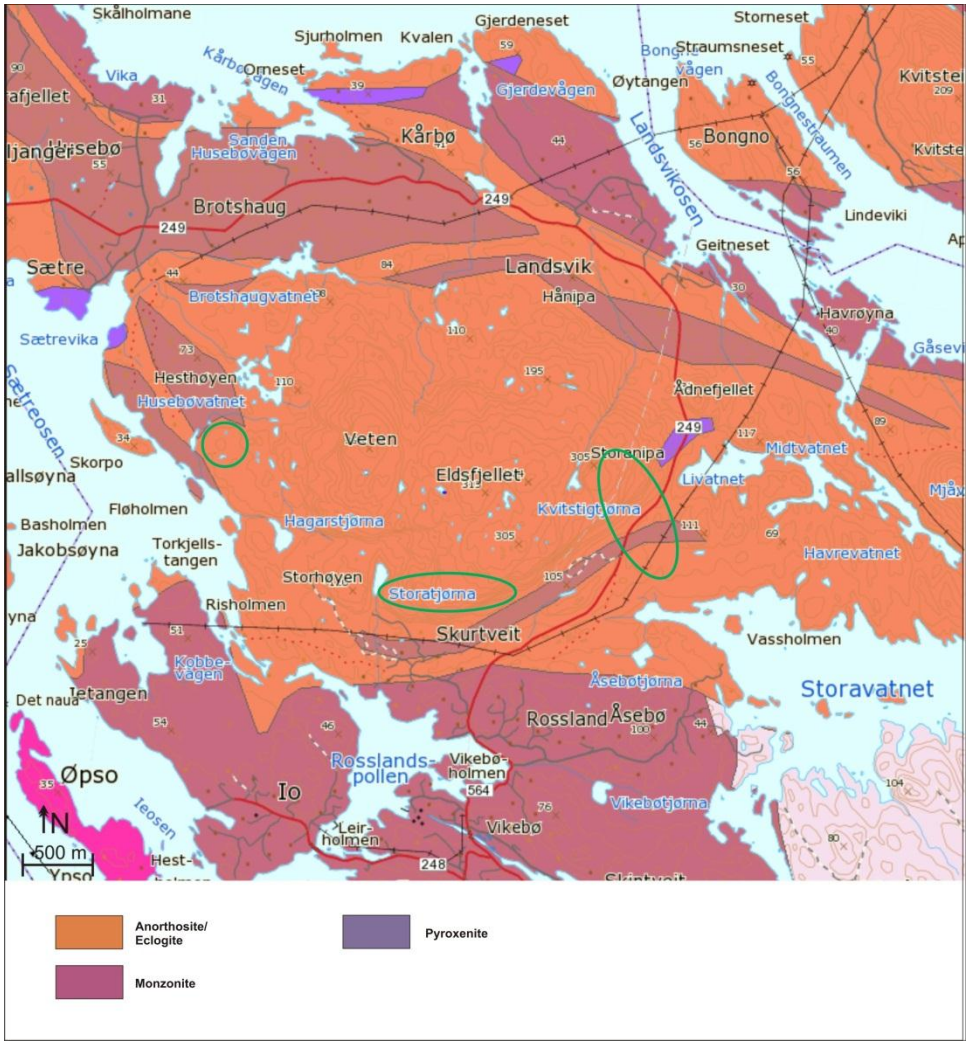

Figure 19: The green circles marking the sampling spots in the field area. They were chosen because of their good accessibility with heavy equipment. Most parts in the north had a vegetation cover or were private property.

Figure 20 shows a rock core from the edge of a corona texture. The left dark part is pyroxene which is the central part of the corona. In the middle is a reddish garnet which produces the rim of the corona texture. In the right part is a whitish anorthosite, partly including garnets and dark mafic minerals. The anorthosite displays the most dominant rock type on Eldsfjellet.

Figure 20: A 7 cm long drilled core from the field area. The sample represents a cut through a corona texture.

4.1.1. Petrography

4.1.1.1. Microscopy

During the laboratory work different rock samples were prepared for microscopy (see methodology chapter 3). The purpose was to classify the different minerals in the rocks and to give them the petrologic correct name. The pictures were taken under linear and cross polarized light to see if there is any extinction visible. In this part of the results chapter, some of the pictures will be described.

4.1.1.2. Interpretation of microscopy pictures

The first thin section (Ef.23.1) (Fig. 21) shows an anorthosite sample. The sample displays fresh rock material from a lower part of a bedrock core. Almost no weathering is visible in the thin section. The figure is divided into two parts. The left picture shows the sample in starting position while the right picture shows the same sample with a changed angle of 60°. This has been done to see the changes in color and the switch of the typical albititic twin in the plagioclase.

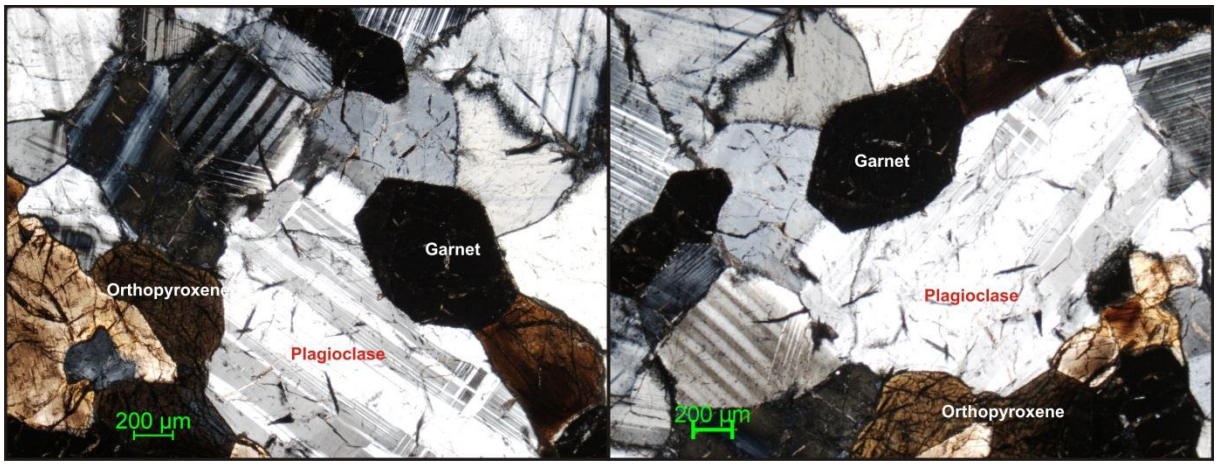

Figure 21: Both thin sections show the same sample, in the right picture the object holder is turned 60°.

There is a high concentration of plagioclase in the sample which is visible in the typical stripes ranging in colour from almost white towards grey and black. A rotation of the sample on the objective table makes other stripes visible. This has to do with crystallographic affects. The plagioclase shows clear signs of weathering on the edge and shows a xenomorphic crystal habitus.

Easy observable are the garnet minerals in the sample; they show a complete mineral extinction and are black at every angle. This is because of their crystal structure which makes garnet always extinct. The garnet in the central part has an almost idiomorphic habitus.

The last visible mineral in the sample is orthopyroxene which has a brownish colour and different extinction with changing angle of the sample, again these minerals show a xenomorphic habitus and can be interpreted as slightly weathered. The mineral combination in the sample, especially the high amount of plagioclase shows that it is an anorthosite.

The next sample (Fig. 22) shows again an anorthosite. Dominant is the plagioclase mineral in the central part of both pictures. Again the samples were rotated approximately 60° on the objective table to see the change in extinction in the sample.

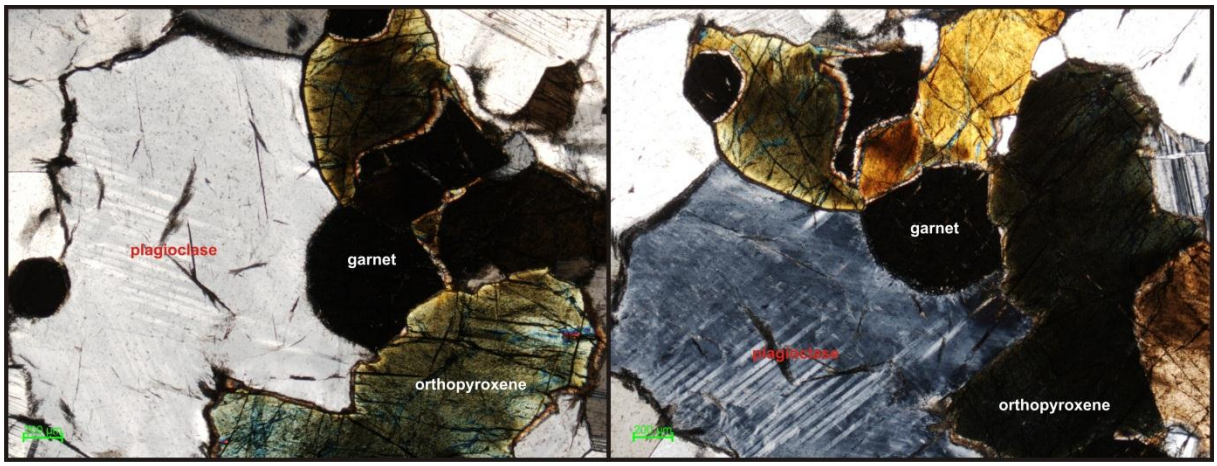

Figure 22: This thin section shows again an anorthosite. The right sample shows the thin section turned 60°. The concentration of orthopyroxene and mica is higher in this thin section.

In the sample shown in Figure 22 the plagioclase is very dominant, a change in colour from light grey in the left picture to bluish grey in the right picture is visible and as in the sample before the typical stripes from the albite twins are observed. This samples shows again a fresh rock sample with almost no weathering features (Orthopyroxene slightly weathered), taken from a lower part in a rock core. Again the plagioclase mineral rims are frayed and show clear weathering features. The habitus of the plagioclase can be classified as xenomorphic.

The thin section in Figure 22 shows again three garnets, a small one in the left and two in the middle-right area. Again they are easy to distinguish because of their total extinction. In this sample the shape of the garnets is hypidiomorphic.

Another dominant mineral in the samples is orthopyroxene with its brownish to brownish-bluish colour. It can be found in the lower right and the upper middle area of the left thin section. It shows weathering features on the rims and can be interpreted as xenomorphic.

The yellow mineral especially visible in the right picture can be interpreted as mica. This is a common mineral in the rocks on Eldsfjellet since types of clay were found which are close related to mica and which have similarities to mica. The sample shows also slight weathering as the samples earlier.

In Figure 23 the thin section shows fine grained minerals in different spectra. A few large minerals are still in the section but they are surrounded by the fine grained minerals. This sample displays weathering and the rim of the different minerals is ragged. This is a sample from an upper part of an rock core which was exposed to weathering.

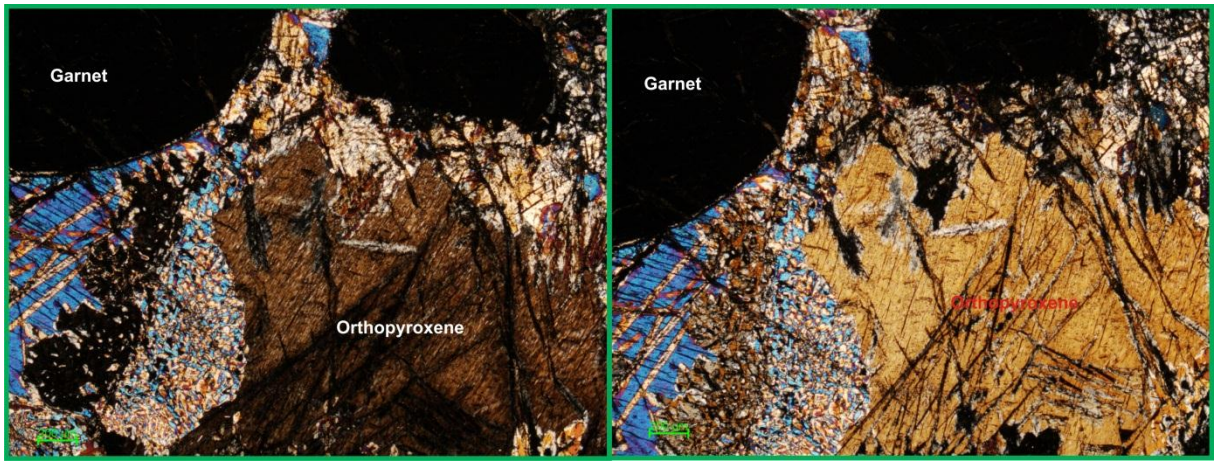

Figure 23: A thin section with strongly weathered material from Eldsfjellet. The bigger minerals are surrounded by strongly altered fine grained minerals.

In the lower central and right area a big brownish orthopyroxene is visible which changes the colour to yellow-brownish (see right picture in Figure 23). The mineral is strongly weathered and shows cracks all over the mineral crossing each other and having a north-south to northeast-southwest trend. The rim of the orthopyroxene is frayed and the mineral has a xenomorphic habitus.

The garnets in the sample are rounded and show no clear typical mineral habitus for a garnet. It shows that the garnets have undergone weathering. Only two garnets can be determined in the thin section, one in the upper left part and one in the upper right part of the thin section.

The larger minerals can be found in a matrix of very fine grained minerals, the wide colour spectra of the small crystals makes it almost impossible to determine single minerals.

A possibility is that the fine grains have their origin from plagioclase. This sample shows a strong degree of weathering.

The thin sections give a good overview of the mineral composition of the field area. It can be seen that the dominant type of rock is anorthosite which also provides the largest amount of rock material for weathering. This is in agreement with other data from the results chapter.

4.1.1.3. Scanning electron microscopy (SEM)

SEM was used for finding micro cracks and weathering structures in the rock samples. For this purpose thin sections were used. The thin sections are cut in a way that they display a sample from the weathered top part into the fresh rock. Of special interest is the part of the thin sections which shows the top part of the sample because weathering will start on the surface between rock and atmosphere. Two thin sections were chosen to show the weathering in the local rocks. The first is shown in Figure 24.

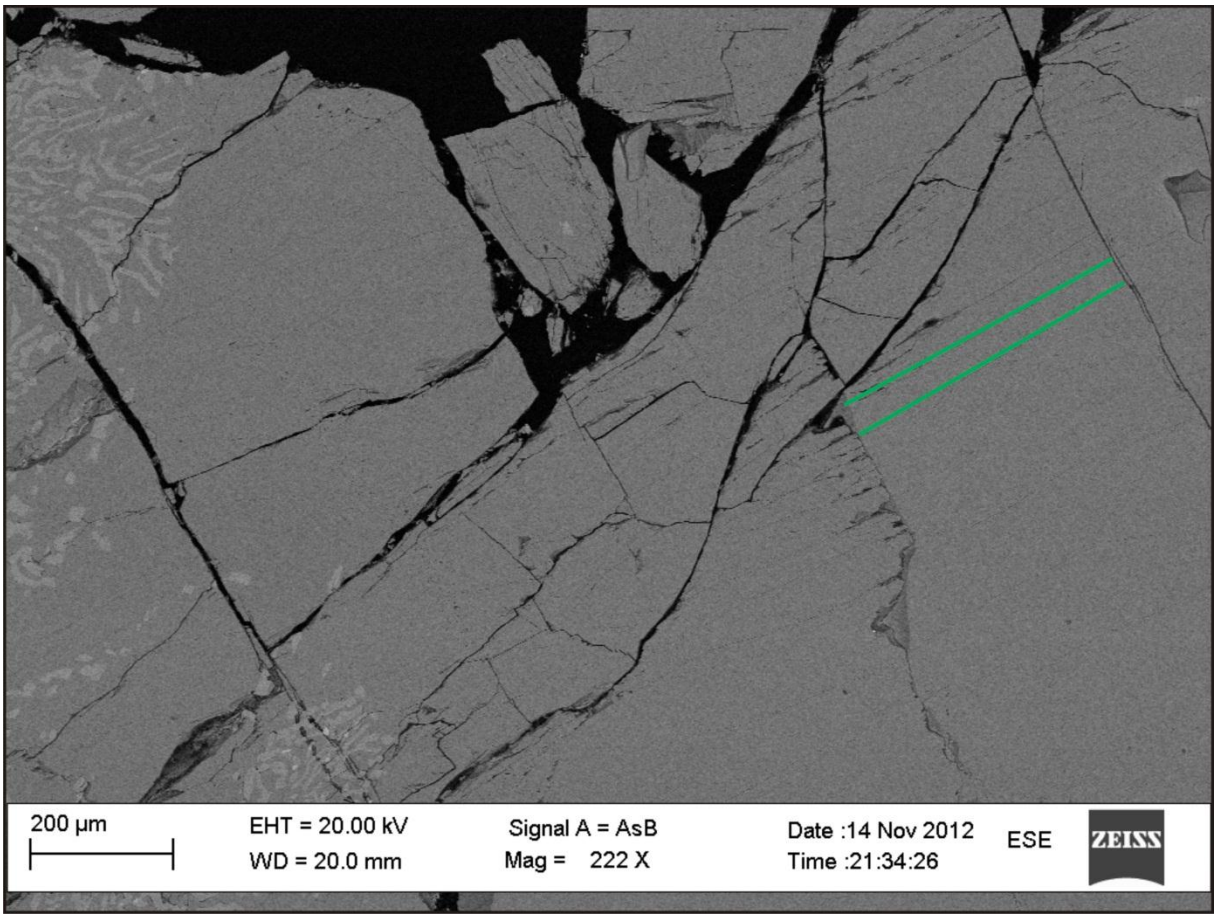

Figure 24: The major rock type in this picture is pyroxene, marked with green are the typical cleavages in a 90° angle. This image Figure shows a weathered surface of a corona texture.

Figure 24 shows the top part of a corona texture. The top part is dominated by pyroxene which is representing the core part of the local corona textures. The cleavages are marked with green lines to make them more visible. Parts of the pyroxene are lose and are already removed from the rock. It can be seen that the weathering is following cracks and the cleavage. In these zones, water can enter and dissolve the minerals. If permanent water supply is given, the weathering can be strong on these mafic minerals. Due to the strong weathering on the corona textures, holes are produced all over the mountain surface (see Figure 34).

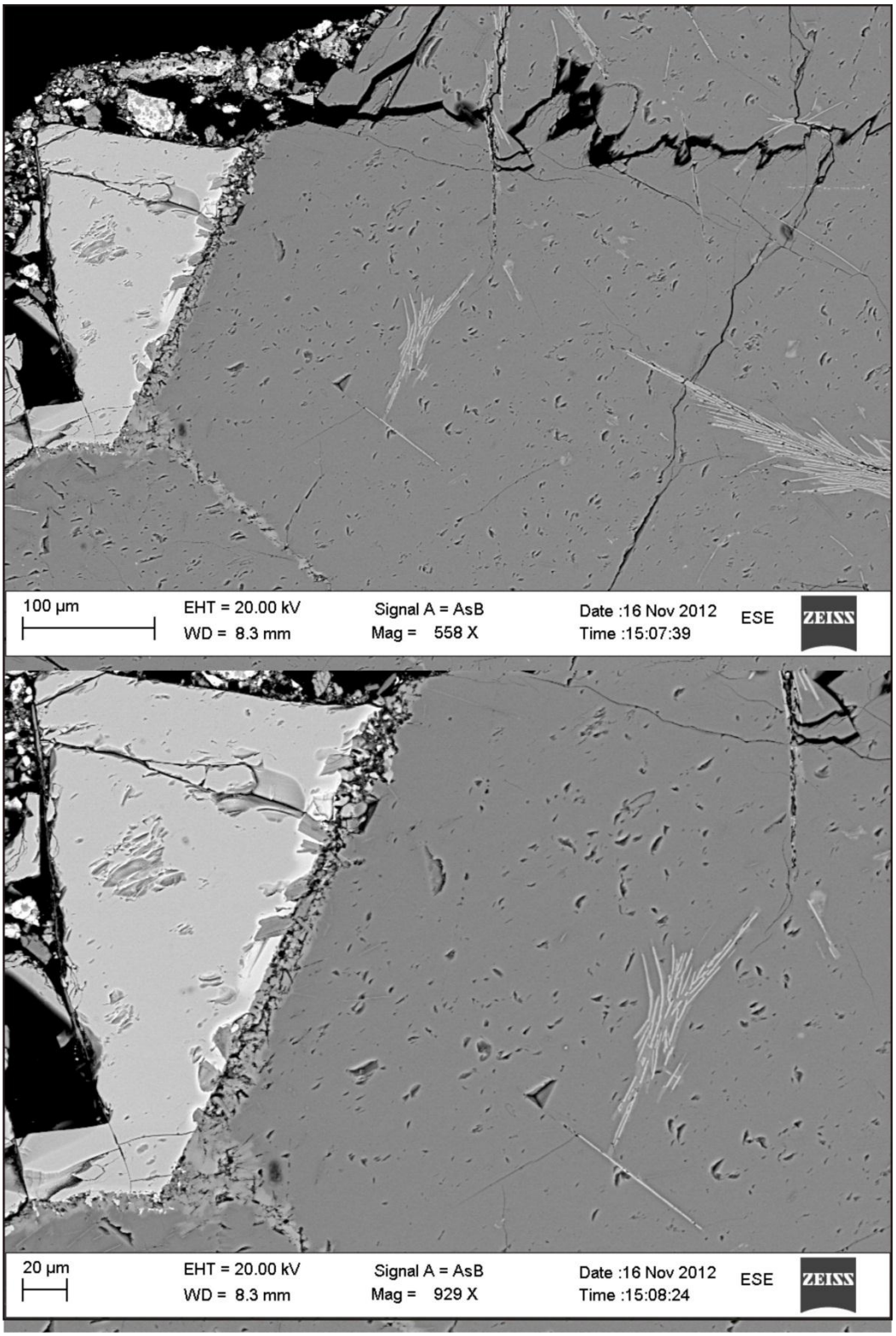

Figure 25: The picture shows parts of a thin section from the surface of a cored rock sample. The light mineral is a garnet and the greyish minerals around it are plagioclase. An open space between both mineral types can be seen which makes it possible for water to enter.

Figure 25 shows two SEM pictures of an anorthosite thin section. These pictures capture the top part. The light mineral is a garnet (Gn) while the darker greyish mineral represents plagioclase (Pc). The upper picture is an overview while the lower picture shows the transition between garnet and plagioclase in more detail. A transition zone between Pc and Gn can be observed. The boundary between both minerals is accessible for water and other fluids. Based on the observations, water can enter the zone between both minerals and dissolve them which lead to a weakening of the bond between both minerals. It can be seen that the minerals them self are not becoming completely dissolved, they are loosen on the mineral interface and fall out from the host rock. During the field work it was possible to find single grains of plagioclase and garnet in sediments which favours the idea of a loose breaking of single minerals from the bed rock. It can be assumed that mechanical processes are also playing an important role. Freeze-thaw weathering can occur on the interface between both minerals and favour the breakdown of bedrock. In the lower picture of Figure 25, free space between both minerals can be seen which leads to the assumption that the garnet mineral will soon fall out from the bedrock.

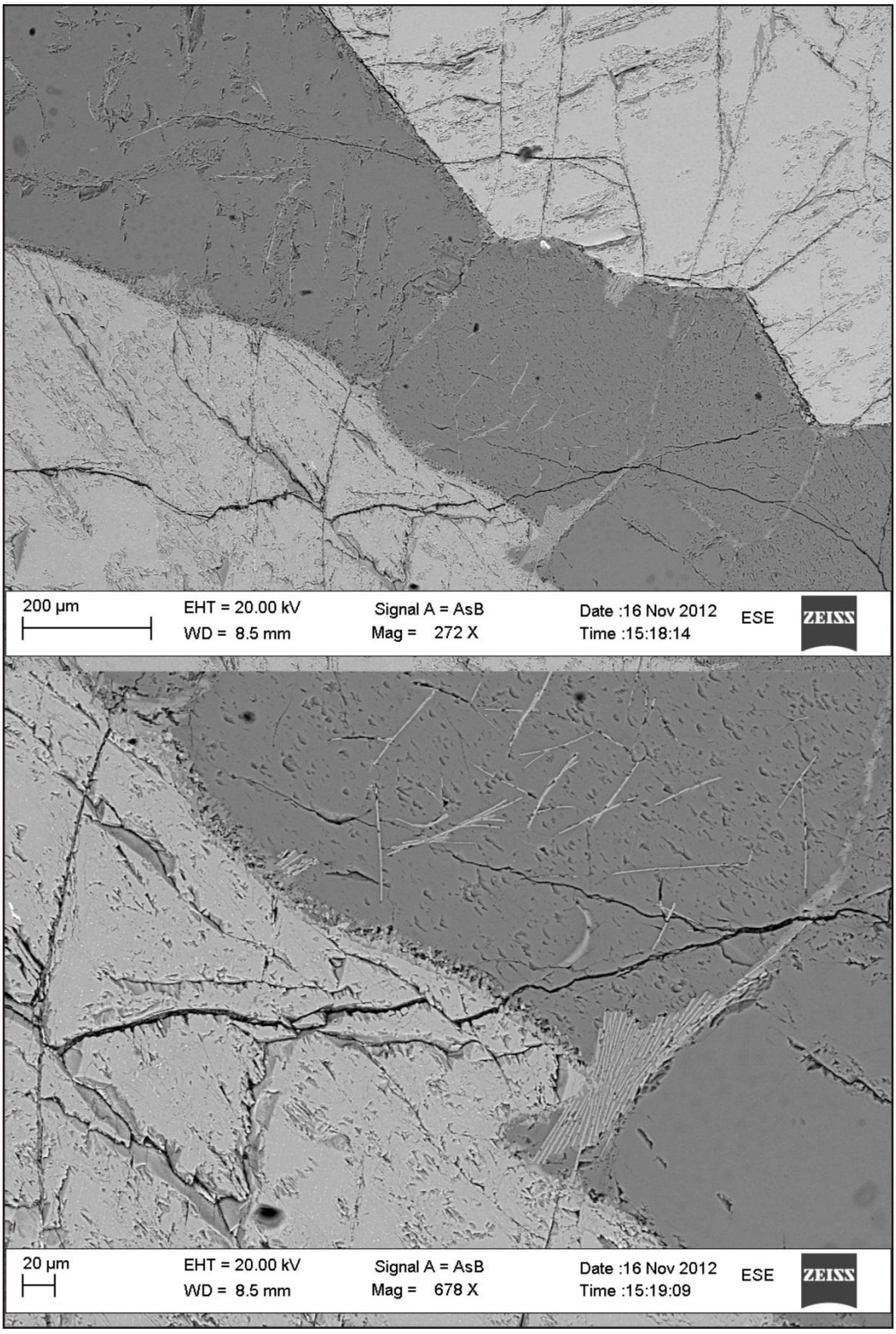

Figure 26: Both pictures show deeper parts of the same thin section in Figure 25. The boundary between garnet and plagioclase is less dominant in the SEM pictures of the rock surface.

Figure 26 shows a deeper part of the same thin section then displayed in Figure 25. The mineral composition is similar. The dominant minerals in the sample are garnet and plagioclase.

The transition between both minerals is less dominant then in the upper part of the thin section. Cracks also exist in the lower part, they can come from cooling processes during uplift or from other stress factors. The interface between both mineral types can still be observed.

Based on the different SEM pictures it can be assumed that chemical weathering is more effective on the upper few millimetres below the surface. Water can easily enter the interfaces and cracks inside the rock and between the different minerals. Dissolution will happen, starting from the interfaces into the different minerals. Mechanical weathering, especially freeze-thaw processes, can have a major influence on the breakdown of the bedrock. The weathering on the surface of the thin section can be observed, but the strength of weathering decreases drastically after a few millimetre. That means the weathering can be described as light in the anorthositic rock bed rock of Eldsfjellet. This is in agreement with other results displayed in the result chapter (chapter 5) of this master thesis.

4.1.2. Geochemical composition

In this section, the results of the geochemical composition of the sample rocks will be displayed.

4.1.2.1. Major element composition of rock samples

During the field work, several rock samples were collected through bedrock coring in the field area (Fig. 19). After processing the samples in the laboratory (for more information see methodology chapter) the major element composition of the samples was measured using XRF. The results of the analysis (Tab. 2) will be shown and interpreted in this chapter. Six different rock samples were taken for geochemical analysis. The decision was based on the mineral composition of the different cores. The major elements were measured as oxides. The measured oxides are: Na_2O, MgO, Al_2O_3, SiO_2, P_2O_5, K_2O, CaO, TiO_2, MnO and Fe_2O_3.

Table 2: Shows the major element composition of different samples from Eldsfjellet. The values are given in weight % of the different oxides.

values in weight %	Na_2O	MgO	Al_2O_3	SiO_2	P_2O_5	K_2O	CaO	TiO_2	MnO	Fe_2O_3
	(%)	(%)	(%)	(%)	(%)	(%)	(%)	(%)	(%)	(%)
EF16	5,5	2,4	27,0	54,1	0,02	0,7	8,2	0,1	0,0	2,4
EF19.1	0,5	14,7	19,0	34,7	0,04	0,1	9,2	0,2	0,2	15,1
EF19.2	0,3	23,6	8,5	49,9	0,02	0,1	2,9	0,2	0,1	15,0
EF19.3	5,0	2,8	27,7	53,1	0,04	0,6	9,1	0,1	0,1	3,4
EF24	1,7	13,7	14,2	47,9	0,04	0,1	13,6	0,3	0,1	10,9

Sample EF.16 has a high concentrations of Al_2O_3 (27 %) and CaO (8, 2 %). It is depleted in MgO and Fe_2O_3. Due to the low concentrations of MgO and Fe_2O_3, which are components in mafic minerals, and the high concentrations of Al_2O_3 and CaO, sample EF16 consists of anorthosite. Anorthosite is the main rock type on Eldsfjellet. They have a high concentration of plagioclase (more than 90 %).

Sample EF 19.1 shows a high concentration of MgO (14, 7 %) and the highest concentration of Fe_2O_3 (15.1 %). It is also rich in CaO (9, 2 %). Due to its relative high concentration in Al_2O_3 (19 %) the sample is interpreted to be garnet. Due to the almost same concentration of Mg and Fe it could be a pyrope or almandin. The garnets are part of the mafic minerals due to their high concentration of Mg and Fe, which are common in mafic rocks.

EF19.2 has the highest MgO concentration of all samples (23, 6 %) and a relatively high concentration of Fe_2O_3 (15 %). It has the lowest CaO (2, 9 %) and Al_2O_3 (8, 5 %) content. This mineral is clearly mafic, based on its composition, an ultramafic mineral. Due to its composition, the sample is interpreted to be pyroxene. Based on the low concentration of CaO in the sample it should be orthopyroxene.

Sample EF.19.3 shows the highest concentration of Al_2O_3 (27, 7 %) and a high concentration of CaO (9, 1 %). The concentrations of MgO and Fe_2O_3 are again very low with only a few percent. The similarities between sample EF16 and EF19.3 are high therefore sample 19.3 is also interpreted to be an anorthosite. The high concentration of elements typical for felsic composition and the low concentration of typical mafic elements like Fe and Mg support this.

The last sample (EF.24) is difficult to predict based on the chemical data. It has high concentrations of MgO and Fe_2O_3 and the highest concentrations of CaO (13, 6 %). The concentration of Al_2O_3 is relatively low with only 14, 2 %. Based on the chemical data, the sample could be of mafic composition. The colour of the material is greenish-white. It does not look like a typical eclogite which could be based on the chemistry. The white coloured parts are probably related to the high CaO concentration which is more typical for anorthosite. Based on the data, the material could be a mixture of eclogite and anorthosite.

Linear and crossed polarized microscopy picture of the different samples can also be found in the results chapter. Here the different minerals are visible and the estimated concentration of them will be described.

4.1.2.2. Rare earth elements

4.1.2.2.1. Introduction to REE

The rare earth elements (REE) are a group in the periodic table called the lanthanides. All of the group members have almost similar chemical properties and have an atomic shell with $5p^6 6s^2$ -structure. There only difference is the filling of the 4f-level. Since the 4f-level is shielded by the outer atomic shell it is not taking part in chemical reactions. Therefore the behavior of all lanthanides is relatively similar (Stosch, 2000). Another similarity is their almost identic ionic radii (Fig. 27)

Element	Ion	Radii [nm] for coordination number:		
		VI	VIII	IX
Lanthan	La^{3+}	0.1032	0.1160	0.1216
Cer	Ce^{3+}	0.101	0.1143	0.1196
	Ce^{4+}	0.087	0.097	
Praseodym	Pr^{3+}	0.099	0.1126	0.1179
Neodym	Nd^{3+}	0.0983	0.1109	0.1163
Samarium	Sm^{3+}	0.0958	0.1079	0.1132
Europium	Eu^{2+}	0.117	0.125	0.130
	Eu^{3+}	0.0947	0.1066	0.1120
Gadolinium	Gd^{3+}	0.0938	0.1053	0.1107
Terbium	Tb^{3+}	0.0923	0.1040	0.1095
Dysprosium	Dy^{3+}	0.0912	0.1027	0.1083
Holmium	Ho^{3+}	0.0901	0.1015	0.1072
Erbium	Er^{3+}	0.0890	0.1004	0.1062
Thulium	Tm^{3+}	0.0880	0.0994	0.1052
Ytterbium	Yb^{3+}	0.0868	0.0985	0.1042
Lutetium	Lu^{3+}	0.0861	0.0977	0.1032

Figure 27: Atomic Radii of the REE (Stosch, 2000).

Nearly all lanthanides are trivalent apart from Ce which can be tetravalent and Eu which can also be bivalent. Therefore the geochemistry of these two elements is more complex. Usually the REE can be divided in light rare earth elements (LREE) from La to Nd, the middle rare earth elements from (Pm or Sm) to Dy and the heavy rare earth elements (HREE) from Ho to Lu (Stosch, 2000). The lanthanides are considered to be lithophile, which means they are bonding with oxygen in nature (oxidic, silicic, phosphatic). In minerals the REE build several coordination polyeder between sevenfold and twelvefold coordination. The sevenfold coordination is typical to find in titanite, the eightfold in zirkon, ninefold in monazite, elevenfold in allanit and twelvefold in perovskite. Most trivalent REE are able to replace Ca^{2+}, Th^{4+} and U^{4+}. Eu^{2+} is able to replace Sr^{2+}. Between La and Lu the variation of the ionic radii is in a range of 15 %, that is the reason why it is possible to have fractionation in this group. The fractionation between to neighboring REE is relatively little, but between LREE and HREE it is distinct.

REE data is usually displayed in a graph showing the concentration (ppm) of the different REE. To make the analysis easier, the data will be plotted on a logarithmic scale since the variation in concentration is large.

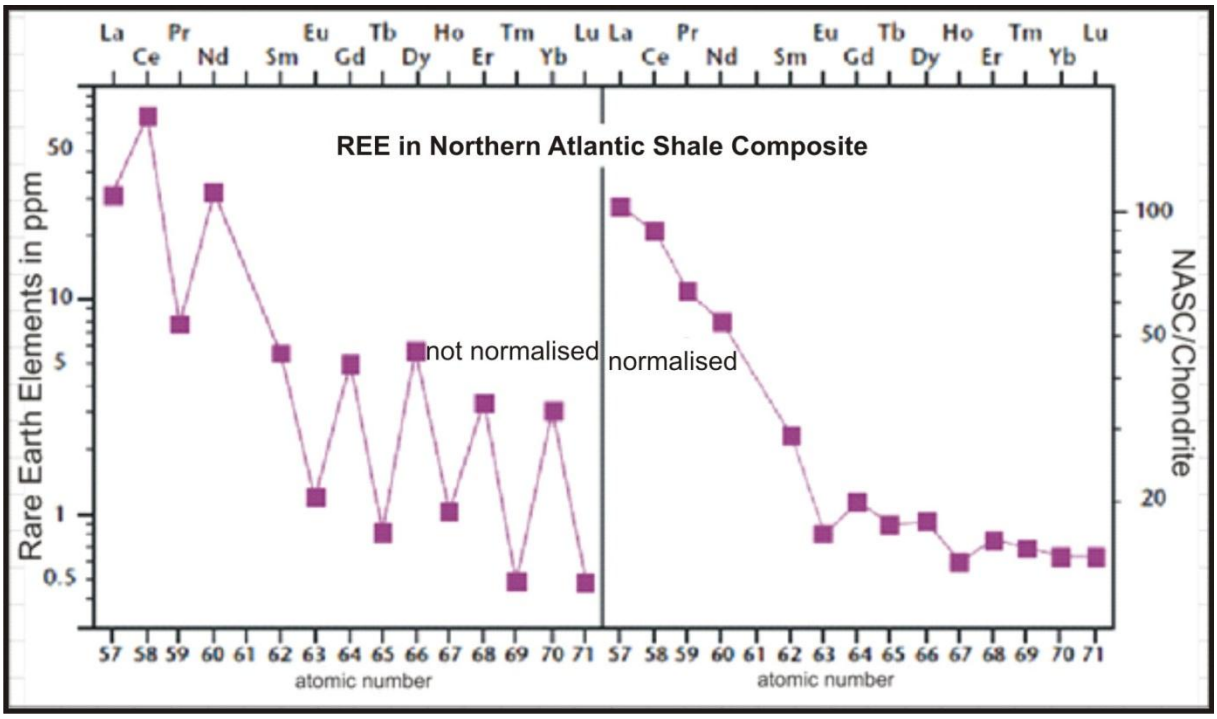

Figure 28: Two different plots of the same data, the left one plots normal REE data and the right one shows the similar data normalised to C1 condrite composition (Stosch, 2000).

In Figure 28 REE data from the North Atlantic Shale Composite illustrates another problem with the analysis of REE. The left plot shows the raw data. The Oddo-Harkins rule states that elements with an even atomic number are more common than elements with an odd number; hence the data plot produces a zig-zag-pattern on the left graph. Therefore the C1 condrite composition is used to standardise the data and even out the zig-zag-pattern. The curve on the right side in Figure 28 is evened out and shows a clear decrease from LREE to HREE which is to be expected since the LREE with the slightly larger ionic radii are more common in the upper crust then the HREE.

4.1.2.2.2. Interpretation of obtained REE Data

During the laboratory analysis of the Eldsfjellet samples, 11 rock samples were analysed for REE. Only 6 of them were used further for analysis because of problems during the sample preparation. Some of the samples had undissolved residue after the chemical digestion which led to uncertainties in the results, therefore they were excluded. The REE analysis was performed parallel with the trace element analysis. The data acquired will be shown in this section.

Table 3 shows the raw data obtained from Bergen geoanalytical facility (BGF). The standards used show a good correlation with the standard values and low uncertainties, therefore it can be assumed that the data is feasible. The data displayed here is in mg/kg which is identical to ppm.

Table 3: The data is the raw data for the rock trace elements, they are given in concentration in ppm. The column with C1 is representing condrite data from Palme and Beer (1993) which is used to normalise the data (see table 13).

Values in ppm	La139	Ce140	Pr141	Nd146	Sm147	Eu153	Gd160	Tb159	Dy163	Ho165	Er166	Tm169	Yb172	Lu175
EF. 6	0,99	2,30	0,33	1,50	0,31	0,46	0,30	0,04	0,24	0,05	0,13	0,02	0,13	0,02
EF. 8	3,52	6,91	0,80	3,07	0,47	0,74	0,30	0,04	0,16	0,03	0,08	0,01	0,07	0,01
EF. 10	5,90	28,98	6,44	38,79	13,28	2,20	14,18	2,31	14,60	2,97	8,19	1,15	7,83	1,30
EF. 3	3,20	6,71	0,77	2,84	0,40	0,49	0,24	0,03	0,12	0,02	0,06	0,01	0,05	0,01
EF. 9	5,07	10,88	1,36	5,89	1,36	1,22	1,30	0,18	1,03	0,19	0,49	0,07	0,42	0,06
Ef19.1	0,70	2,46	0,38	2,07	0,50	0,56	0,54	0,07	0,52	0,10	0,28	0,03	0,26	0,04
ef 19.2	0,25	0,97	0,11	0,67	0,13	0,14	0,17	0,02	0,19	0,03	0,12	0,01	0,13	0,02
C1	0,25	0,64	0,10	0,47	0,15	0,06	0,20	0,04	0,25	0,06	0,17	0,03	0,17	0,03

The data in Table 3 is acquired from ICP-MS measurements. The C1 row shows the condrite data which used for normalising the other data. All condrite data is obtained from geochemical earth reference model called GERM (http://earthref.org/GERM/) which combines geochemical data for the whole earth. The data used for these samples is from Palme and Beer (1993).

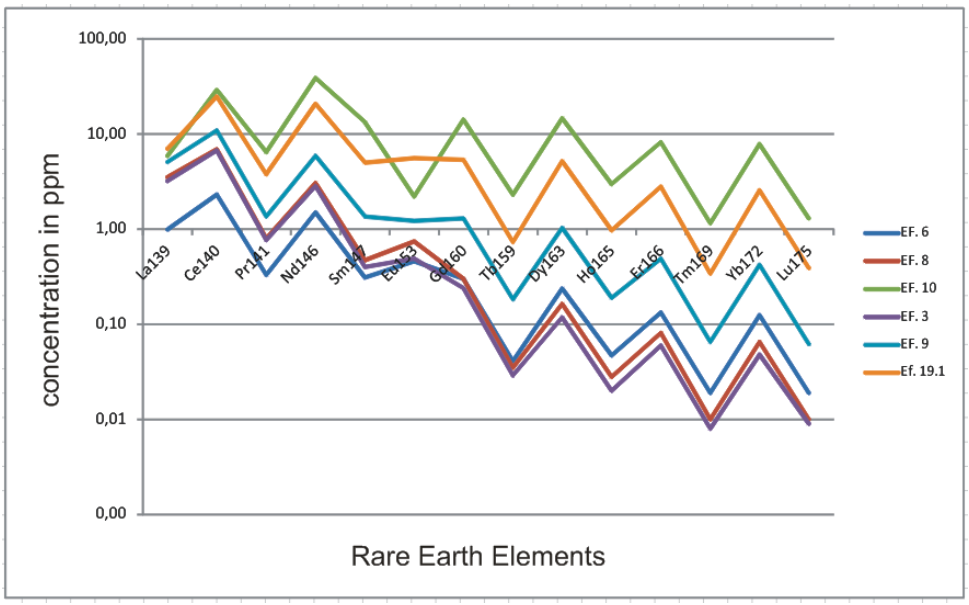

Figure 29: The plot shows the raw data without normalising it to C1 condrite, a dominant zig-zag-pattern can be seen, and this is due to the higher abundance of elements with even numbers.

Figure 29 shows the data from Table 3 and the before explained zig-zag-pattern can be seen. Also observable is that most samples plot in an almost similar range except from Ef.10 which

has, especially for the HREE, much higher concentrations compared to the other samples. The decreasing trend from LREE to HREE is clearly apparent except for Ef.10. This zig-zag-pattern is due to the higher concentration of elements with even numbers as explained before.

Table 4: In this table the data from table 3 has been normalised to C1 condrite composition to even out the zig-zag-pattern. The data is displayed in concentration in ppm.

Values in ppm	La139	Ce140	Pr141	Nd146	Sm147	Eu153	Gd160	Tb159	Dy163	Ho165	Er166	Tm169	Yb172	Lu175
EF. 8	4,0	3,6	3,4	3,2	2,0	7,9	1,5	1,1	0,9	0,8	0,8	0,7	0,8	0,7
EF. 9	14,4	10,8	8,3	6,5	3,1	12,8	1,5	0,9	0,6	0,5	0,5	0,4	0,4	0,4
EF. 10	24,1	45,4	66,8	81,8	86,2	37,9	69,5	61,6	57,5	52,4	49,3	44,9	47,5	51,2
EF. 3	13,1	10,5	8,0	6,0	2,6	8,4	1,2	0,8	0,5	0,4	0,4	0,3	0,3	0,4
EF. 9	20,7	17,1	14,1	12,4	8,8	21,0	6,4	4,9	4,1	3,4	3,0	2,5	2,6	2,4
Ef. 19.1	2,9	3,9	3,9	4,4	3,2	9,7	2,6	1,9	2,0	1,7	1,7	1,3	1,6	1,5

Normalisation of the data was done by dividing each sample value with the associated C1 value derived from Palme and Beer (1993). Therefore the values given here represent a multiple of the C1 condrite. The condrite has a composition and element concentration which is assumed to represent the composition and concentration of the suns photosphere. Therefore these values were used to normalise the data.

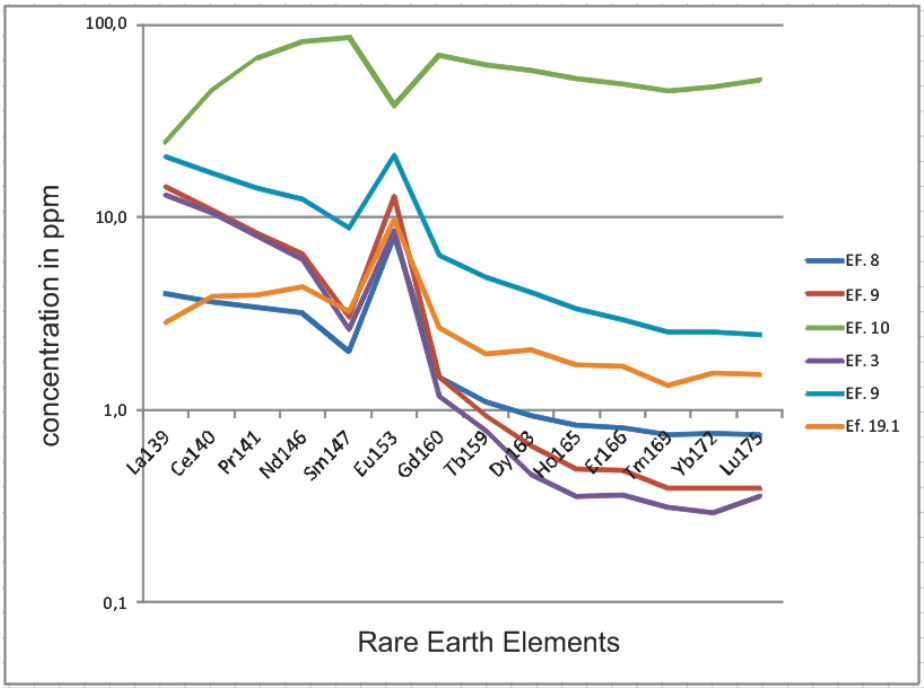

Figure 30: After the data from table 12 has been normalised to C1 condrite (see table 13) the data shows a different pattern. All samples except of the green line (Ef. 10) show an anorthosite pattern with a decreasing concentration from LREE to HREE except from the positive Eu anomaly. Sample Ef.10 (green) shows a N-Type MORB pattern with a high concentration of most REE and a dominant negative Eu anomaly. The y-axes represent the concentration in ppm on a logarithmic scale while the x-axes shows the different REE.

After the data was evened out (Fig. 30), the different sample plots show distinct similarities. Except from sample Ef.10, the plots show a constant decrease from the LREE to the HREE. Another prominent feature is the positive Eu anomaly. Based on field observations, most of the material is anorthositic rocks with a high feldspar concentration. From all major rock forming minerals, the feldspar group has the most distinct preference of LREE in comparison to HREE. Another characteristic for Eu^{2+} is that it can substitute for Ca^{2+} in plagioclase. Since the major part of the local rocks is of anorthositic composition, they have a high abundance on Ca^{2+} in their structure. This supports the observed positive Eu anomaly in the samples. The replacement of Ca^{2+} by Eu^{2+} is not possible for clinopyroxene because the compact clinopyroxene structure excludes it (Stosch, 2000). Sample Ef.10 differs from the other samples in several aspects. First of all it has a negative Eu anomaly, it also has much higher REE concentrations than the other samples and there is no clear decrease in the HREE.

Based on the specific pattern of sample Ef.10 the material is interpreted to be an N-type MORB.

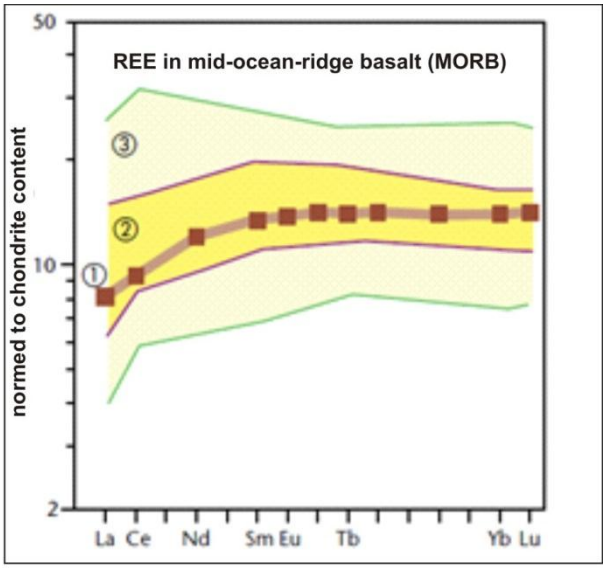

Figure 31: This is a figure which shows the general distribution of typical MORB pattern. 90% of all MORB are in field 3, 40% of all MORB are in field 2 and number 1 marks an average MORB composition compared to C1 condrite composition. The figure shows that most MORB have a concentration between 4 and 50 ppm compared to C1 condrite which is relatively high in comparison with the anorthosite data in figure 9 which is only between 0, 1 and approximately 20 (ppm).

Figure 31 shows the usual REE distribution in MORB, the amount of the LREE is lower than the HREE. The negative Eu anomaly for Ef.10 is not included in this diagram. Based on Stosch

(2000) this happens when an N-type MORB is strongly fractionated and due to plagioclase fractionation a negative Eu anomaly gets produced.

C.C. Lundstrom (1995) describes a pattern similar to Ef.10 from a basalt. The N-type MORB (Ef.10) describes a magma which has been undergone partial recrystallization. This is due to the fact that the REE are incompatible in basaltic minerals as well as in the crystallization of olivine, clinopyroxene, plagioclase and others. Since the REE are incompatible, they will be enriched in the declining residual melt. As mentioned before there is an Eu anomaly which is due to the possible replacement of Ca^{2+} by Eu^{2+}.

Due to these patterns and the information above it is assumed that all samples except from Ef.10 are cumulates from a melt. They are enriched by Eu which shows that they have taken out Eu from the melt. It is also assumed that based on the data, Ef.10 is considered to be an N-type MORB and got produced during partial crystallization. First the anorthositic samples were produced as cumulates. Afterwards the residual melt, which is enriched in REE, crystalised. The crystalised melt includes all of the REE except from Eu which has already been incorporate into the anorthosites.

This result leads to the suggestion that parts of the Lindås nappe contain of oceanic crust material instead of being of a pure continental origin. The literature suggests a continental origin of the local material (e.g. Austrheim and Griffin 1985, Jolivet et al. 2005, Raimbourg et al. 2005). To confirm the data it is necessary to collect and analyse further samples, beyond the scope of this work.

4.1.2.2.3. Uncertainties of the measurements

Because of high uncertainties, to low concentrations on certain elements and pollution of the digested rock samples with particles, the data in Figure 32 is not included in the results.

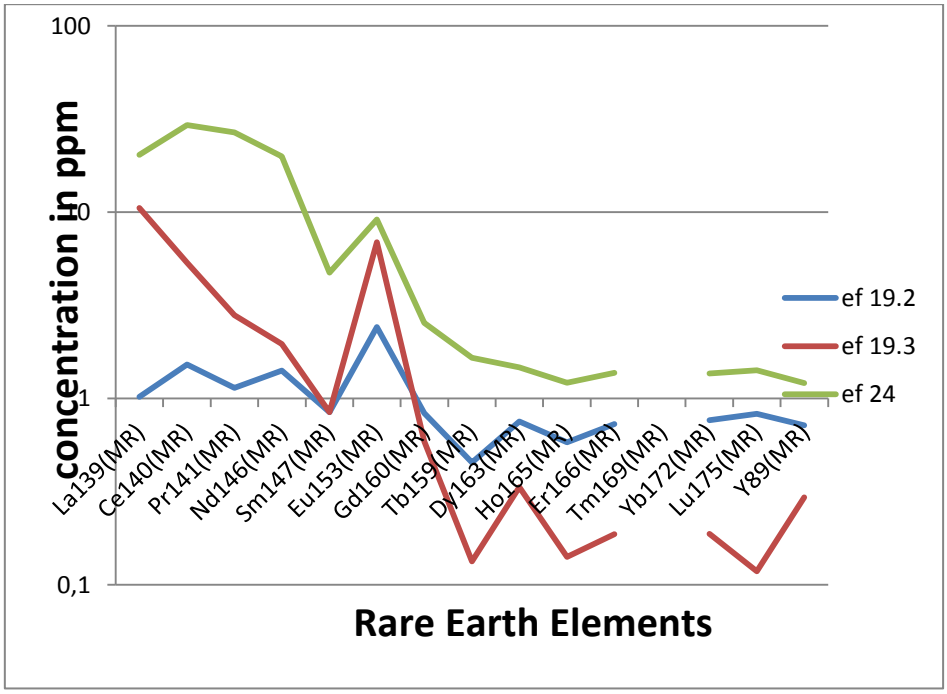

Figure 32: The graphs show that Tm could not be included because of to low concentration in the samples. In comparison with the plot in figure 9 the pattern shows zig-zag-patter especially in low concentration, that is because of values below the detection limit and inaccurate sample preparation which led to flawed results. Because of the named reasons, the data has been excluded from the interpretation. The y-aches shows the concentration in ppm in displayed in logarithmic scale and the x-axes displays the different REE

Figure 32 shows the results from the first REE analysis. The data in Figure 32 was excluded from interpretation because of the high uncertainty displayed by the curves. First of all the data for Tm concentration was below the detection limit and is therefore excluded from the interpretation. Another problem is that parts of the data show large differences for the LREE (left side of the graph). The main reason for excluding the data is the strong variation of the concentrations especially for the HREE, this shows that the results are questionable. That means the data has high uncertainties in the low concentrations. In comparison with figure 30, the differences are distinct. To avoid incorrect interpretations, the data was excluded. A possible reason for the high uncertainties can be the presence of undissolved residue after the chemical digestion. The particles can disturb the ICP-MS measurements and can lead to higher or lower concentrations than they are in reality.

4.2. Sediment samples

During the field work, two sediment cores were taken from the local catchment lake. One core was subdivided in 3 cm slices which were dried slowly and prepared for clay mineral analysis and to acquire the chemical composition.

4.2.1. Clay minerals

During the field work, lake sediment cores from Storatjørni (local catchment lake) (Fig. 2) were retrieved. The samples were bagged in 2-3 cm slices. The whole core had a length of 30 cm and 4 samples were taken out at different depths to determine the clay content of the samples and the amount of different clays. Due to the short length of the core, all sediments should represent deposits after the deglaciation. The samples were sent to a clay laboratory (www.claylabs.de) at the University Of Greifswald, Germany.

4.2.1.1. Methodology

Four samples were prepared for XRD. Since the samples were very rich in organics, they had to be cleaned, which took approximately 6 weeks. The cleaning procedure included mixing of 5 g sample material with 20 ml deionized water and 0, 5 ml 30 % H_2O_2. After 24 h the solution was mixed again with 0, 5 ml 30 % H_2O_2 and the sample was heated to 60 °C. This process was repeated until the solution was clear and had no organic smell left (Peltz and Grathoff pers. com.).

Afterwards the samples were sieved in a <32 µm grain size fraction to enrich the 32 µm fraction. For the <32 µm fraction, smear samples were produced. From the left 32 µm the <2 fraction was separated following the Stok law. The samples were measured on a Bruker D8 Advance with a xyz sample stage and a cobalt irradiation of 49 kV and 30 mA. The measurement range was between 3 and 34 °2 Θ. First the air dried (AD) samples were measured (AD), afterwards the samples have been saturated with ethylene glycol (EG) and stored in a desiccator overnight and then measured. In the last step the samples were heated in a muffle furnace to 550 °C for 1h. After the samples cooled down, they were measured again (550). (Information from Peltz and Grathoff, Clay Lab).

4.2.1.2. Clay Mineral Results

During the analysis, different techniques were used to plot the clay mineral data. Figure 33 shows the plotted data for the <2µm clay fraction for the sediment samples in a depth of 4-6 cm. A peak at 14 Å is the 001 reflection of chlorite. The glycolized plot (red graph) shows no change in the position but in the plot obtained after the heating to 550 °C the peak is shifting between 0,1 to 0,2 °2 Θ towards higher °2theta values.

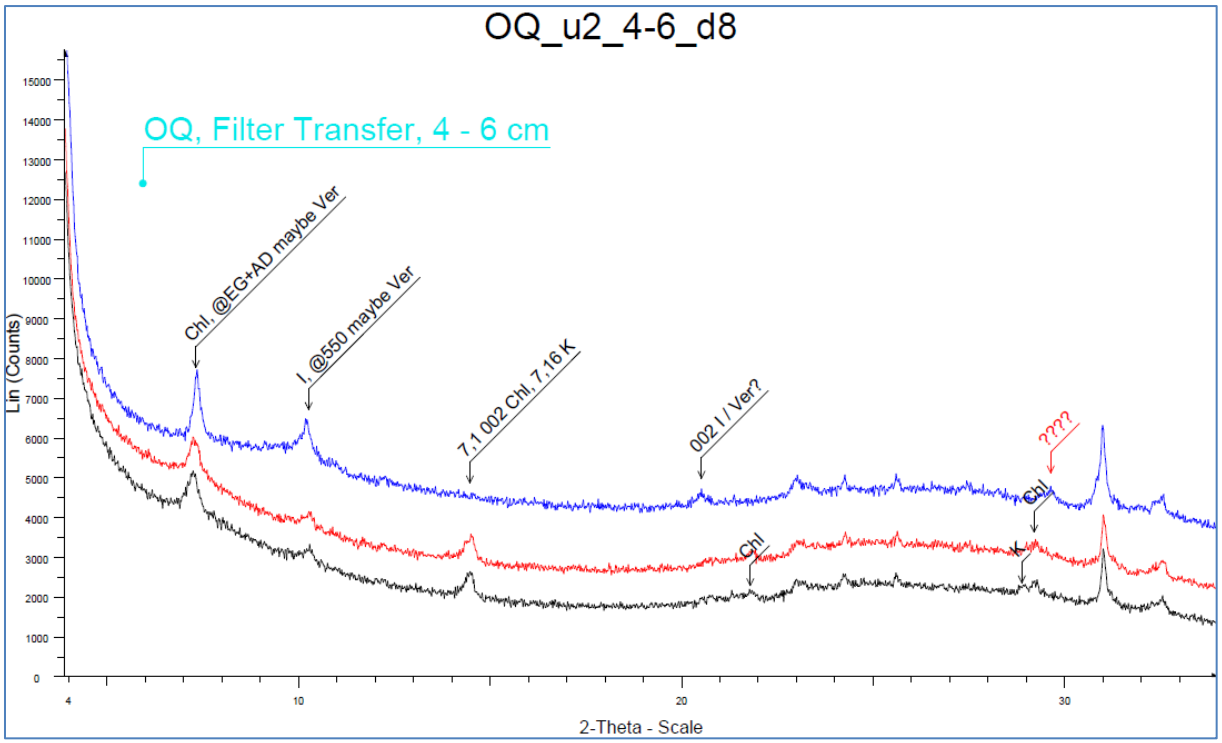

Figure 33: Shows the plotted data for sediment samples of 4-6 cm depth. The black line shows air dried samples (AD), the red line shows Ethylene Glycol saturated samples (EG) and the blue line shows samples after heating to 550 °C. This were done to see if the clay minerals will change their structure and the position of the peaks might move.

At approximately 10 Å is the 001 peak for illite/muskovite and at ca. 14, 5 °2 Θ are two peaks which overlap. At 7, 1 Å is the 002°2 Θ reflection of chlorite and at 7, 16 Å the 001 reflection of kaolinite. Both peaks disappear when the material becomes heated to 550°, because kaolinite becomes X-ray amorph. At 21 °2 Θ there is a weak signal of the 002 reflection of illite observable. At approximately 22 °2 Θ the 003 chlorite reflection is visible in the air dried and glycolized samples.

In the AD and EG measurements is the kaolinite 002 reflection at 3.55 Å and the 004 chlorite reflection at 3.55 Å.

The observed 001 illite peak could also be vermiculite. At 7 °2theta both reflections could overly each other because the illite peak is asymmetric. In the AD and EG curves both minerals have peaks at the same position. When heated the peak at 7 °2theta is more distinct and more symmetrical and the intensity of the 10 Å peak increases. This could have occurred due to a collapse of vermiculite during the heating to 10 Å. Since the 001 illite is at the same position, vermiculite and illite would fall again on the same position.

For the smear-slides <32 µm the results are similar. Figure 31 shows the ethylene glycol (EG) graphs plotted with depth starting from the shallowest sample on top. It is visible that the peaks are all at the same position and the variation to depth is very little.

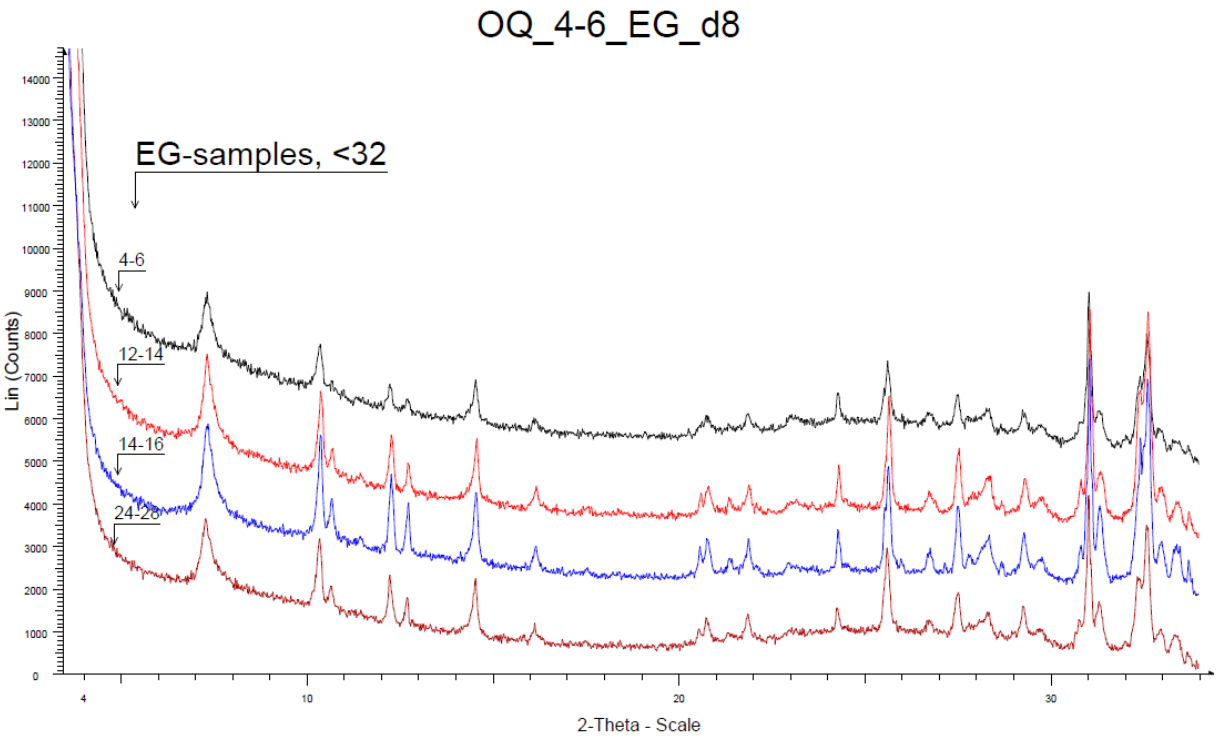

Figure 34: This is a comparison of all EG data from 4 cm sediment core depth up to 26 cm depth. The results show no large difference with depth, which means the clay minerals are relatively even distributed and there was no significant shift in chemistry which would lead to the production of other secondary minerals.

The samples consist mainly of chlorite, illite, kaolinite and maybe vermiculite.

Illites and vermiculites are closely related to the micas. The strongest similarity to mica has the illite group because their principal interlayer cation is potassium. Most illites are di-octahedral like muscovite and some are tri-octahedral like biotite. The major

difference from muscovite is a higher silica concentration and a lower amount of potassium. Illite is one of the most abundant clay minerals and can be formed from for example: feldspar, kaolinite or muscovite. A typical way to produce illite is by low grade metamorphism but also a process called sericitization is common, it produces illite/smectite from feldspar in lower parts of weathering zones (Deer et al. 1966). This could be a process which explains the illite production in the sediments, it could have been derived from the weathering of feldspar rich anorthosite.

Another possible clay mineral is vermiculite which can be produced as an alteration product of chlorite. As explained before it has almost a similar peak in the analysis as illite and therefore it is difficult to distinguish between them. Vermiculite is chemically similar to tri-octahedral micas and smectites. When vermiculite is heated it undergoes a peculiar exfoliation phenomenon which gives it excellent thermal and acoustic insulation properties. In nature the most common cation in vermiculite interlayers is Mg, but also Ca and more rarely Na can take this position (Deer et al. 1966). Vermiculite is a typical weathering product from ultrabasic and basic rocks where it is an alteration product of for example: pyroxene, phlogopite/biotite and chlorite. It can also derive from hydrothermal systems or through percolating waters. Another typical environment were vermiculite is produced is on the contact between acidic intrusive rocks and basic or ultrabasic rocks (Deer et al. 1966).

Another mineral found in the samples is chlorite, it has a relatively similar layered structure than mica. Chlorite is usually found in low grade metamorphosed rocks, hydrothermal alteration products of ferromagnesian minerals in igneous rocks and together with clay minerals in fine grained sediments. Chlorite is a common product of hydrothermal alterated pyroxenes, amphibole and biotite in igneous rocks. There is often a very close relationship between the chlorite composition and the original igneous minerals. They are also common in argillaceous sediments (clay rich sediments). In these sediments chlorites are often in regular interstratification with vermiculite which also might have been observed in the lake samples (Deer et al. 1966).

Kaolinite can also be found in the samples. The typical way to produce kaolinite, is weathering or low-temperature hydrothermal alteration of feldspar, muscovite and other Al-rich silicates, normally in acidic rocks. It can also occur in secondary deposits in deltaic,

lagoonal or non-marine environments. The transport must have happened under non-alkaline conditions (Deer et al. 1966).

All of the identified clay minerals can be produced in the environment on Eldsfjellet. Figure 35 shows possible mineral transformations in metagabbroic rock material which can be adapted to the Eldsfjellet area.

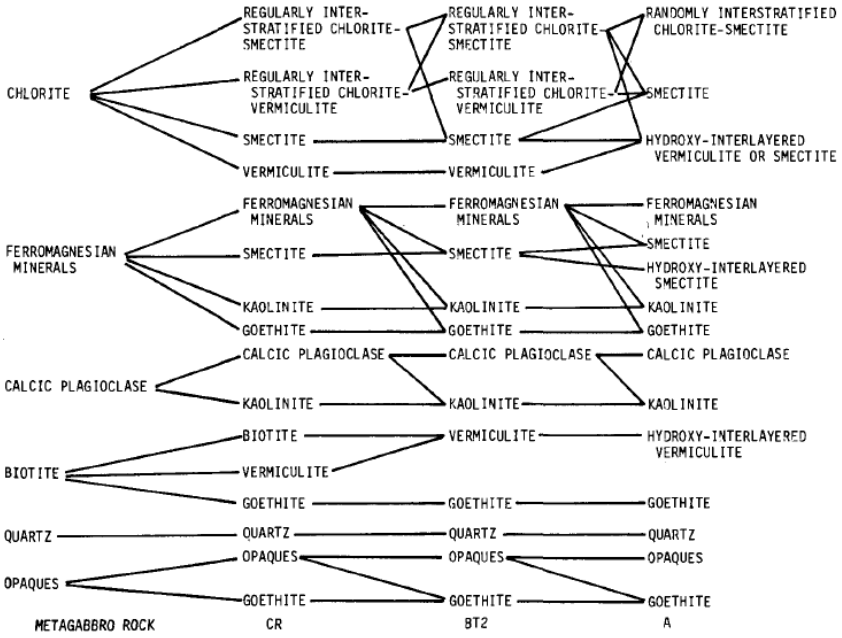

Figure 35: Mineral transformation starting from different major rock types and their associated secondary minerals (Rice et al. 1985). Of special interest is the calcic feldspar which has a high abundance in the field area.

Following the transformation from chlorite in Figure 35, one of the possible transformation products is vermiculite which could have been a product found in the sediments instead of illite. Another interesting group to check is the ferromagnesian minerals, for example pyroxene which is part of the lithology in the field area. During the transformation it will produce smectite (same as chlorite) and kaolinite. No smectite has been found in the samples, but kaolinite. The third and very interesting group is the transformation of calcic plagioclase which is part of the dominant rock type in the field area, the anorthosite. As visible in Figure 35, calcic plagioclase will produce kaolinite which is also observed in the samples from Eldsfjellet. Based on the data from Rice et al. (1985) and using it as background for interpretation it is likely that instead of illite, vermiculite is found in the samples. No smectite has been observed during the analysis; therefore it can be excluded

from the interpretation. Kaolinite is a common clay mineral in the lake samples from Eldsfjellet. The fact that there are no large differences in the clay mineral distribution with depth (Fig. 34) shows that the processes happened in the time period were the lake sediments were deposited have not changed. That means for the period represented by the 28 cm sediment thickness, the local process have been uniform.

4.2.2. Geochemical composition of the lake sediments

The sediment samples were prepared for XRF analysis to acquire the major element composition and see if changes occur with depth. Table 5 displays the major element composition of the lake sediments.

Table 5: The table shows major element compositions of sediment samples from the local catchment lake.

Sample Name	Na_2O	MgO	Al_2O_3	SiO_2	P_2O_5	K_2O	CaO	TiO_2	MnO	Fe_2O_3
	wt%	wt%	wt%	wt%	wt%	wt%	wt%	wt%	wt%	wt%
EF4_6	2,59	1,84	24,46	55,38	0,32	0,69	6,10	0,33	0,02	5,18
EF10_12	3,06	2,04	25,56	56,04	0,26	0,70	7,32	0,33	0,03	4,10
EF12_14	2,97	2,15	26,45	56,30	0,31	0,78	7,09	0,37	0,03	4,40
EF14_16	3,29	2,12	25,30	56,30	0,31	0,79	6,84	0,36	0,03	4,20
EF20_22	3,05	2,16	24,57	57,12	0,30	0,78	7,26	0,36	0,03	3,79
EF24_28	2,42	1,73	21,08	64,11	0,34	0,68	5,72	0,36	0,02	3,48

The major elements compositions in Table 5 are given in weight per cent. The depth of the core increases from the upper most sample downwards. There is no general decreasing or increasing trend of certain elements observable with depth. All samples have a high concentration in Al_2O_3, Na_2O, CaO and Fe_2O_3. The concentration of P_2O_5 is relatively similar in all samples. P_2O_5 concentrations indicate if samples are rich in organic materials.

4.3. Water samples

Eleven water samples were taken during the field work. The samples were distributed over the same area as the rock samples (see Fig. 33). Samples were collected from local puddles with one exception. Sample Eldsfj. Vann 1 was taken from the local catchment lake.

4.3.1. Major element composition of water samples

The collected samples were analysed for major and trace element composition (Tab. 7). The water samples were taken from standing water in puddles because the concentration of dissolved elements from the bedrock will be higher than in running water. Samples were taken to analyse the major and trace element concentrations in the puddles

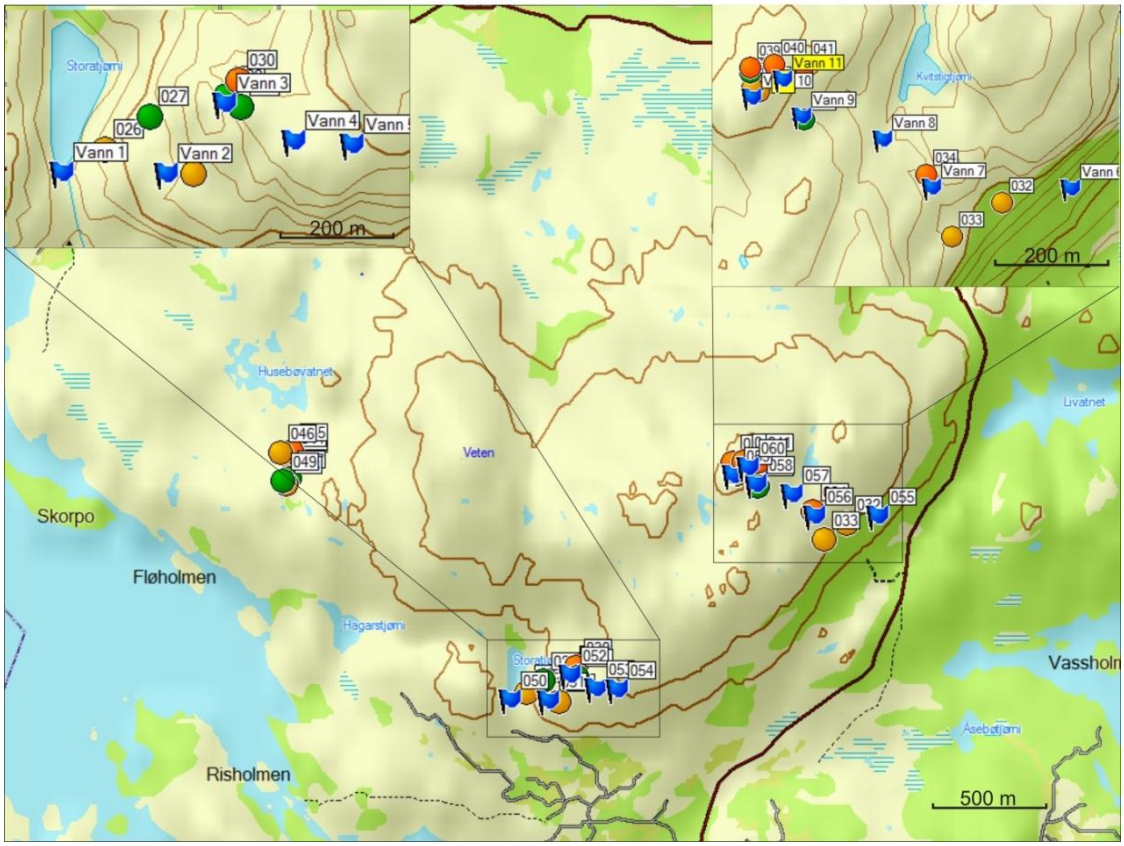

Figure 36: A map was constructed which shows the distribution of all rock samples (different dots) and the water samples (blue flags) collected in the field area (MapSource).

In Figure 36 the distribution of all water sample locations are shown (blue flags). Three areas were examined on Eldsfjellet, but water samples were only collected from two of these. They were chosen because of the number of available puddles in the area which can be related to the drilled rock cores. In the north western area, no puddles were available because of difficult accessibility.

Before evaluating the samples, it is important to examine the standards measured and compare them with nominal values. The results of the comparison are shown in Table 6.

Table 6: A comparison of measured standard samples (marked with UiB) and given standard values marked with MPI (Max Planck Institut). The green marked column shows the deviation in per cent between the samples measured in the Department and the once derived from the GeoReM data base.

Values in ppm	CA	Fe	K	Mg	Na	S	Si
sps-sw2 UiB	10,1	0,1	0,8	2,1	9,6	9,8	5,0
sps-sw2 MPI	10	0,1	1	2	10	10	5
diviation in %	1,4	7,8	28,6	4,0	4,1	2,4	0,2

Generally the results for sps-sw2 are good in agreement with the values from MPI. Deviation less than 10 % are considered to show reliable results. The value for Fe (7.8 %) is less than 10 % and therefore still acceptable (for major elements). Only the result for K (28.6 %) is too high and therefore questionable.

Table 7: The major element composition of water samples from the field area is displayed in this table. The values are given in ppm

Values in ppm	Ca	Fe	Mg	Na	S	Si
Eldsfj. Vann 1	0,38	0,02	0,43	2,78	0,62	0,46
Eldsfj. Vann 2	0,40	0,02	0,43	3,30	0,53	0,52
Eldsfj. Vann 3	0,34	0,03	0,41	3,44	0,73	0,14
Eldsfj. Vann 4	0,21	0,49	0,40	2,79	0,21	0,87
Eldsfj. Vann 5	0,55	0,02	0,47	3,34	0,58	0,40
Eldsfj. Vann 6	0,81		0,62	4,49	1,04	1,26
Eldsfj. Vann 7	0,66	0,02	0,43	3,16	0,61	0,63
Eldsfj. Vann 8	0,77	0,02	0,40	2,46	0,72	0,94
Eldsfj. Vann 9	0,29	0,04	0,38	2,55	0,75	0,86
Eldsfj. Vann 10	5,53	0,01	0,61	1,58	1,02	1,23
Eldsfj. Vann 11	0,16	0,39	0,31	1,92	0,65	0,07

Due to K values lower than the detection limit and a high uncertainty in the standard values, K is not included in the table (Tab. 7). The concentration of different major elements is in general low. That is probably due to the high amount of precipitation in the area. The supply of freshwater is high enough for rapid exchange of water in the puddles so that the concentration cannot increase significantly. Also, the overall concentration of the measured major elements is low, there are differences in concentration between the samples. The concentration of Ca is 5.5 ppb at Eldsfj. Vann 10 which is significantly higher than all the other samples which have a concentration less than 1 ppm. This can be explained because the puddle is located in anorthositic rocks which have a high Ca concentration. The Fe concentration is, except from two samples, around 0.015 to 0.040. In Eldsfj. Vann 4 and 11

the concentration is much higher with values between 0.49 and 0.39. The two puddles are located in bedrock which is richer in mafic minerals, for example eclogite. The Mg concentration in all samples is generally low and not uniform. The values are between 0.31 and 0.62 (ppm). The highest concentration of all measured major elements has Na. Its concentration is in a range of 1.58 and 4.49 ppm. It is low in Eldsfj.Vann 10 which has the highest Ca concentration. This is probably due to the suggested anorthositic composition which is on the opposite side of the An-Al plagioclase system. In this sample anorthosite dominate, therefore no albite rich plagioclase material is present.

The S concentration is again relatively low and between 0.21 and 1.04 ppm. The lowest concentration can be found in Eldsfj.Vann 4 and the highest concentration in Eldsfj.Vann 6.

The concentration of Si in the samples varied from 0.07 up to 1.26 ppm. The highest concentrations are in samples Eldsfj.Vann 6 and 10 with 1.26 and 1.23 respectively. These to samples also show a very low concentration of Fe. In sample 6 the concentration is not detectable.

4.3.2. Trace element composition of water samples

In this section, the focus is on the trace element composition of water samples from the same puddles as in the previous section. For this analysis, two different standards are used to determine the accuracy of the analyses. The standards are SPS-SW2 and NISTRM1643e.Table 8 and 9 show the standard deviation from the certified values. The geographical distribution of the water samples is shown in Figure 36.

Table 8: The deviation between the measured standards and the certified values are between 4 % and up til 32 %. Values above 10 % are assumed to be too uncertain for the further usage. That means Sr, Pb, Th and U are above the maximum uncertainty.

Values in ppb	Sc	V	Cr	Mn	Co	Cu	Rb	Sr	Y	Cs	Ba	Pb	Th	U
sps1	2,7	54,9	11,0	55,1	10,8	111,0	53,7	277,9	2,6	10,1	239,2	22,2	1,9	2,2
SPS2	2,6	54,6	15,1	50,3	10,9	117,7	53,8	283,1	2,8	9,6	230,1	22,3	1,9	2,1
sps1-2	2,7	53,1	10,7	52,7	10,0	104,4	52,4	263,1	2,5	9,3	227,9	21,0	1,5	1,8
sps1-3	2,8	54,2	11,1	54,8	10,2	109,9	51,9	281,8	2,4	9,4	226,5	19,3	1,5	1,8
sps2-2	3,0	55,9	11,7	52,7	10,6	109,2	55,0	283,4	2,7	9,7	237,2	22,6	1,8	2,0
sps2-3	2,6	53,4	11,2	47,9	10,5	101,0	50,7	265,4	2,4	9,3	229,6	20,7	1,8	1,9
average SPS	2,8	54,3	11,8	52,2	10,5	108,9	52,9	275,8	2,6	9,6	231,7	21,4	1,7	2,0
certified value	2,5	50,0	10,0	50,0	10,0	100,0	50,0	250,0	2,5	10,0	250,0	25,0	2,5	2,5
diviation in %	12	8.6	18	4.4	5	8.9	5.8	10.3	4	4	7.3	14.4	32	20

The standard deviation values for SPS-SW2 show a wide range of error from 4% up to 32%. The highest uncertainties are in Pb, Th and U which are together parts of a radioactive decay series. Since they are so closely related, it might be the reason for the uncertainty. Except for the three named elements and Sc, the uncertainty is good. Because of their large uncertainties, the measured concentrations of Pb, Th and U are not included in further data interpretation.

Table 9: In comparison with the values in table 5, the results show better certainties. The highest uncertainty has Pb with 10,3 %.

Values in ppb	V	Cr	Mn	Co	Cu	Rb	Sr	Ba	Pb
nist1643-1*	36,4	19,7	35,8	26,4	22,4	14,5	341,7	509,1	18,2
Nist1643-2*	41,3	23,9	41,1	29,2	22,4	16,0	371,8	517,1	16,4
NIST1643-3*	39,1	22,2	38,5	27,5	18,6	14,7	345,0	513,8	18,3
average NIST	38,9	21,9	38,5	27,7	21,1	15,1	352,8	513,3	17,6
certified value	37,9	20,4	39,0	27,1	22,8	14,1	323,1	544,2	19,6
diviation in %	2,7	7,4	1,3	2,4	7,3	4,7	9,2	5,7	10,3

The results from standard NISTRM1643e are shown in Table 9. The values for NIST are generally in better agreement with the certified standards than the SPS-GW2 values. The range of error is between 1.3 and 10.3 %. In this measurement uranium and thorium are not included. Pb is included and has again the highest error which is in between the maximum excepted error range.

The trace element concentration for the different puddles are in Table 10.

Table 10: The values in the table represent trace element concentrations in the water samples. The concentrations are given in ppm. Empty columns display values which were below the detection limit.

values in ppb	Cr52	Zr90	Ti47	V51	Ba138	Pb208	Sr88
Vann 1	0,1	ND	0,3	0,3	1,3	0,4	4,2
Vann 2	0,1	0,01	0,3	0,4	1,4	0,6	4,8
Vann 3	0,2	0,01	0,6	0,5	0,9	0,6	3,1
Vann 4	0,1	0,02	1,5	0,6	1,5	1,3	3,4
Vann 5	0,1	0,01	0,6	0,4	1,0	0,9	4,8
Vann 6	ND	ND	0,2	0,2	4,2	0,1	7,8
Vann 7	ND	ND	0,4	0,3	2,3	0,4	6,7
Vann 8	ND	ND	0,1	0,2	1,3	0,2	6,6
Vann 9	ND	ND	0,1	0,2	1,8	0,3	3,5
Vann 10	0,5	0,21	5,9	1,7	2,3	1,9	7,0
Vann 11	0,3	0,05	6,1	0,8	1,9	1,4	2,5

In Table 10 certain elements are blow the detection limits, for example in Cr and Zr (all 0,005 values), these are not displayed.

5. Discussion

In the Discussion chapter all the results, which were interpreted separately in the results chapter (Chapter 4), will be put together. The aim is to create a picture of the weathering history on Eldsfjellet from source to sink. Another part of this chapter will be the evaluation of the degree of post-glacial weathering in the field work area with help of weathering indexes (see Chapter 4). In the first section, the focus will be on the dominant weathering structure on Eldsfjellet, corona textures.

5.1. Corona textures

Corona textures can be observed on the whole mountain (Fig. 37) they have a spherical shape and a length between a few centimeters up to several meters. The corona textures are less weathering resistant than the bedrock and therefore leave holes all over the mountain, since the inner part is weathered out and removed. In the field area a spatial difference in the degree of weathering can be observed. West and north-west facing areas, as well as the summit of Eldsfjellet show much more weathering holes then the south and south-east facing areas. Based on the weather data (Chapter 1), which shows that the major rain direction is from west, it can be assumed that heavy precipitation and strong wind increases the weathering. This can be explained by the permanent exposure to rainwater, therefore the chemical disequilibrium on the west/north west facing surfaces will maintain and chemical weathering will be more effective.

Figure 37: The boot in this picture is used for comparing it with the size of a corona in the field area. The reddish colour is inside the corona texture is garnet, the blackish coloured parts are pyroxene minerals (unknown).

The corona textures are homogenously distributed all over the field area. The weathering pits were observed on horizontal, as well as vertical surfaces. Their abundance on vertical surfaces can be explained by the strong westerlies which have the ability to press water into the micro cracks of the textures. Subsequent reactions between water and mineral will dissolve the minerals in the texture. A higher concentration of NaCl in droplets in the wind can lead to salt weathering in the micro cracks when pressed into them. When the rain water evaporates, salt crystals can grow in the micro cracks, this leads to a further break down of the rocks.

The difference in the weathering rates between the anorthositic host rock and the corona textures is not described in accessible literature. One reason for the faster weathering can be the free space between the different mineral layers which makes it easier for water to penetrate and therefore to dissolve or mechanically break the minerals out of the strcutre due to freeze and thaw processes. This can only work if the space between the mineral layers is large enough to create a laminar water flow. Another likely reason is the difference in mineralogy, anorthosite is a felsic rock mainly consisting of elements with large ionic radii common in the upper crust. The minerals in the coronas are mafic minerals which are less weathering resistant, with a tendency to react strongly with the atmospheric oxygen and the water. A good example is olivine which disintegrates very fast when exposed to meteoric conditions at the surface. This is due to less oxygen incorporated in the minerals produced at greater depth, therefore a lag of oxygen. When a corona texture becomes

exposed at the surface, the mafic minerals will react with atmospheric oxygen and water, causing fast weathering of the minerals.

5.2. Rare earth element patterns (REE)

The REE are a very useful tool for determining the crystallization history of rocks. Specific REE patterns provide information on the fractionation history of a melt (see chapter 4.4.). The results show clear plagioclase patterns for most of the samples (Fig. 38). The pattern for plagioclase is very distinct because of the positive Eu anomaly and a decrease of the REE from LREE to HREE. The whole area is dominated by anorthositic rocks with a high abundance of plagioclase ($CaAl_2Si_2O_8$), the Ca^{2+} from the plagioclase is readily exchanged with Eu^{2+} since both have an almost similar ionic radii. The residual melt therefore becomes depleted in Eu^{2+} due to the uptake in the cumulate. What is left afterwards is a melt which is still rich in most REE but depleted in Eu. This can be seen in Figure 35. Sample Ef.10 shows a completely different REE´s pattern than the other samples. It is strongly enriched in most REE and shows a prominent negative Eu anomaly. The amount of REE in Ef.10 is up to 1000 times higher than in the plagioclase-rich samples. The pattern for Ef.10 observable in Figure 35 shows a close relation to an N-Type MORB (Stosch, 2000).

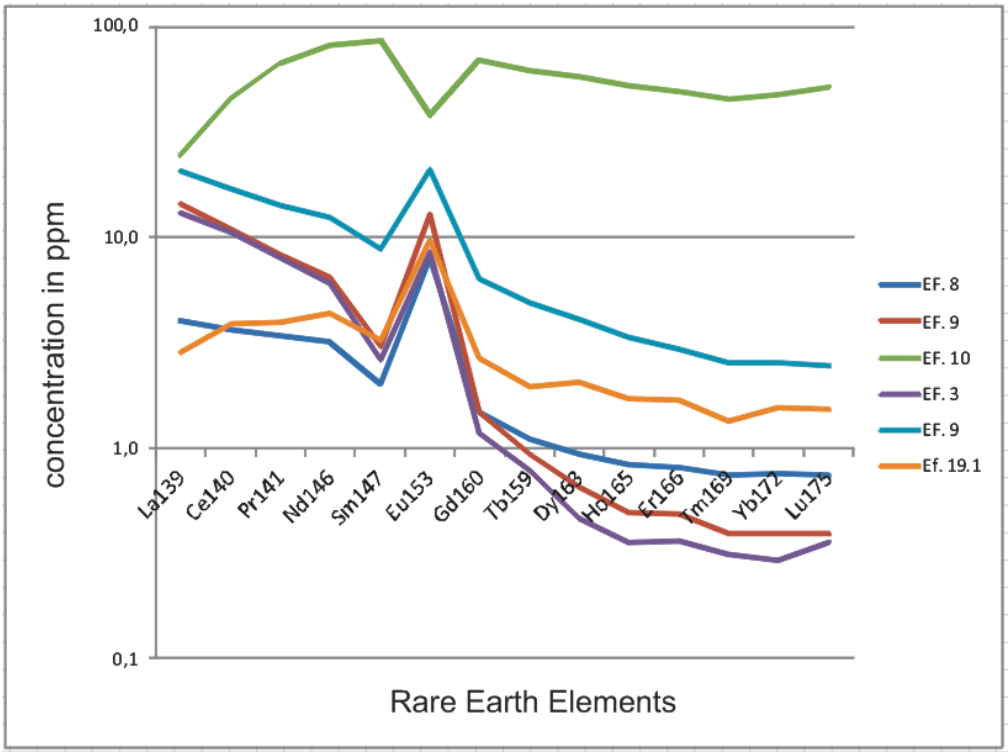

Figure 38: After normalising the data from table 12 to C1 condrite (see table 13) it shows a different pattern. All samples except of the green line (Ef. 10) show an anorthosite pattern with a decreasing concentration from LREE to HREE except from the positive Eu anomaly. Sample Ef.10 (green) shows an N-Type MORB pattern with a high concentration of most REE and a dominant negative Eu anomaly. The y-axis (n=1) represent the concentration in ppm on a logarithmic scale while the x-axis show the different REE.

The N-Type MORB shows that there is partly oceanic crust material incorporated in the continental rocks of the Lindås Nappe. This has not been described before in literature for this area. To obtain further information to support the findings it is necessary to collect more samples in the area and do further geochemical analysis. The samples were taken on in-situ rock material therefore it can be excluded that the sample material is cored from erratic which got transported by the ice. Compared to the standard values used for ICP-MS analysis and the values for standards from MPI, the error is low and therefore the results can be expected to be precise.

5.3. Weathering trends based on ternary plots of Nesbitt and Young

It is possible to use geochemical data from different sources to predict a weathering chain from source to sink. Nesbitt and Young (1984, 1989) showed there data by plotting it on a ternary plot (Fig. 36). This technique can be used for different purposes and is often used in geological classifications; an example is the QAPF diagram for determining the type of rock

based on the different amount of minerals. The ternary plot from Nesbitt and Young works in a similar way.

5.3.1. Ternary plot for felsic minerals

Figure 39 shows a general ternary plot for weathering. The four dots on the plot are marking different oxides. The lower left corner is CaO and Na_2O, the lower right corner is K_2O and the upper corner show Al_2O_3.

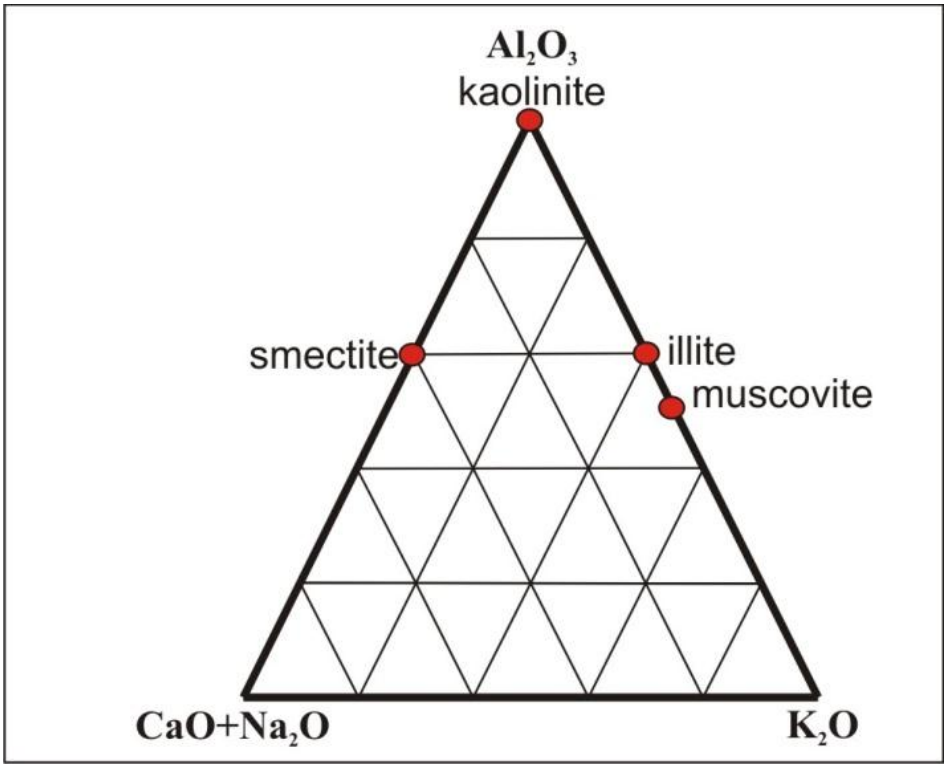

Figure 39. An example of a ternary plot for oxides, the plot is used to display the weight % of different oxides. Samples which plot in the lower part are considered to be fresh rock material and the more the composition plotted moves up to Al_2O_3, the more weathered the sample will be. This is because almost all of the mobile components like CaO will be transported away and Al_2O_3 as an immobile component will be left. The red points mark concentrations which lead to the production of different secondary minerals like illite. The plot displays the degree of weathering and was first presented by Nesbitt and Young (1984).

Every corner stands for a 100 % mineral composition. The lower left corner stands for plagioclase dominated rocks like anorthosites. These samples are rich in CaO and Na_2O and have almost no K_2O. The lower right corner shows rocks with a high concentration of K_2O and which are strongly depleted in CaO and Na_2O. This corner represents orthoclase. The upper corner is rich in Al_2O_3 and depleted in the other oxides. Data which plots in the upper corner consists of high amounts of kaolinites and chlorites which are both secondary

minerals. This means that this corner represents the most mature weathering products. Between the two lowermost corner points and the Al_2O_3 point different other minerals can be produced. These minerals are part of the weathering chain and get produced on the way up from the source rock (plagioclase rich or orthoclase rich) towards the highest degree of weathering expressed as kaolinite and chlorite.

The amount of the particular oxides on this plot will make it possible to determine the degree of weathering. For example a sample rich in CaO and Al_2O_3 will plot somewhere on the line between the lower left corner and the upper corner. If the concentration of Al_2O_3 is higher than the concentration of CaO, the sample will most likely produce smectite as a secondary clay mineral. If the Al_2O_3 concentration is even higher, kaolinite or chlorite will be produced. The same happens on the other side except that muscovite and illite will be produced. Based on the data acquired from laboratory work it is possible to describe the direction of the weathering chain. The data used in this thesis was obtained from fresh rock material from Eldsfjellet and sediments in a local lake.

A different ternary plot can also be used to display the data (Fig. 40)

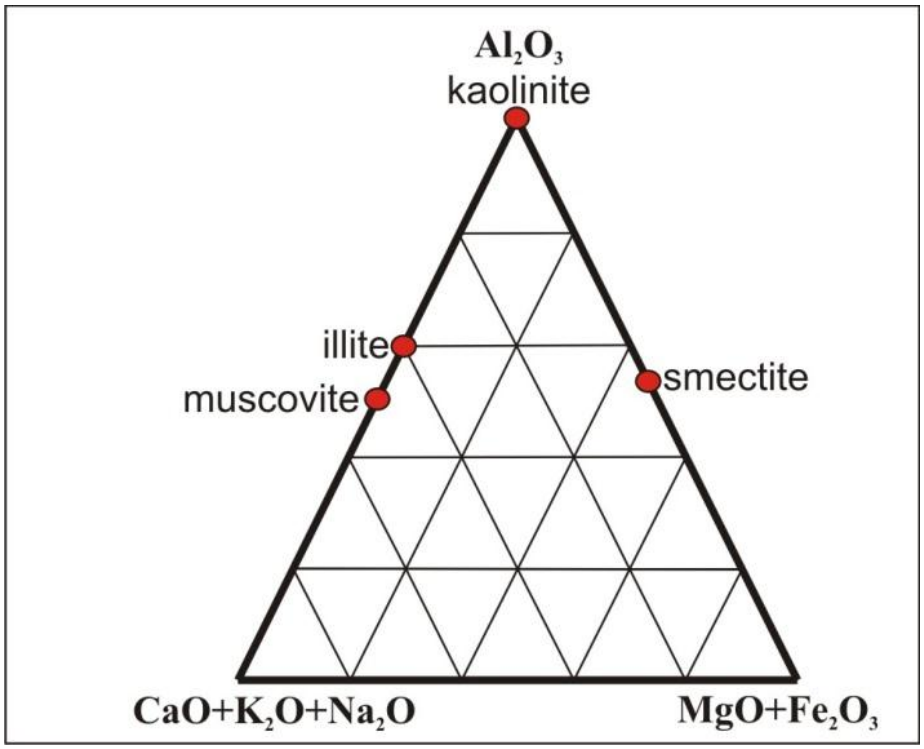

Figure 40: The ternary plot shows a different dataset than the one before. The lower right corner displays oxides often found in mafic rocks while on the lower left side typical oxides of felsic rocks are displayed. Again the lower part of the ternary plot shows fresh rock samples and the higher up the data plots, the higher the degree of weathering will be.

In this ternary plot (Fig. 40) CaO, K_2O and Na_2O are represented in, the lower left corner, while the lower right corner is representing MgO and Fe_2O_3. The secondary minerals are now plotted on the opposite sides since a higher concentration in Mg and Fe will move the samples closer to smectite. Other than that the technique behind is the same. This ternary plot takes also the element content (Mg, Fe) of more mafic minerals into consideration.

5.3.2. Plot of the Eldsfjellet data

The obtained data from Eldsfjellet is plotted in the two before mentioned types of ternary plots to be able to display the direction of weathering.

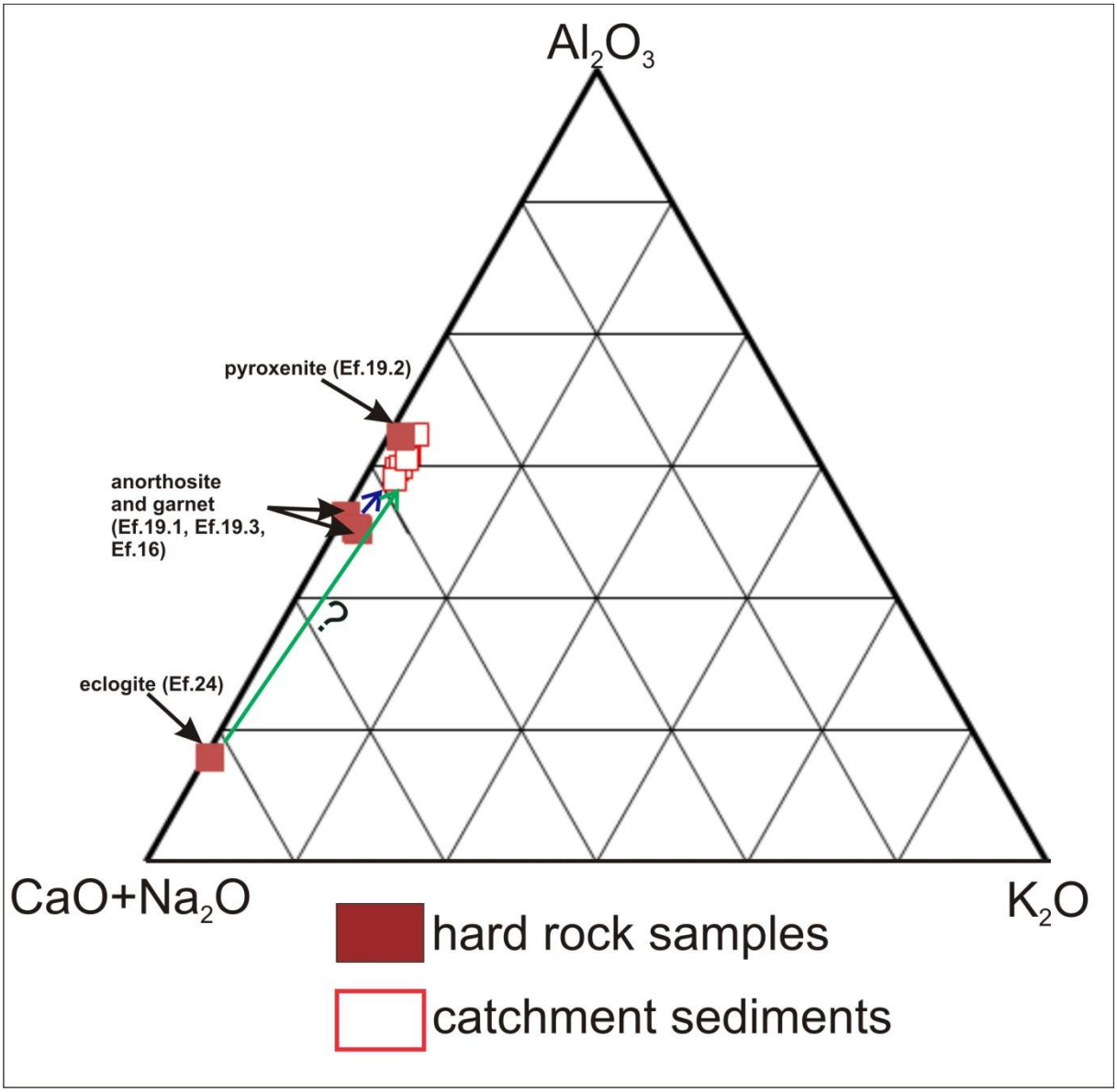

Figure 41: The XRF-data from Eldsfjellet samples is plotted in the ternary plot. The samples are all on the left boundary because of the low amount of K_2O in the samples. Since the dominant rock type in the area is a plagioclase the catchment

sediments have a high Ca content. The degree of weathering is increasing towards the sediments which, is expected since the sediments are weathering products of the local bedrock.

The data in Figure 41 shows the results from the major element analysis of hard rock samples (filled squares) and catchment sediments. One sample plots in the lower most left corner and is interpreted to be an eclogite. The other two samples above representing anorthosites based on their chemical composition. Above them the lake sediment samples are plotting as a cluster. That means the overall composition of the lake sediment samples with depth is not varying much (see also chapter 4). Above that, a pyroxene can be found, based on the chemistry and on its optics. To see differences in the amount of mafic mineral it is necessary to use the before mentioned C-N-K to M-F plot (example in Fig. 42).

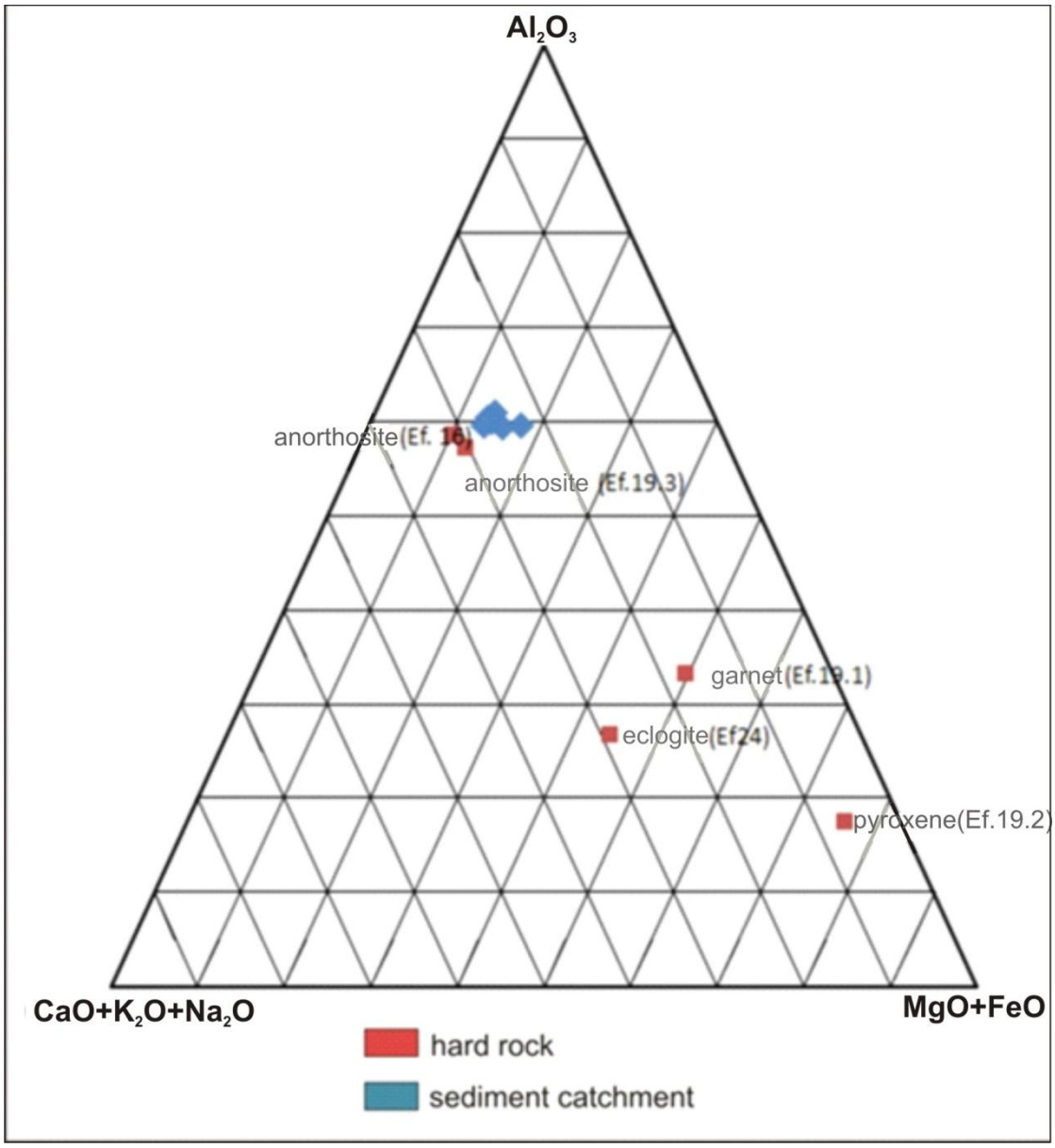

Figure 42: The MgO and FeO content lead to a different plot than in Figure 5. Sample Ef.19.2, which is interpreted to be a pyroxene, plots close to the MgO+FeO corner because of the high concentration in both oxides. The anorthositic rocks plotting close to the sediment catchment samples which were expected since the main rock type is anorthosite and therefore it is also the main rock for weathering.

In comparison with the first plot, some differences are observable in Figure 42, first the different samples move further away from the left side to the middle, which has to do with the abundance of Mg and Fe in all samples. The second difference is that garnet is now visible; it has been in a cluster with the anorthosites before. The pyroxene sample is moving down to the MgO + FeO corner due to its high concentration in these oxides (see chapter 4). The eclogite moved towards the middle of the plot that means it contains both felsic and mafic components.

Both plots show a close relationship between the anorthosites and the lake samples. This can be explained by the abundance of anorthosite in the area. Anorthosite is the dominating type of bedrock and therefore it will be also the major rock affected by weathering. The other samples do not show a close relationship to the lake sediments and can therefore be excluded being of major importance for the production of the lake sediments.

5.3.3. Comparison with other ternary plots

To investigate the degree of weathering at Eldsfjellet it is necessary to compare the data with other areas. For this reason the work of Rajamani et al. (2009) was chosen. The data in this publication is obtained from a region in western India called the Western Ghats. It is an area with high temperature (average annual temperature up to 24 °C) and high precipitation (between 3.000 and 4.000 mm/a up to 9.000 mm/a). Because of the named conditions it can be expected that chemical weathering plays an important role and that weathering will be advanced. Eldsfjellet is in a relatively cold temperate region with an average temperature of around 5.5 °C and less precipitation (approximately 2.000 mm/a). It can therefore be expected that the chemical weathering is less advanced. To compare data from the two areas, results were plotted together in ternary plots. These plots can be seen in Figure 40. Rajamani et al. (2009) divided their data in three different groups which are independently plotted. The first group is marked with F which represents the rocks with a dominant content of felsic minerals. The second group are the rocks marked with M which representing rocks with a high concentration of mafic minerals. The third group is called MF and represents rocks with a mixed composition of felsic and mafic minerals. The yellow lines drawn on the different plots represent the direction of weathering. The large blue spherical point represents the lake sediments, the red dots indicate the positions of the anorthosites and the green dot represents the eclogite. The numbering on the samples of Rajamani et al. (2009) indicates the direction of weathering. The lowest number represents the freshest rock material.

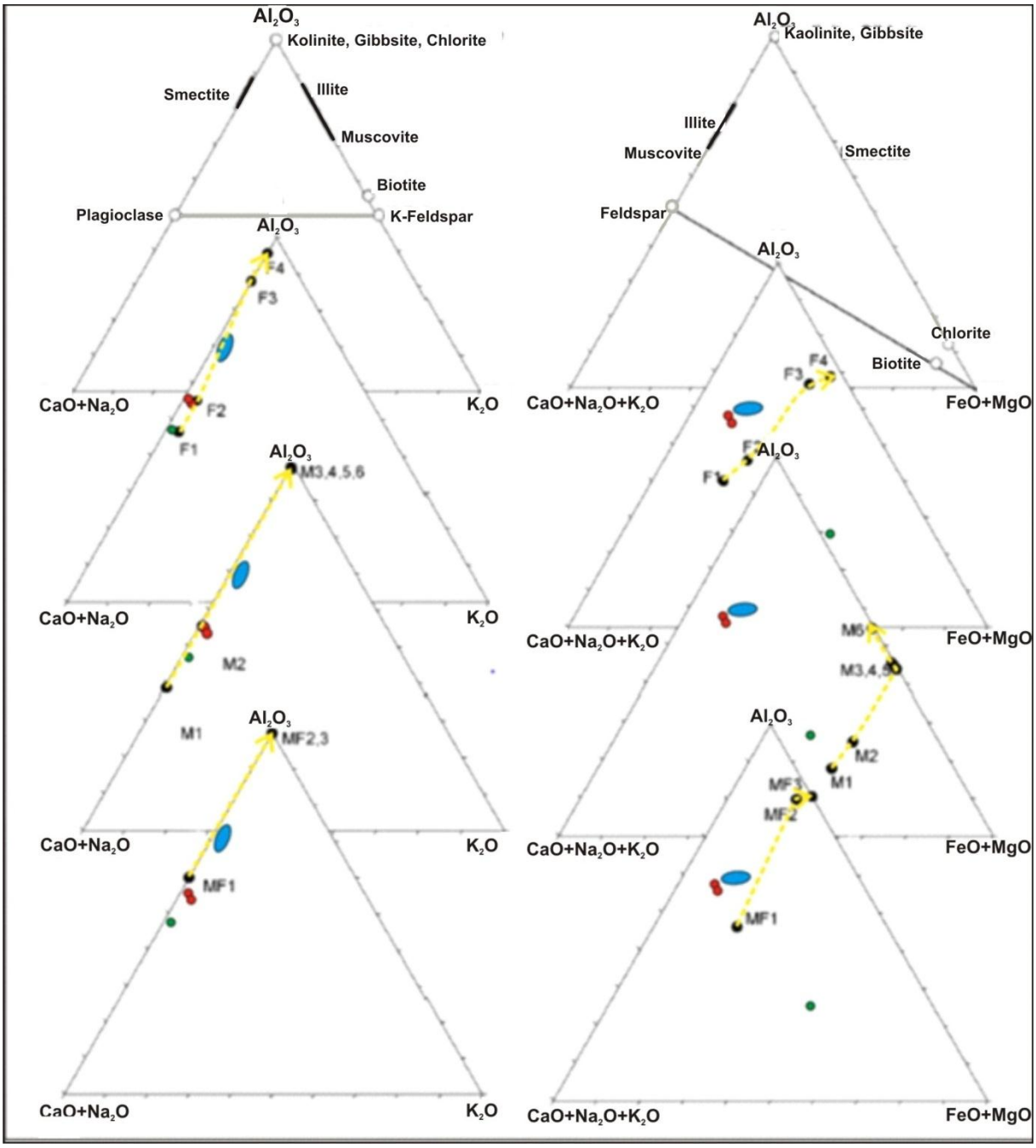

Figure 43: A comparison of data from Rajamani et al. (2009) with data from Eldsfjellet. M stands for mafic composition, F for felsic and MF for mafic-felsic rocks. The yellow arrow shows the direction of weathering for the Rajamani samples. The red dots show the plotted anorthosite content, the green dot represents an eclogite composition and the blue circle shows the composition of the catchment sediments.

The ternary plots on the left side are representing the CaO-Na_2O to K_2O type which divides the rocks rich in felsic minerals into plagioclase-rich and orthoclase-rich. The left plots show that both the values from Rajamani et al. (2009) and Eldsfjellet are following the same direction. The weathering chain marked with the yellow arrow moves along the left axes of the plot up to Al_2O_3. Based on the plot of the Eldsfjellet data the weathering chain can be

closely related to the felsic samples from Rajamani et al (2009). The starting point of weathering is almost similar. The most distinct difference is the degree of weathering at the end. While the lake sediments plotting a bit further towards the Al_2O_3 point, the samples F3 and F4 almost reach the level at which only kaolinite and chlorite are produced. The system here works as a comparative system. CaO, Na_2O and K_2O represent mobile oxides, whereas Al_2O_3 is considered to be an immobile oxide. The more one of the mobile oxides is removed by weathering, the higher becomes the concentration of Al_2O_3 in the sample and therefore the more mature is the weathering. This is a technique which is applied in many different approaches and it gives a good overview of the degree of weathering.

The plots on the right side in Figure 39 represent the CaO-Na_2O-K_2O to FeO-MgO plot. As written earlier they represent the comparison of felsic against mafic minerals. The pattern here looks slightly different, the data which plots above the starting point of F3 and F4 of Rajamani et al. (2009) has a distinct trend towards the production of smectite as seen from the samples from the Western Ghats but is not obvious from the Eldsfjellet samples. There is a slight trend between the anorthositic samples and the catchment sediment leaning towards the production of smectite. Again the trend of Rajamani et al. (2009) is much more distinct due to the stronger weathering.

The plots show that the weathering at Eldsfjellet starts at plagioclase and moves upwards towards kaolinite, chlorite and gibbsite as end products. In comparison with the data from Rajamani et al. (2009), the weathering trend is less distinct due to the colder climatic conditions and the lower precipitation at Eldsfjellet, compared to the Western Ghats region.

5.4. Clay mineralogy of the lake sediments

Since the ternary plot shows the general trend of chemical weathering in the field area and the most likely weathering product to be produced, it is now interesting to see which clay minerals can be found in the catchment lake (Results see chapter 4.6).

Figure 44 compares the different XRD results from the catchment sediments. Samples were analysed from a depth of 4-6 cm, 12-14 cm, 14-16 cm and 24-28 cm. The results show different peaks and each of them represents a specific clay mineral.

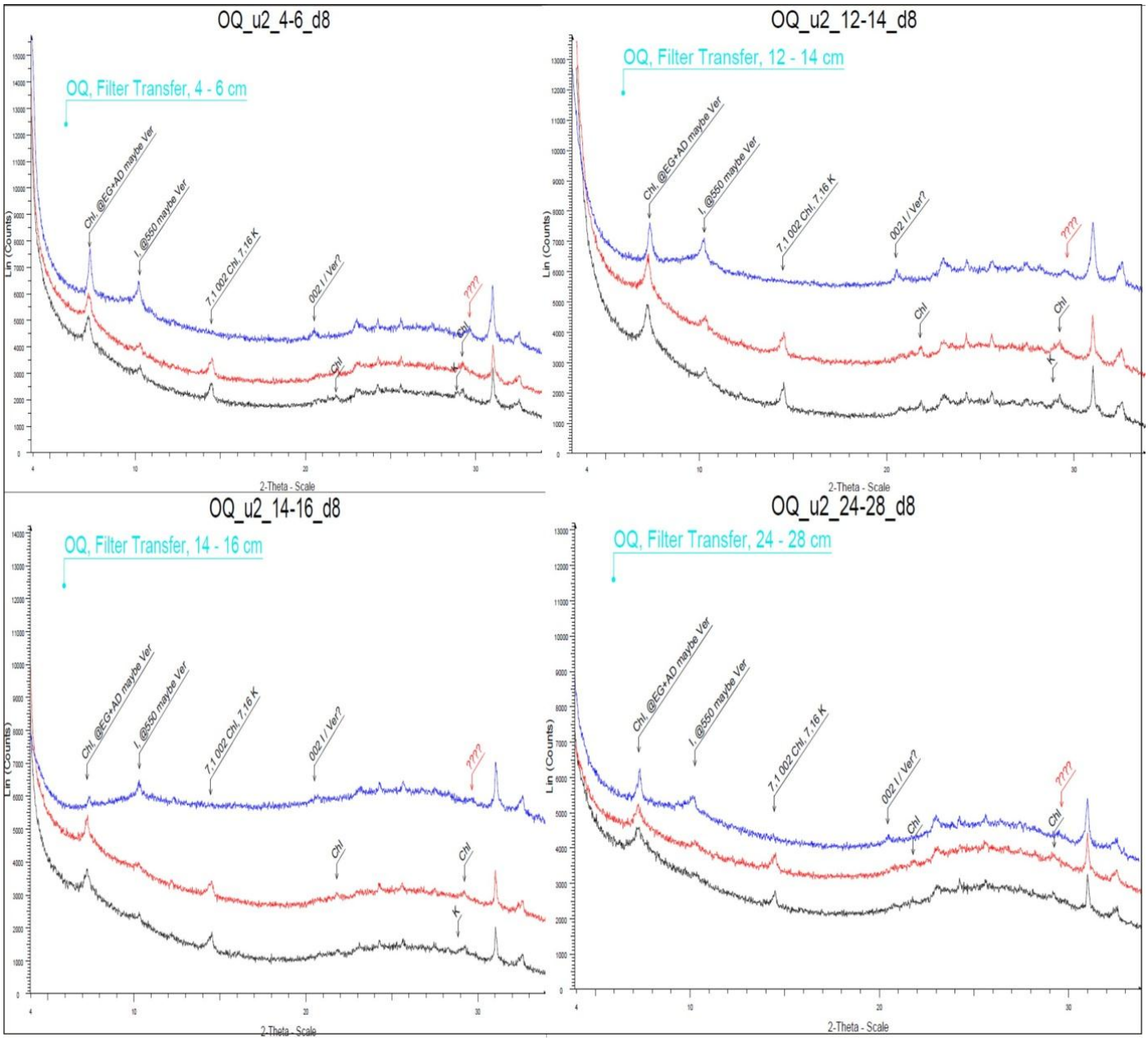

Figure 44: The graphs in this figure are a comparison of the different catchment sediment XRD analysis. The sediment depth increases from upper left to the lower right data set. The black line represents the results for the samples after organics got removed. The red line shows the values after they were mixed with ethylene glycol. The blue line stands for the results after heating the same samples up to 550°C. The warming of the samples led to a change in the position of the peaks in the graphs. This difference can be explained by destruction of existing clays and the formation of new clay minerals during the warming.

The results in Figure 44 show very distinct peaks for chlorite and illite and based on the report from the Clay Lab, kaolinite was also found. There is also a possibility that vermiculite in the samples could be hidden by the chlorite and illite peaks. The results are in agreement with the ternary plots, kaolinite and chlorite were expected in the sediments. It is also likely that vermiculite exists in the sediments due to the abundance of Mg, Fe, Ca and Na in the

sediments. Based on the report it is difficult to separate between vermiculite and chlorite/illite.

An unusual result is the abundance of illite in the sediments; based on the plots by Nesbitt and Young (1984, 1989) the expected clay mineral would be smectite as one of the secondary minerals since the plotted results move upwards on the smectite axis. The same problem was observed by Rajamani et al (2009). In their article, they suggest no explanation for this problem.

To solve this problem, an attempt was made in this thesis to compare the catchment lake water chemistry with Norwegian meteoric water. The idea was to compare the rainwater values with the lake water to see if there is any uptake of particular elements. A focus was on major elements like Ca, Na and K to see a loss of them in the system due to uptake in other environments and if there is an increase in K into the system from other sources. The increase of K is important since it is necessary for illite production, but the concentration of K in rocks, sediments and water is relatively low. The attempt was not successful and no gain of K has been observed. The process responsible for producing illite instead of smectite could not be explained from the dataset in this study and requires further geochemical analysis.

5.5. Water as weathering agent

Since the chemical finger print of the main rock types of Eldsfjellet can be connected to the sediments in the catchment lake a link can be made between source and sink. Another question is: what is the major weathering and transportation agent between mountain and Catchment Lake, due to the high precipitation and the weathering properties of water, it is thought to be of major importance for weathering and transportation.

5.5.1. Water chemistry

To find out if water has a major effect on the weathering, trace element data acquired from different water samples in the field area were compared with the rock chemistry of the local bedrock (see Results chapter 4.5.2). Trace elements were chosen due to their sensitivity to changes in the system. Figure 45 compares the water chemistry from local ponds with the rock chemistry in the same area.

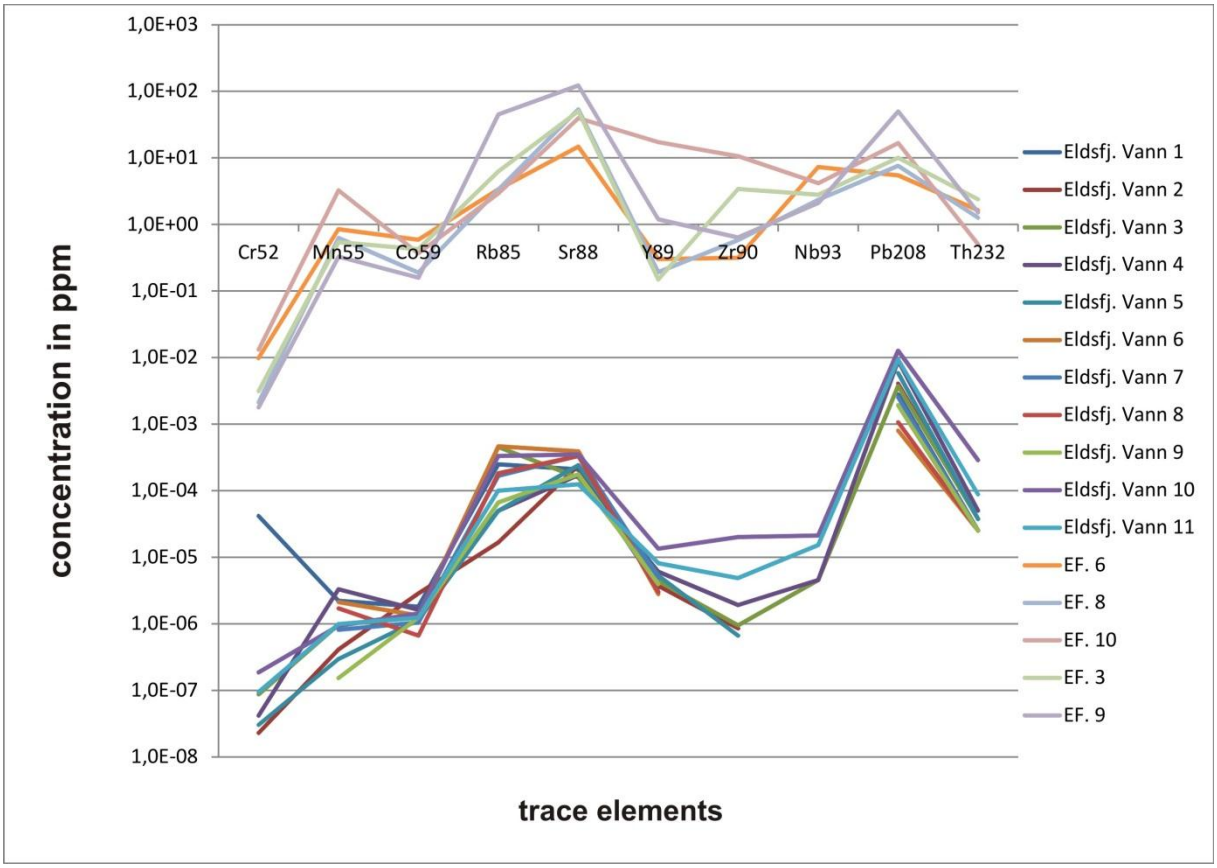

Figure 45: The graphs show a comparison of rock samples upper cruves with the water samples from puddles in the field area (lower curves)). The decrease and increase of concentrations is in a good agreement with each other. The concentration of trace elements in the water samples (lower curves) is lower than in the rock samples. This is expected since the concentration of trace elements in the water samples is mainly due to the uptake from the local bedrock by weathering. Both sets of curves show a high concentration in Pb, Rb and Sr. The concentration of Cr is low in both groups except from Eldsfj. Vann 1 which has a higher Cr concentration. This might be directly related to anthropogenic effects.

Figure 45 compares the concentrations of trace elements in water and rock sample with each other. The data in the upper part of the diagram are from rock samples; they have a higher concentration than the water samples. To make it possible to compare the graphs, the data is plotted on a logarithmic scale. The results are explained in detail in the above mentioned part of the results chapter. The high concentration of Cd in Eldsfj. Vann 1 can be

explained by anthropogenic contamination. The difference in the element concentration of Y and Zr can be explained by a different rock composition of Ef.10 in comparison with the dominant anorthosites in the field area (see 4.4.2).

By comparing the data, an overall agreement between water and rock samples can be stated. The pattern between them is almost similar. The relative increase and decrease of certain element concentrations can be found in both rock and water samples. Some differences can be explained by processes in the ponds which might have affected the composition and by possible uncertainties due to slight differences in the measurements methods. The rock samples were warmed to 1000 °C and therefore they might have lost volatile elements which could lead to uncertainties in the concentrations.

Since the increase and decrease of concentrations in water and rock samples are in a good agreement, water will be the major weathering agent in the area. Due to the heavy precipitation in the region, the weathering by water will stay effective since there is a constant supply of water. The transportation of dissolved material by water to the catchment lake is the most likely way.

5.6. Chemical weathering indexes

In this section, background information about the chemical weathering indexes will be given and their use will be explained.

5.6.1. Principles behind CIA and CIW

In the past 30-40 years, many different chemical weathering indexes were developed. Different approaches were used to compare element concentrations with each other to use these values as indexes for the intensity of weathering. Price and Velbel (2003) compared different chemical weathering indexes with each other to find out which once are the most reliable. In their paper Price and Velbel (2003) set up a list of requirements for a weathering index. A weathering index should be:

1.) Easy to use, involving chemical elements common in soil analysis (Harnois, 1988).

2.) An Index should incorporate elements with a range of mobility in the weathering environment (Harnois, 1988). It is not advantageous to use only highly mobile elements, because if a weathering profile is at an advanced stage, it might be already depleted on highly mobile elements.

3.) A good weathering index should show chemical trends with increasing weathering and the numbers should clearly show a change in the index with rising weathering.

4.) A weathering index should be applicable to many different types of rocks and should show clear differences in values between fresh and weathered material (Fedo et al. 1995).

For this thesis the best fitting weathering indexes are CIA (Nesbitt and Young 1989) and CIW (Harnois 1988). The CIA (chemical index of alteration) is using the conversion of feldspar to for example kaolinite. It therefore includes oxides like Al_2O_3, Na_2O, K_2O and CaO. The CIW (chemical index of weathering) is using the same oxides as CIA except for K_2O. The calculation formulas for CIA and CIW are:

CIA: $(100)*[Al_2O_3/(Al_2O_3+Na_2O+ K_2O+ CaO)]$

CIW: $(100)*[Al_2O_3/(Al_2O_3+Na_2O+CaO)]$

Both indexes have their weight on the conversion of feldspar, therefore these methods were preferred. The major rock composition in the fieldwork area is anorthositic, that means a high concentration of feldspar can be found. Since the concentration of feldspar is high, it is assumed that during the weathering, feldspar will play an important role.

Based on the two different methods used and their calculations with focus on the kaolinite production, the index values should increase with increasing weathering. The methods were applied in different geological settings, lately on sediments of 44 rivers worldwide by Li et al. (2010). He found that the CIA values are sensitive to surface temperature, latitude of the river mouth and soil depth at the watershed and that CIA reflect the integrated weathering history. Based on Nesbitt and Young (1989), which developed the CIA method, there are basic values for different major minerals. Of special interest is plagioclase since it is the most abundant mineral in the upper crust. The basic CIA values for plagioclase and biotite are 50. The change from plagioclase to the secondary minerals (clay

minerals) is from 55 to 80. The CIA value for illite is approximately 75 and for kaolinite is 100. Orthoclase weathers more slowly than plagioclase (Fig. 46).

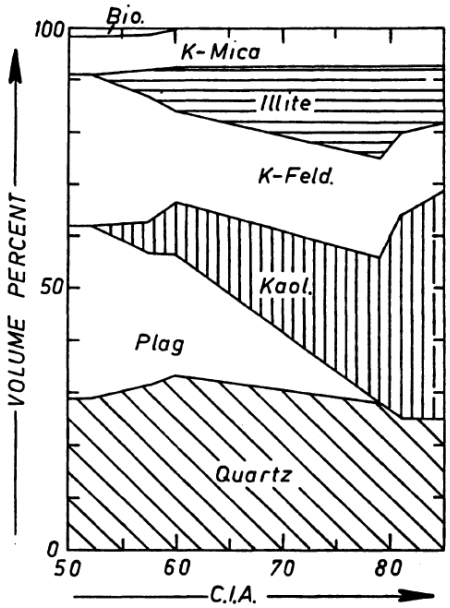

Figure 46: In this figure is the abundance of different minerals with increasing CIA values displayed. The amount of plagioclase decreases strongly with increasing weathering while for example the amount of quartz is almost constant. (Nesbitt and Young 1989).

Figure 46 shows the increased degree of weathering for the two different feldspars and the parallel increase of the secondary minerals, like illite and kaolinite. Quartz, as a weathering resistant mineral shows no strong decrease in the figure. Plagioclase vanishes at a CIA of approximately 80 whereas K-feldspar is still present. The formation of illite depends on K-feldspar, due to the mass balance considerations (source of K) coupled with the antipathetic relationship between the amount of K-feldspar and the in situ produced amount of illite (Brock 1943; Wahlstrom 1948; Sand and Bates 1953; Grant 1963; Nesbitt et al. 1980). The weathering of phyllosilicate is also an important process, but due to the volumetrically small amount in the crust, minerals like amphibole, pyroxene and olivine are not considered to be of major importance. The determination of clay minerals is important when doing chemical weathering analysis because the clay minerals are the major weathering product of the primary mineral phase. The understanding of chemical processes, which lead to certain types of clay minerals make it possible to determine paleoenvironments and paleoclimates (Nesbitt and Young 1982). During the weathering of anorthositic rocks, the majority of clay minerals produced are kaolinite, illite and smectite, as can be seen in the clay section in this

chapter. One of the reasons for using the CIA and CIW approach is that neither take the mobility of Fe into account. Fe is problematic because of its different oxidation states. The Fe^{3+} is relatively immobile, while the Fe^{2+} is highly mobile. During the weathering process, the amount of FeO decreases while the amount of Fe_2O_3 increases. That means with advancing weathering Fe becomes more immobile. (e.g., Reiche 1943). This is because of the extra oxygen in Fe^{3+}, in oxide analysis the weight percentage of Fe^{3+} is greater than the one for Fe^{2+} even without a change in the abundance of Fe. The increase in Fe will offset the decrease of alkalis and alkali earth elements during the weathering and therefore create less advanced weathering state (Price and Velbel 2003). Another problem is that if Fe should be considered in a weathering index, it would be necessary to evaluate the exact concentration of both Fe^{3+} and Fe^{2+} in the material, since the evaluation has to take potential complexes and varied initial values of Fe^{2+} and Fe^{3+} in to account, the results for weathering indexes might be less good then results from other indexes. The second problem with Fe is that Fe reflex redox conditions in the environment and might not be consistent throughout the whole weathering profile (Price and Velbel 2003).

As mentioned before, the major difference between CIA and CIW is that CIW does not incorporate K_2O in its calculation. The reason is that K is usually leached during soil formation, but K is enriched in Precambrium paleosols which is possibly a diagenetic feature (Retallack, 1986). After entering solution K^+ can produce K-minerals, adsorbed on other clays through ion exchange or removed by fluid migration (Harnoi 1987). If K is incorporated in a chemical weathering index then it has to be assumed that K was leached. Harnoi (1988) avoids this problem by not incorporating K in his calculation. He also excludes Fe from his calculation due to the prior explained reasons. Like CIA the CIW method uses the immobile Al_2O_3 in comparison with the mobile oxides CaO and Na_2O. This can provide information about the level of leaching of the mobile elements.

	Rock type	Fresh rock					Most weathered residue
Precambrian paleosols							
[1]Denison	basalt	76	87	90	95	94	96
[1]Pronto	granite	61	61	69	96	95	94
[2]Dominion Reef	granite	59	60	66	93	94	98
Soil profiles							
[3]Tishomingo T1	granite	57	58	70	81	91	92
[3]Tishomingo T2	granite	63	64	71	72	88	82
[4]Kiama	latite	48	63	81	87	89	85
[4]Inverell	basalt	44	85	89	94	95	99
[4]Casino	basalt	32	32	48	62	82	92
[4]Guyra	basalt	39	42	74	85	86	81

The reader is referred to the original publications for a detailed description of the profiles.
[1] Gay and Grandstaff (1980)
[2] Holland (1984)
[3] Harris and Adams (1966)
[4] Craig and Loughman (1964).

Figure 47 These are examples of CIW values for different rock sample (Harnoi, 1988).

Figure 47 shows calculated CIW values from different rock types based on their chemical data. The data is from various publications and compiled by Harnoi (1988) to show the differences from fresh rock to the strongest weathered material. In the paleosol samples, the basalt material shows the most advanced weathering from the beginning, while in the other soil profiles the weathering of basaltic material is very low. The difference between paleosols and soil profiles is not very distinct on granitic material. It starts relatively high and increases to values up to 98. The range for basaltic material is from 32 to 99. The diagram shows that the CIW can be applied to felsic and mafic rocks.

5.6.2. CIA and CIW evaluation of laboratory data

The following chemical weathering index values are calculated from major element data obtained with XRF analysis. The data was derived from rock samples collected in the field area using a coring device and sediment samples from lake cores taken in the main catchment in the field.

Table 11: The CIA and CIW values calculated show a small range of weathering values. The values displayed are sediment samples from the catchment lake and they are organised with increasing depth from the upper to the lower most sample.

Sample	CIA	CIW
EF4-6	72	74
EF10-12	70	71
EF12-14	71	72
EF14-16	70	71
EF20-22	69	70
EF24-28	70	72

Table 12 shows the calculated CIA and CIW values from the lake sediments. The depth of the sediment samples increases from the uppermost to the lowermost sample number. The numbers used denotes the depth at which the sample material was taken. Table 12 and Figure 44 show that the variation between the samples is relatively small, the maximum CIA value is 72 and the minimum is 69. Likewise the CIW values show a similar small variation from maximum 74 to minimum 70. It is displayed that the CIW values in general are slightly higher the CIA values. This difference can be explained by the fact that CIA includes K_20 in its calculation while CIW is omitting it. In comparison with the data derived from Harnoi (1988), especially compared to granitic compositional material, the values can be interpreted to be almost fresh rock material. Weathering has clearly occurred since fresh plagioclase material has a CIA value of approximately 50 (Nesbitt and Young 1989) but in comparison to other data it is not strongly weathered. That is probably due to relatively cool climate in the field area compared to data obtained from tropical areas. Another factor will be the short transport distance between source and sink; therefore the weathering effects will be limited.

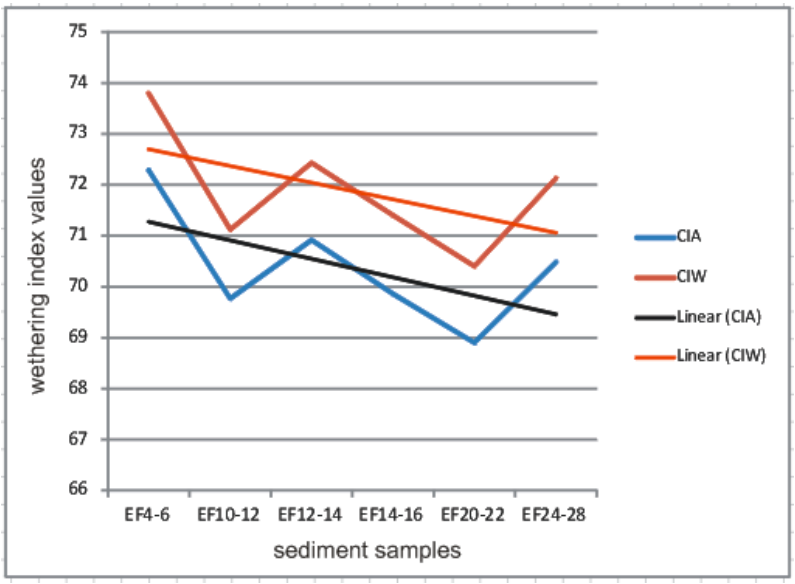

Figure 48: The graphs are plots of the calculated weathering index values for CIA and CIW. The general trend is a decrease of weathering intensity with depth. Both weathering indexes show a decrease with depth.

Figure 48 shows the CIA and CIW data from the lake core, depth increases from left to right from 4 to 28 cm. The samples were taken from a catchment lake core and represent a depth of 4 cm down to 28 cm. There is an obvious difference in the degree of weathering through the core. The uppermost part of the core is more weathered than the lower part. This is similar to results from Harnoi (1988). This is due to the stronger weathering on close to surface material which will be more affected by processes occurring at the water/sediment boundary because of the stronger ion exchange.

The second chemical weathering index calculations were done on in situ rock samples collected from the field area. The major element composition from the samples was determined by using XRF. Sample Ef.19 is divided into 3 different parts, one part which is mainly consisting of garnet, the second part consists of anorthosite and the third part consists of pyroxene. This was done to see if there is a difference in the degree of weathering observable in one sample. Since the samples represent different minerals, a difference in the composition can be expected. The results show that the pyroxene Ef.19.2 is much stronger weathered then the other two minerals (Ef.19.1 and Ef.19.3), which can be expected because pyroxene is a mafic mineral which weathers easier under surface conditions.

Table 12: The data from rock samples, left table and sediments in the right table are displayed together to show the difference in the degree of weathering between them.

	CIA	CIW
EF16	65	66
EF19.1	66	66
EF19.2	72	73
EF19.3	65	66
EF24	48	48

	CIA	CIW
EF4-6	72	74
EF10-12	70	71
EF12-14	71	72
EF14-16	70	71
EF20-22	69	70
EF24-28	70	72

The data in Table 13 compares the chemical weathering index data of rock samples (left table) with the catchment sediment samples (right table). The comparison shows, in average, slightly lower CIA and CIW values on the fresh rock material. That is in agreement with the system behind CIA and CIW which assume that with rising index values, the weathering is increasing. The difference in values between the least and most weathered index values are in range of 2-5. The only value which is significantly lower is EF.24, it shows a value of 48 which implies fresh rock material. The values for Ef.19.2 indicate the strongest degree of weathering and represent pyroxene. To find the reason for the high values on Ef.19.2 and the very low values on Ef.24 it is necessary to check the major element data (see Chapter 4.1.2.).

Table 13: Comparison of table 1 and 2.

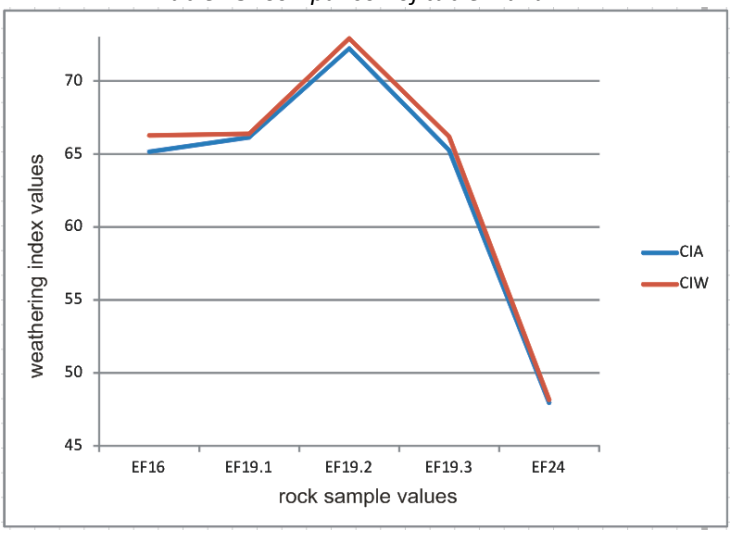

Figure 49: The x-axes displays the different rock samples which are plotted in this diagram while the y-aches represents the weathering index values ranging from 48 up to 73. Based on the calculations (tab. 9) EF24 has the lowest degree of weathering and can be interpreted as fresh rock while sample EF19.3 has the highest degree of weathering with a value of 74.

Figure 49 shows the plot of the calculated CIA and CIW values for the rock samples. Most values range between 65 and 72 and the differences to the sediment samples from the drainage lake are small. There are two values which stick out and that is Ef.19.2 with a high

value of 72 (CIA) and 73 (CIW) and the values for Ef.24 which are low in comparison with the other values The CIA for Ef.24 is 48 and CIW is also 48. The plotted data shows very good agreement with the exception of Ef.16 which show a slight difference between the calculated CIA and CIW value.

Sample 19.2 shows low concentrations for some of the elements compared to the other samples. The values for K_2O, CaO, Al_2O_3 and Na_2O are the lowest of all samples. These values are important for the calculation of CIA (incl. K_2O) and CIW (excl. K_2O). Since the values are in comparison with Al_2O_3 it can be assumed, the lower the mobile element values are, the higher is the chemical weathering index. In this case it explains the high chemical weathering index values for sample Ef.19.2. The high values of the rock samples agree well together with the type of mineral. Mafic minerals have the tendency to weather more rapidly at the surface than felsic minerals as explained in chapter 2.

Sample Ef.24 shows a strong degrease in the degree of weathering compared to the other samples. Based on different literature it is supposed to be a fresh rock sample. The major element composition shows the highest concentration of CaO (13.6 %) which is much higher than in the other samples and the sample has a relatively low Al_2O_3 concentration of only 14.2 %, which is the second lowest concentration. The comparison of a relatively low concentration on Al_2O_3, which represents the immobile elements, with a high concentration on one of the mobile elements leads to a drop in the weathering index, therefore the value is very little compared to the other samples. Based on the derived major element composition, the sample is interpreted to be an anorthosite which is a very common rock type in the area and it explains the high CaO concentration.

The different weathering indexes are good to characterise the chemical weathering. Therefore they are useful in giving information about the degree of weathering. But these methods are not applicable for determining the amount of weathering or the amount of removed material. It is not possible to gain a quantitative number of weathered materials.

5.6.3. Weathering Index by Parker (WIP) and Vogt index of weathering

After describing the approaches of CIA and CIW in this section, two other indexes will be described. They are chosen because they also gain good results on this type of rock material (Price and Velbel 2003). Both methods working in a different way than the two proposed earlier and therefore will give a different range of index values.

The Weathering Index by Parker, WIP (Parker 1970) is focused on the proportion of alkali and alkali earth metals present in the sample. These elements are chosen because they are the major elements with the highest mobility (Price and Velbel 2003).

$$WIP= (100)[2Na_2O/0,35)+(MgO/0,9)+(2K_2O/0,25)+(CaO/0,7)]$$

In this formula Parker (1970) considered the susceptibility of these elements to weathering by including Nicholl´s value of bond strength in the dominator. This is the measure necessary to break the cation to oxygen bond of the oxides. These values are believed to represent the probability of an element becoming mobilized during the weathering. The approach assumes that all CaO is incorporated in silicate minerals. If the sample material includes a large amount of carbonates or cements, it will lead to an imprecision of the data and to incorrect values. Another problem arises because Al_2O_3, as a relatively immobile oxide is not considered as a reference phase to monitor relative changes of composition of relevant mineral components (Bahlburg and Dobrzinski 2011). The CIA approach was proposed by Nesbitt and Young (1982) to circumvent then mentioned problems associated with WIP. The difference between CIA and CIW is that if weathering increases, the WIP values become smaller. A normal range is between 100 (fresh rock) down to 1 (completely weathered). The results for WIP are in a good agreement with the CIA and CIW data (Tab. 15). They show slight to moderate weathering with values between 35 and 29 for the catchment sediments. Worthwhile to mention is that the data from lake sediments can have a potential bias due to uptake and loss of elements and oxides in the lake environment. Therefore all the weathering index values should be considered as relative information about the degree of weathering and not as absolute results.

Another index proposed by Vogt (1927) is the Vogt residual index (V). This index was used by Roaldset (1972) to characterize the degree of weathering of clays in Quaternary deposits in Norway. She compared the bulk chemistry of moraine and marine clays and found out that the moraine clays were more weathered (Price and Velbel 2003). The formula for the calculation of the Vogt residual index is:

V: $(Al_2O_3+K_2O)/(MgO+CaO+Na_2O)$

As it can be seen, the formula includes the already known mobile oxides and the alkali and earth alkali metals. The formula also includes Al_2O_3 as immobile component which is added to K_2O. The results for the Vogt´s residual index data are shown in Table 15.

Table 14: To compare different results for weathering indexes, the Vogt´s Residual Index and the weathering index by Parker (WIP) have been selected. The values were chosen because of their different calculation approach. The calculations were carried out on the sediment samples from the local catchment lake.

Sample	WIP	Vogt (V)
EF4-6	36	2,1
EF10-12	36	2,2
EF12-14	37	2,1
EF14-16	36	2,0
EF20-22	29	2,2
EF24-28	31	2,4

Table 15 shows the results for the calculated V data, the values starting with minimum 1 and theoretically going to infinite. The values are usually between 2 and 2.4 which again show a slight weathering. This method is more adapted to sediments and therefore it is not used on rock samples.

The four described weathering indexes CIA, CIW, WIP and V show all a good correspondence in the results. They all display a low, but detectable degree of weathering in the Eldsfjellet area. Again these derived values give only an indication about the degree of weathering and they are not absolute.

5.6.4. Interpretation of chemical index values from Eldsfjellet

The range of obtained values for saprolites and regoliths are between 69 up to 72 for CIA and between 70 up to 74 for CIW. The CIW values are on average higher than the CIA values, because of the exclusion of K_2O in the CIW calculation. Based on the interpretation by Bahlburg and Dobrzinski (in press 2009), values around 70 can be seen as slightly weathered.

In comparison with the calculated values in this thesis, Rajamani et al. (2009) obtain CIA values between 89 and 95 for their regoliths and saprolites. Compared to the data produced from Eldsfjellet samples, the weathering in the Western Ghats is clearly more extensive. The Western Ghats values mainly reflect the destruction of plagioclase, pyroxene and amphibole.

The results for CIA and CIW for Eldsfjellet are in a good agreement with the analysed data, the degree of weathering in the fieldwork area is not very mature due to climate conditions and a short transportation distance between source and sink.

5.7. Calculating the amount of weathering

If the amount of the different oxides in the fresh rock material and corresponding saprolites is known, it is possible to calculate the percentage gain and loss of oxides during weathering. The major element compositions which were used for the calculations are all obtained on samples with a weight of 1 g. This makes the calculation and multiplication easier and the data comparable. Average values for fresh rock material and average values for catchment sediments were used for the calculation. This gives a fairly good impression of the amount of gain and loss in the weathering system at Eldsfjellet.

The calculation used was adapted from Faure (1998). To create the formula an immobile oxide has to be found. In case of this calculation Al_2O_3 was used. If the Al_2O_3 value from the fresh rock sample is divided by the value for the weathered sample it is possible to calculate the *weight-loss factor (w)*. In case of the Eldsfjellet data the factor was 0.784. This factor will now be used to calculate the weight of remaining material from the other oxides. An example for that is CaO, the fresh rock value is 8.6 weight % and in the sediments the value is 6.72 weight %. By multiplying the weight % of sediments with the *weight-loss factor*

(6.72*0.784), it is possible to obtain the number for the remaining CaO in gram. In this case it is 5.27 g. This was done for all the oxides and can be found in table 16. The values used in Table 2 are average values of the rock and catchment sediment samples.

Table 15: A comparison of weight % concentration of fresh rock samples with catchment sediment. The values are average values for the different oxides and display the average concentration for fresh rock and sediment concentration. It is possible to calculate the gain and loss of oxides based on the weight % values in gram. They show a loss for most of the oxides except from P_2O_5 and TiO_2. The increase of P_2O_5 is related to a high organic content in the sediments which leads to an increase in the chemical data.

Oxides	Rocks (%)	Sediments (%)	Amount remaining in 100 g	gain+/loss- in 100 g	gain+/loss- in %
Na_2O	2,60	2,90	2,27	-0,33	-12,7
MgO	11,46	2,01	1,57	-9,89	-86,3
Al_2O_3	19,27	24,57	19,27	0,00	0,0
SiO_2	49,73	57,54	45,10	-4,63	-9,3
P_2O_5	0,03	0,31	0,24	0,21	650,0
K_2O	0,33	0,74	0,58	0,25	75,0
CaO	8,60	6,72	5,27	-3,33	-38,7
TiO_2	0,16	0,35	0,27	0,11	68,8
MnO	0,11	0,03	0,02	-0,09	-78,6
Fe_2O_3	9,34	4,19	3,28	-6,06	-64,8
Sum	101,63	99,36	77,88	-23,75	

Table 16 shows the results from the calculations based on Faure (1998). The results show that between the fresh rocks and the sediments an overall loss of 23.75 g of all oxides can be measured. This means that from the source area down to the sink (lake) and due to processes in the catchment lake ca. 23.37 % of the material is removed and transported away. A high loss of MnO, Fe_2O_3 and MgO can be seen, these oxides are all typical elements in mafic minerals like pyroxene, olivine and amphibole. This supports the idea of preferential weathering of mafic minerals. The strongest gain was for P_2O_5 (650 %) and K2O which can be related to an uptake from the organic rich sediments in the lake. The concentration of P_2O_5 itself is still low compare to most of the other oxides. There is also a relatively strong increase in K_2O (+75 %), while Na_2O (-12.7 %) and CaO (-38.7 %) decreases. The increase in K_2O and the decrease of the other two oxides could partly explain why illite is produced instead of smectite. It is due to the loss of the other two oxides from the system.

The amount of lost material on the mountain surface due to weathering is relatively low which is in good agreement with the calculated weathering indexes.

5.8. Further suggestions

To achieve an even better understanding of the weathering processes in the area it would be useful to acquire additional sample material, especially in the northern and eastern part of Eldsfjellet to support the results from this work and extend the knowledge further.

To estimate the degree of weathering, it is advisable to collect 2-3 core samples next to each other to be able to extract enough material from the alteration rims to calculate the CIA and CIW between fresh rock and weathered rock. This will give even more detailed information about the degree of weathering.

Of interest will also be deteiled clay analysis from the rock surfaces and detailed water analysis to find out why the clay minerals transported to the lake include illite instead of the expected smectite.

6. Conclusions

- Major and trace element data was acquired from rock and water samples (1. in Fig. 50) distributed over Eldsfjellet. The comparison of trace element data from rock and water samples shows a good agreement; therefore water is expected to be of major importance for the chemical weathering processes on Eldsfjellet.

- Water samples were taken from local ponds (2. in Fig. 50) and compared with local bed-rock trace element composition. The data is in good agreement and shows that water is the major weathering and transport agent (3. in Fig. 50).

- It was possible to determine the clay content from the highly organic top part of a sediment core (5. Fig. 48) taken in the local catchment lake. The clays were produced directly on the bedrock surface (4. Fig. 50) and are consistent with the local bedrock, therefore it can be shown which kind of clay mineral will be produced during chemical weathering. One exception is the production of illite instead of smectite. It was not possible to solve this problem, but it is expected that there is an exchange of certain elements which favor this process.

- Chemical weathering indexes were used to display the degree of weathering. The indexes used were CIA, CIW, Vogt´s Index and WIP. All show slight to moderate weathering.

- In comparison with the chemical weathering indexes, the gain and loss of oxides was calculated by using the average major element values from rocks and sediments and multiplying the sediment values with a *weight-loss factor* (Faure, 1998). The results show a loss of 23.75 % which is low weathering and consistent with the chemical weathering indexes. That means it can be assumed that approximately 24 % of the today bed rock surface is removed.

- Eldsfjellet major element data were plotted on a ternary plot with data from Rajamani et al. (2009). The plot shows low weathering compared to the data of Rajamani et al. (2009) from the Western Ghats, India as expected. An explanation is the much higher annual temperature, higher precipitation and a longer transport distance which favors the

weathering. The weathering trend is consistent with the Rajamani et al. (2009) data. That means temperature and precipitation conditions play a crucial role for chemical weathering.

- REE data shows an anorthositic origin for most samples except from Ef.10 which is interpreted to be an N-Type MORB and therefore of oceanic crust origin, this is the first data describing material of oceanic crust origin in the field area.

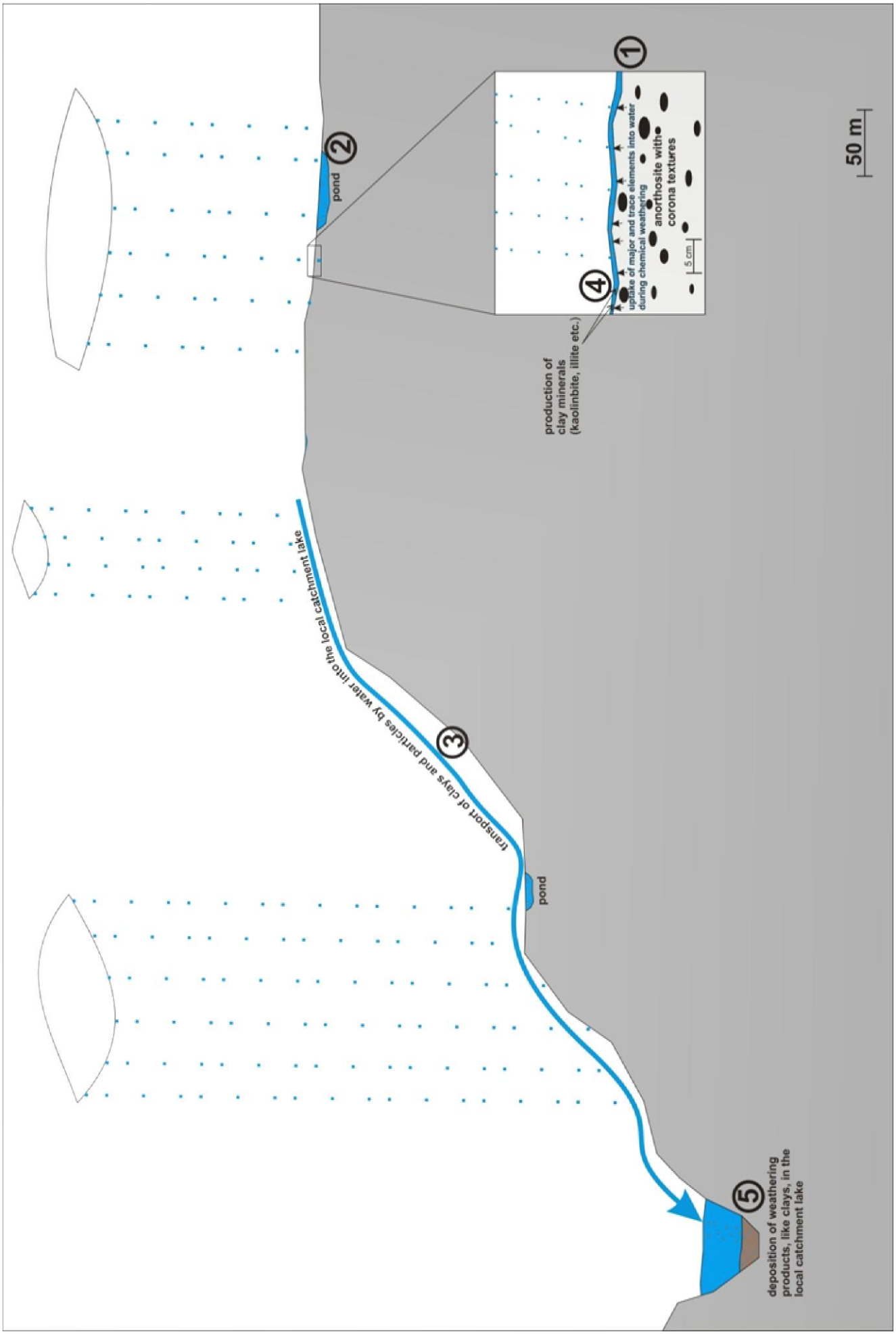
1
2
pond
uptake of major and trace elements into water during chemical weathering
anorthosite with corona textures
5 cm
4
production of clay minerals (kaolinite, illite etc.)
50 m
transport of clays and particles by water into the local catchment lake
3
pond
5
deposition of weathering products, like clays, in the local catchment lake

Figure 50: An overview of the processes between source and sink. Precipitation on the mountain surface leads to a supply with fresh water which will react with the bed rock surface (2). Clay minerals will be produced on the rock surface (1 and 4). Due to permanent fresh water supply, the chemical weathering will be consistent. Particles and clay minerals will be transported away by the water (3) and deposited in the local catchment.

7. References

Montanini, A., Tribuzio, R., Anczkiewicz, R., 2006. Exhumation History of a Garnet Pyroxenitebearing Mantle Section from a Continent–Ocean Transition (Northern Apennine Ophiolites, Italy). *Journal of Petrology.***47**, 1943–1971

Andersen, B.G., Mangerud, J., Sørensen, R., Reite, A., Sveian, H., Thoresen, M., Bergstrom, B., 1995. Younger Dryas ice-marginal deposits in Norway. *Quaternary International*. **28**, 147-169 (1995)

Aulbach, S., Griffin, W.L., O´Reilley, S.Y., McCandless, T.E., 2004. Genesis and evolution of the lithospheric mantle beneath the Buffalo Head Terrane, Alberta (Canada). *Lithos.***77**, 413-451.

Austrheim, H., Griffin, W.L., 1985. Shear deformation and Eclogite formation within Granulite-Facies Anorthosites of the Bergen Arcs, Western Norway. *Chemical Geology*. **50**, 267-281 (1985)

Austrheim, H., Griffin, W.L., 1986/87. Eclogitization of lower crustal granulites by fluid migration through shear zones, *Earth and Planetary Science Letters*. **81**, 221-232.

Austrheim, H., Erambert, M., Boundy, T.M., 1996. Garnets recording deep crustaly earthquakes, *Earth and Planetary Science Letters*. **139**, 223-238

Bahlburg, H., Dobrzinski, N., 2010. A review of the Chemical Index of Alteration (CIA) and its application to the study of Neoproterozoic glacial deposits and climate transitions, *The Geological Record of Neoproterozoic Glaciations. Geological Society, London, Memoir*.

Bahlburg, H., Breitkreuz C., 2004, Grundlagen der Geologie. *Spektrum Akademischer Verlag*. 403 pages.

Bingen, B., Austrheim, H., Whitehouse, M.J., Davis, W.J., 2004. Trace element signature and U–Pb geochronology of eclogite-facies zircon, Bergen Arcs, Caledonides of W Norway, *Contributions to Mineralogy and Petrology*. **147**, 671-683.

Bondevik, S., Mangerud, J., 2002. A calendar age estimate of a very late Younger Dryas ice sheet maximum in Western Norway, *Quaternary Science Review*. **21**, 1661-1676.

Boundy, T.M., Fountain, D.M., Austrheim, H., 1992. Structural development and petrofabrics of eclogite facies shear zones, Bergen Arcs, western Norway: Implications for deep crustal deformation processes, Journal of Metamorphic Geology. **10**, 127-146.

Brock, R.W., 1943. Weathering of igneous rocks near Hong Kong, *Geol.Soc.America Bull.* **54**, 717-738.

Boundy, T.M., Mezger, K., Essene, E.J., 1997. Temporal and tectonic evolution of the granulite-eclogite association from the Bergen Arcs, western Norway, *Lithos*. **39**, 159-178.

Charlier, B., Auwera, J.V., Duchesne, J-C., 2005. Geochemistry of cumulates from the Bjerkreim–Sokndal layered intrusion (S. Norway) Part II. REE and the trapped liquid fraction, *Lithos*. **83**, 255-276.

Deer, W.A., Howie, R.A., Zussman, J., 1966. Introduction to the Rock-Forming Minerals, *Longmans, London*. p. 528.

Davydova, V.V., Perchuk, A.L., Stoeckhert, B., 2009. Petrology of Coronite from the Bergen Arcs Complex, Norway, *Moscow University Geology Bulletin*. **64**, 166-176.

Deer, W.A., Howie, R.A., 1966. An introduction to the rock-forming minerals, *Longman, London*.

de Haas, G-J.L.M., Nijland, T. G., Valbracht, P. J., Maijer, C., Verschure, R., Andersen, T., 2002. Magmatic versus metamorphic origin of olivine-plagioclase coronas, *Contributions to Mineralogy and Petrology*. **143**, 537-550.

Deepthy, R., Balakrishnan, S., 2005. Climatic control on clay mineral formation: Evidence from weathering profiles developed on either side of the Western Ghats, *Journal of Earth System Science*. **114**, 545-556.

Erambert, M., Austrheim, H., 1993. The effect of fluid and deformation on zoning and inclusion patterns in poly-metamorphic garnets, *Contrib. Mineral. Petrol*. **115**, 204-214.

Fassel, V. A., Kniseley, R. N., 1974. Inductively Coupled Plasma-Optical Emission Spectroscopy, *Analytical Chemistry*. **46**, 1110A-1111A.

Faure, G., 1998. Principles and Applications of Geochemistry, *Prentice Hall*. 600 pages 2nd edition.

Fedo, C.M., Nesbitt, H.W., Young, G.M., 1995. Unraveling the effects of potassium metasomatism in sedimentary rocks and paleosols, with implications for paleoweathering conditions and provenance, *Geology*. **23,** 921-924.

Grant, W.H., 1963. Weathering of Stone Mountain Granite, *in E. Ingersol (ed.), Clays and Clay Minerals: Oxford, Pergamon*. 65-73.

Harnois, L., 1988. The CIW index: a new chemical index of weathering, *Sedimetary Geology*. **55**, 319-322.

Hawkins, D.B., Roy, R., 1963. Experimental hydrothermal studies on rock and clay mineral formation, *Geochimica et Cosmochimica Acta*. **27**, 1047-1054.

Hölting, B., Coldewey, W. 2008, Einführung in die Allgemeine und Angewandte Hydrogeologie. *Spektrum Akademischer Verla. 384 pages*.

Jolivet, L., Raimbourg, H., Labrousse, L., Avigad, D., Leroy, Y., Austrheim, H., Andersen, T.B., 2005. Softening trigerred by eclogitization, the first step toward exhumation during continental subduction, *Earth and Planetary Science Letters*, **237**, 532-547.

Kühn, A., Glodny, J., Iden, K., Austrheim, H., 2000. Retention of Precambrian RbrSr phlogopite ages through Caledonian eclogite facies metamorphism, Bergen Arc Complex, W-Norway, *Lithos*. **51**, 305-330.

Latypov, R. M., Mitrofanov, F.P., Alapieti, T. T., Halkoaho, T. A. A., 1999. Petrology of the Lower Layered Horizon of the Western Pansky Tundra Intrusion, Kola Peninsula, *Petrology*. **7**, 482-508.

Lekens, W.A.H., Haflidason, H., Sejrup, H.P., Nygard, A., Richter, T., Vogt, C., Frederichs, T., 2009. Sedimentation history of the northern North Sea Margin during the last 150ka, *Quaternary Science Review*. **28**, 469-483.

Li, C., Yang, S., 2010. Is Chemical Index of Alteration (CIA) a reliable proxy for chemical weathering in global drainage basins?, *American Journal of Science*. **310**, 111-127.

Liu, Z., Colin, C., Huang, W., Le, K. P., Tong, S., Chen, Z., Trentesaux, A., 2007. Climatic and tectonic controls on weathering in south China and Indochina Peninsula: Clay mineralogical and geochemical investigations from the Pearl, Red, and Mekong drainage basins, *G^3- Geochemistry, Geophysics, Geosystems*. **8**.

Liu, Z., Zhao, Y., Colin, C., Siringan, F. P., Wu, Q., 2009. Chemical weathering in Luzon, Philippines from clay mineralogy andmajor-element geochemistry of river sediments *Applied Geochemistry*. **24**, 2195-2205.

Lohne, Ø.S., 2006. Late Weichselian related sea-level changes and glacial history in Hordaland, Western Norway, *PhD Thesis, University of Bergen*.

Lohne, Ø.S., Bondevik, S., Mangerud, J., 2007. Sea-level fluctuations imply that Younger Dryas ice-sheet expansion in Western Norway commenced during the Allerød, *Quaternary Science Reviews*. **26**, 2128-2151.

Lohne, Ø.S., Mangerud, J., Svendsen, J.I., 2012. Timing of the Younger Dryas glacial Maximum in Western Norway, *Journal of Quaternary Science*. **27**, 81-88.

Lundstrom, C.C., Gill, J., Williams, Q., Perfit, M.R., 1995. Mantle Melting and Basalt Extraction by Equilibrium Porous Flow, *Science*. **270**, 1958-1961.

Maji, A. K., Patra, A., Ghosh, P., 2010. An overview on geochemistry of Proterozoic massif-type anorthosites and associated rocks, *J. Earth Syst. Sci*. **119**, 861-878.

Markl, G., Foster, C. T., Bucher, K., 1998. Diffusion-controlled olivine corona textures in granitic rocks from Lofoten, Norway: calculation of Onsager diffusion coefficients, thermodynamic modeling and petrological implications, *Journal of Metamorphic Geology*. **16**, 607-623.

Mangerud, J., Gyllencreutz, R., Lohne, Ø.S., 2011. Glacial History of Norway, *in Quarternary Glaciations-Extent and Chronology, Part IV-A Closer Look. (eds) J. Ehlers, P. Gibbard.* Elsevier: Amsterdam, 279-298.

McDonough, W. F., Sun, S.-S., 1995. The composition of the earth, *Chemical Geology*. **120.**

Nesbitt, H. W., Young, G. M., 1984. Prediction of some weathering trends of plutonic and volcanic rocks based on thermodynamic and kinetic considerations, *Geochimica et Cosmochimica Acta*. **48**, 1523-1534.

Nesbitt, H. W., Young, G. M. 1989. Formation and Diagenesis of Weathering Profiles, *The Journal of Geology*. **97**, 129-147.

Noack, Y., Colin, F., Nahon, D., Delvigne, J., Michaux, L., 1993. Secondary-mineral formation during natural weathering of pyroxene: reviews and thermodynamic approaches, *American Journal of Science*. **293**, 111-134.

Okland, I. Huang, S., Dahle, H., Thorseth, I. H., Pedersen, R. B., 2012. Low temperature alteration of serpentinized ultramafic rock and implications for microbial life, *Chemical Geology*. **318-319**, 75-87.

Ollier, C., 1984. Weathering, *Longman London*. 270 pages.

H. Palme, C., Beer, H., 1993. in Landolt Börnstein Group VI, *Astronomy and Astrophysics*. **2A.**

Pe´rez del Villar, L., Delgado, A., Reyes, E., Pelayo, M., Ferna´ndez-Soler, J. M., 2005. Thermochemically induced transformations in Al-smectites: A Spanish natural analogue of the bentonite barrier behavior in a radwaste disposal, *Applied Geochemistry*. **20**, 2252-2282.

Price, J. R., Velbel, M. A., 2003. Chemical weathering indices applied to weathering profiles developed on heterogenous felsic metamorphic parent rocks, *Chemical Geology*. **202**, 397-416.

Raimbourg, H., Jolivet, L., Labrousse, L., Leroy, Y., Avigad, D., 2005. Kinematics of syneclogite deformation in the Bergen Arcs, Norway: implications for exhumation mechanisms, (Eds.) D. Gapais, J. P. Brun, P. R. Cobbold, Deformation Mechanisms, Rheology and Tectonics: from Minerals to the Lithosphere, *Geological Society, London, Special Publications*. **243**, 175-192.

Rajamani, V., Tripathi, J. K., Malviya, V. P., 2009. Weathering of lower crustal rocks in the Kaveri river catchment, southern India: Implications to sediment geochemistry, *Chemical Geology*. **265**, 410-419.

Ramberg, I. B., Bryhni, I., Nottvedt, A., Ragnes, K., 2008. The Making of a Land-The Geology of Norway, *Geological Society of Norway*. 624 pages.

Reiche, P., 1943. Graphic representation of chemical weathering, *Journal of Sedimentary Petrology*. **13**, 58-68.

Renberg, I., 1991. The HON-Kajak sediment corer, *Journal of Paleolimnology*. **6**, 167-170.

Renberg, I., Hansson, H., 2008. The HTH sediment corer, *Journal of Paleolimnology*. **40**, 655-659.

Reusch, H., 1894. Strandfladen, et nyt traek i Norges Geografi, *Norges Geol. Undersökelse*. **15**, 1-14.

Rice Jr., T. J., Buol, S. W., Weed, S. B., 1985. Soil-Saprolite Profiles Derived from Mafic Rocks in the North Carolina Piedmont: I. Chemical, Morphological, and Mineralogical Characteristics and Transformations, *Soil Science Society of America Journal*. **49**, 171-178.

Roaldset, E., 1972. Mineralogy and geochemistry of Quaternary clays in the Numedal Area, sothern Norway, *Norsk Geol. Tidsskr*. **52**, 335-369.

Rockow, K. M., Haskin, L. A., Jolliff, B. L., Fountain, D. M., 1997. Constraints on element mobility associated with the conversion ofgranulite to eclogite along fractures in an anorthositic complex on Holsnøy, Norway, *Journal of Metamorphic Geology*. **15**, 401-418.

Sand, L.B., Bates, T.L., 1953. Mineralogy of the residual kaolins of the Southern Appalachians, *Am.Mineral*. **38**, 358-372.

Schneider, J., Bosch, D., Monié, P., Bruguier, O., 2007. Micro-scale element migration during eclogitisation in the Bergen arcs (Norway): A case study on the role of fluids and deformation, *Lithos*. **96**, 325-352.

Sejrup, H.P., Aarseth, I., Haflidason, H., 1995. Quaternary of theNorwegian Channel - glaciation history and paleoceanography, *Norsk Geologisk Tidsskrift*. **75**, 65-87.

Shao, J., Yang, S., Li, C., 2012. Chemical indices (CIA and WIP) as proxies for integrated chemical weathering in China: Inferences from analysis of fluvial sediments, *Sedimentary Geology*. **265-266**, 110-120.

Singer, A., 1984. The Paleoclimatic Interpretation of Clay Minerals in Sediments - a Review, *Earth - Science Reviews*. **21**, 251-293.

Srivastava, A. K., Randive, K. R., Khare, N., 2012. Mineralogical and geochemical studies of glacial sediments from Schirmacher Oasis, East Antarctica, *Quaternary International*. **XXX**, 1-12.

Stosch, H.-G., 2000. Geochemie der Seltenen Erden, lecture notes from 1988-1993, updated 1998 and 2000, *Department of Petrography and Geochemistry, University of Karlsruhe*.

Taylor, S. R., Campbell, I. H., McCulloch, M. T., McLennan, S. M., 1984. A lower crustal origin for massif-type Anorthosites, *Nature*. **311**, 372-374.

Thomas, R., 2001. A Beginner's Guide to ICP-MS Part VII: Mass Separation Devices — Double-Focusing Magnetic-Sector Technology, *Spectroscopy*. **16**, 22-26.

Tomilenko, A. A., Kovyazin, S.V., 2008. Development of Corona Textures around Olivine in Anorthosites of the Korosten' Pluton, Ukrainian Shield: Mineralogy, Geochemistry, and Fluid Inclusions, *Petrologiya*. **16**, 92-109.

Velbel, M. A., Berker, W. W., 2008. Pyroxene weathering to smectite: conventional and cryo-field emission scanning electron microscopy, Koua Bocca Ultrmafic Komplex, Ivory Coast, *Clays and Clay Minerals*. **56**, 112-127.

Vogt, T., 1927. Sulitjelmafeltets geologi og petrografi, *Nor. Geol. Unders.* **121**, 1-560.

Wahlstrom, E.E., 1948. Pre-Fountain and recent weathering o Flagstaff Mountain near Boulder, Colorado, *Geol.Soc.America Bull.* **59**, 1173-1190.

Wilson, M., 1993. Magmatic differentiation, *Journal of the Geological Society, London*. **150**, 611-624.